INSTITUTO
UNIVERSITÁRIO
DE LISBOA

ROADM architectures for multi-band optical networks

João Frederico de Almeida Raposo do O'Ramos

Master degree in Telecommunications and Computer Engineering,

Supervisor:
PhD, Luís Gonçalo Lecoq Vences e Costa Cancela, Assistant Professor
Iscte-Instituto Universitário de Lisboa

Co-Supervisor:
PhD, João Lopes Rebola, Associate Professor
Iscte-Instituto Universitário de Lisboa

October, 2023

TECNOLOGIAS
E ARQUITETURA

Department of Information Science and Technology

ROADM architectures for multi-band optical networks

João Frederico de Almeida Raposo do O'Ramos

Master degree in Telecommunications and Computer Engineering,

Supervisor:
PhD, Luís Gonçalo Lecoq Vences e Costa Cancela, Assistant Professor
Iscte-Instituto Universitário de Lisboa

Co-Supervisor:
PhD, João Lopes Rebola, Associate Professor
Iscte-Instituto Universitário de Lisboa

October, 2023

Família

Acknowledgment

With the completion of this work, six years at Iscte-Instituto Universitário de Lisboa come to an end. I want to acknowledge and thank Iscte-Instituto Universitário de Lisboa, my teachers and colleagues for all the experiences and challenges I have had and faced. Special thanks to the Instituto de Telecomunicações (IT) and Iscte-Instituto Universitário de Lisboa my supervisors Professor Luís Cancela and Professor João Rebola, for their constant guidance and support throughout this dissertation.

I would also like to thank my family, and friends for encouraging me and helping me through the most complicated moments. Special thanks to my parents and sister for being there for me.

Finally, I would like to make an honourable mention to my grandmother Maria Helena, who always had a special affection for me, and my deceased grandparents, Ângelo, Maria Manuela and Virgílio.

Resumo

Atualmente com o aumento exponencial das comunicações 5G, das comunicações entre *datacenters* e dos serviços de baixa latência, o aumento da capacidade e da flexibilidade das atuais redes óticas é uma prioridade para os atuais fornecedores de serviços e conteúdos. A transmissão multibanda (MB) é vista como uma solução a curto e médio prazo para aumentar a capacidade e ultrapassar as limitações de transmissão na banda C. Esta dissertação analisa o impacto de várias arquiteturas de nós no projeto de redes MB C+L+S.

Três arquiteturas MB - *baseline*, *common-band* e *compact* - são estudadas em termos do custo-por-bit e das limitações introduzidas pela camada física (PLIs). Desenvolveu-se uma ferramenta de planeamento de redes que resolve o problema do encaminhamento, da atribuição do formato de modulação e do espectro (RMSA), e que incorpora o impacto da arquitetura dos nós e dos PLIs. Esta ferramenta RMSA calcula a capacidade total da rede e o custo-por-bit de uma determinada topologia de rede, para as diferentes arquitecturas MB.

A arquitetura *common-band* apresenta o menor custo-por-bit comparativamente às restantes arquiteturas MB, quando os PLIs são desprezados, uma vez que apenas são utilizados componentes da banda C de menor custo. Num cenário de rede, com o efeito dos PLIs, a arquitetura *common-band* conduz à menor capacidade total de rede e ao maior custo-por-bit, devido ao elevado ruído adicional dos conversores de comprimento de onda óticos. O custo-por-bit da arquitetura *common-band* é quase o dobro do custo-por-bit das arquiteturas *baseline* e da *compact*, devido à degradação induzida pelos PLIs.

Palavras-Chave: Redes óticas; multibanda; multiplexador ótico de inserção/extracção reconfigurável; conversor de comprimento de onda ótico; custo-por-bit; limitações da camada física.

Abstract

Nowadays with the exponential increase of 5G mobile, datacenter communications and low-latency services, there is a huge demand for more data capacity and flexibility in optical networks. The multi-band (MB) is a mid-term solution to increase capacity and surpass the C-band transmission limitations. This dissertation analyzes the impact of several node architectures on the design of C+L+S MB networks.

Three MB node architectures - baseline, common-band and compact - are studied in terms of cost-per-bit and induced-physical layer impairments (PLIs). We develop a routing, modulation format and spectrum assignment (RMSA) network planning tool, based on a Monte-Carlo simulation, that incorporates the impact of the node architecture and PLIs. This RMSA tool calculates the total network capacity and cost-per-bit of a given network topology, for the different MB node architectures.

The common-band architecture presents the lowest cost-per-bit compared to the remaining MB architectures when the PLIs are neglected, since only lower cost C-band components are used. In a network scenario, with the PLIs impact, the common-band architecture leads to the lowest total network capacity and highest cost-per-bit due to additional noise from all-optical wavelength converters. The common-band cost-per-bit is almost twice the compact and baseline cost-per-bit due to the PLIs-induced degradation.

Keywords: Optical networks; multi-band; reconfigurable optical add-drop multiplexer; all-optical wavelength converter; cost-per-bit; physical layer impairments.

Contents

List of Figures

List of Tables

List of Acronyms

A/D: Add/Drop

AO-WC: All-Optical Wavelength Converter

ASE: Amplified Spontaneous Emission

B&S: Broadcast and Select

BER: Bit Error Rate

C: Colorless

CD: Colorless and Directionless

CDC: Colorless, Directionless and Contentionless

COI: Channel Of Interest

DEMUX: Demultiplexer

EDFA: Erbium-Doped fiber Amplifier

FEC: Forward Error-Correction

FF: First-Fit

FS: Frequency Slot

IL: Insertion Loss

ISRS: Inter-channel Stimulated Raman Scattering

ITU-T: International Telecommunication Union - Telecommunications

LCoS: Liquid Crystal on Silicon

MB: Multi-Band

MC: Monte Carlo

MCS: Multicast Switch

MEMS: Micro-Electromechanical Systems

MUX: Multiplexer

NLI: Nonlinear Interference

OA: Optical amplifier

OS: Optical Switch

OSNR: Optical Signal-to-Noise Ratio

PIC: Photonic Integrated Circuit

PLI: Physical Layer Impairments

QAM: Quadrature Amplitude Modulation

QPSK: Quadrature Phase-Shift Keying

R&S: Route and Select

RM: Residual Margin

RMSA: Routing, Modulation Format and Spectrum Assignment

ROADM: Reconfigurable Optical Add-Drop Multiplexer

ROSNR: Required Optical Signal-to-Noise Ratio

S/C: Splitter/Coupler

SDM: Spatial-Division Multiplexing

SM: Safety Margin

SMF: Single-Mode Fiber

SNAP: Statistical Network Assessment Process

SPM: Self-Phase Modulation

TDFA: Thulium-Doped fiber Amplifier

TR: Transponder

WDM: Wavelength Division Multiplexing

WSS: Wavelength Selective Switch

XPM: Cross-Phase Modulation

List of Symbols

α	Multiplicative factor that influences the cost of S-band components
α_b	Fiber attenuation coefficient in dB/km for the band b
β	Multiplicative factor that influences the cost of AO-WC
β_2	Group velocity dispersion parameter
β_3	Third order dispersion parameter
$\Delta\nu_{ch}$	Channel spacing
$\eta_{corr}(f_m)$	Modulation correction factor
$\eta_{N_{spans}}(f_m)$	NLI coefficient accounting for the modulation correction
$\eta_{SPM,j}$	NLI coefficient corresponding to the SPM effect
$\eta_{XPM,j}$	NLI coefficient corresponding to the XPM effect
γ	Fiber nonlinear coefficient
λ_0	Reference wavelength
ν_{ch}	Frequency of the last channel for the desired band
$\nu_{m,b}$	Nominal frequency of the central WDM channel
ν_m	Channel frequency of channel m
$\overline{\alpha}$	Generic attenuation coefficient
$\overline{L}_{span}$	Average span length
Φ	Excess kurtosis
ϕ	Phase mismatch term
ε	Coherence factor
A/D_{ratio}	Add/Drop ratio
B_0	Optical bandwidth
B_k	Bandwidth of k-th interfering channel
B_m	Bandwidth of the m-th channel (COI)
BP	Blocking probability after N_{sim} MC iterations
c	Speed of light
C_r	Raman gain slope
$Cost_{A/D,CD,b}$	Cost of the CD A/D structure for the band b

$Cost_{A/D,CDC,b}$	Cost of the CDC A/D structure for the band b
$Cost_{AO-WC}$	Cost of the AO-WCs
$Cost_B$	Cost of component B (A/D structure)
$Cost_{EDFA,b}$	Cost of the EDFA for the band b
$Cost_{express,b}$	Total cost of the ROADM express structure for the band b
$Cost_{fiber}$	Fiber lease cost per km during 5 years
$Cost_{MB,MUX/DEMUX}$	Cost of the MB MUX/DEMUX
$Cost_{Network,a,n}$	Total network cost for a specific ROADM architecture a and network topology n
$Cost_{TR}$	Cost of the transponder
$Cost_{WSS,1\times M'}$	Cost of the WSS present in Drop structure (CD type)
$Cost_{WSS,R\times 1}$	Cost of the route WSS
$Costperbit$	Total cost-per-bit
$Ctotal$	Total network capacity
$D_{\lambda 0}$	Fiber dispersion parameter at the reference wavelength λ_0
$F_{m,b}$	Noise figure of each OA in dB
f_m	Nominal central frequency
g_{AO-WC}	Conversion gain of AO-WC in linear units
$G_{in,i,b}$	Gain of each in-line amplifier in link i and in band b in dB
G_{max}	Maximum gain considered for each OA in dB
$g_{pos,i,b}$	Post-amplifier gain in linear units
$G_{pre,b}$	Pre-amplification gain in dB for the band b
h	Planck constant
$IL_{add,b}$	ILs of the add path of the baseline, AO-WC, common-band and compact architectures architectures for the band b
$IL_{drop,b}$	ILs of the drop path of the baseline, AO-WC, common-band and compact architectures architectures for the band b
$IL_{MBWSS,route,1\times Y}$	ILs of the route MB WSS
$IL_{MBWSS,select,Y\times 1}$	ILs of the select MB WSS
$IL_{WSS,add,M'\times 1,b}$	ILs of the CD add structure WSSs for the band b
$IL_{WSS,drop,1\times M',b}$	ILs of the CD drop structure WSSs for the band b
$IL_{WSS,route,1\times Y,b}$	ILs of the route WSS for the band b
$IL_{WSS,select,Y\times 1,b}$	ILs of the select WSS for the band b

k_{paths}	Number of candidate paths
L_{sec}	Length of each link in km
M'	Number of transponders in one A/D card
M	Total number of transponders in the A/D structure
$N_{A/D}$	Number of A/D cards
N_{AO-WC}	Number of AO-WCs
N_{bands}	Number of bands
N_{ch}	Number of WDM channels arriving to the ROADM node in one direction
N_{fibers}	Number of fibers considered per direction in the node
$N_{gen,max}$	Number of generated demands in the i-th iteration of the RMSA simulator
$N_{i,p}$	Number of links in candidate path p
$N_{in,i}$	Number of in-line amplifiers in link i
N_{OLAs}	Number of OAs
N_{ROADMs}	Number of ROADMs
N_{WSS}	Number of WSSs
$osnr_{total,m,p,b}$	Total OSNR at the end of a path for channel m, candidate path p and band b
$p_{ASE,m,AO-WC,i,b}$	Additional ASE noise power due to the AO-WC losses compensation in link i
$p_{ASE,m,pre,i,b}$	ASE noise power of each OA in each band b for each link i
$p_{ASE,m,total,i,b}$	Total ASE noise power in each band b for each link i
$p_{ch,opt,m,i,b}$	Optimal power for channel m in band b and link i
$P_{d,p}$	Demand d and candidate path p
P_{filt}	Filtering penalty
p_m	Launch power of channel m
$p_{NLI,m,i,b}$	NLI noise power
p_{tot}	Total power transmitted
P_{xtalk}	Crosstalk power penalty
R	Number of directions per node
RM_p	Residual margin in candidate path p
$ROSNR$	Required OSNR

S_0	Fiber dispersion slope at the reference wavelength λ_0
SM_p	Safety margin in candidate path p
$Total_{Length}$	Total length of the network considered
Y	Size of the components used in the express structure

CHAPTER 1

Introduction

1.1. Motivation, context and goals

Nowadays, optical networks require technological innovation and more flexibility due to the growth of many consuming high data capacity and low-latency services, such as autonomous driving, virtual reality, cloud, datacenter communications and 5G services [1]. Many innovations have been introduced over the years that contribute to the use of the available C-band of an optical fiber in a more efficient way, such as advanced modulation formats, flexible grid, coherent-detection, reconfigurable optical add-drop multiplexer (ROADM) and ultra-sophisticated advanced signal processing [2].

Despite using the referred technologies, an optical network capacity crunch is foreseen in a near future [3]. So, currently, there are two solutions that are mainly discussed in the literature to expand the capacity of the existing C-band optical networks [4]. These two solutions are spatial-division multiplexing (SDM) and the multi-band (MB) solution. The MB solution consists in the exploitation of the full low attenuation spectrum available in a single optical fiber, allowing transmission beyond the C-band, and is seen as a near to medium-term solution to solve the capacity problem [4–6]. SDM is seen as a more long-term solution and can be implemented using multi-core, multi-mode, or multi-parallel fibers. However, SDM requires the deployment of new fibers, which may be more expensive in relation to the MB solution that exploits the fibers that are already installed [4]. SDM is considered more suitable for submarine networks [6], due to the huge amount of data traffic carried by these networks that can only be transported with multiple fibers, or multi-core fibers. Google is currently exploring these two solutions to meet their network infrastructure requirements [6].

In recent years, several works have studied MB optical networks [7–11]. In particular, in [9], a cost analysis considering a C+L+S network scenario is studied considering both transmission and node architecture issues. The node architectures considered were the MB baseline architecture, where switching between bands is not possible, and the MB common-band architecture, which uses mainly C-band components [7–9]. In [8], a MB all-optical wavelength converter (AO-WC) node architecture was presented and, in [10, 11],

a MB architecture called compact architecture that only uses components that work in all bands has been proposed and its performance on optical networks has been analyzed. Despite there are already, at least, four types of MB ROADM architectures proposed in the literature to the authors best knowledge, a comprehensive cost analysis comparison between these architectures remains to be done.

The MB optical networks raise novel questions and concerns compared to C-band networks, like the equipment used on other bands not being so mature with characteristics not yet optimized, different fiber attenuations for each band, the influence of the inter-channel stimulated Raman scattering (ISRS) on signal transmission and the proper design of the MB node architecture [7–11]. Besides the study of these network physical layer challenges, new planning tools have to be developed so that the much larger spectrum available in the MB scenario can be efficiently used. So, well designed routing, modulation format and spectrum assignment (RMSA) tools capable of satisfying all traffic demands are of paramount importance [12]. These tools typically use the optical signal-to-noise ratio (OSNR) metric in order to take into account the physical layer impairments (PLIs) impact in the RMSA tool and network design [12].

The main goal of this dissertation is to study different MB ROADM architectures and their suitability to answer the demand for the growing traffic capacity. In particular, four different MB architectures proposed in the literature working on the C+L+S bands are analyzed and compared, in terms of their internal structure, hardware count, capacity provided, and cost-per-bit. The influence of these architectures in a C+L+S MB network scenario is assessed and compared with networks based on the SDM solution. Moreover, the design of a RMSA planning tool incorporating the impact of the PLIs and also the impact of the node architecture is performed. In particular, the total OSNR is computed for each possible path in different optical networks and the frequency slots (FSs) assignment for the optical paths that meet the minimum residual margin is performed. The main outputs of the developed RMSA planning tool are the total network capacity and cost-per-bit.

1.2. Dissertation organization

This section describes how this dissertation is organized.

In **Chapter 2**, a brief review of the MB optical transmission and amplification topics is presented, and then the node architectures proposed in the literature for MB transmission, such as the baseline, AO-WC, common-band and compact nodes and their corresponding

architectures and hardware components are presented and studied. The cost-per-bit of these MB nodes will be evaluated and compared with the cost-per-bit of SDM nodes. Then, the cost-per-bit of two different networks employing the different MB node architecture solutions is studied considering also the fiber lease cost. These two network MB scenarios are compared with a SDM network scenario considering 3 fibers per direction.

In **Chapter 3**, the impact of the network PLIs, such as the amplified spontaneous emission (ASE) noise, nonlinear interference (NLI) noise and ISRS effect on optical networks with these MB node architectures is assessed through the OSNR and residual margin (RM) computation, considering different modulation formats. The PLIs are computed for the BT-UK network topology and the baseline, common-band and compact architectures, considering two different technologies for the wavelength selective switch (WSS) components implementation, the photonic integrated circuit (PIC) and Liquid Crystal on Silicon (LCoS).

In **Chapter 4**, the C+L+S MB network simulator developed in Matlab is presented and explained. This simulator is used to solve the RMSA problem and to compute the total network capacity and cost-per-bit, considering the BT-UK and CONUS-60 network topologies with the MB node architectures proposed in the literature. Firstly, the main characteristics of the BT-UK and CONUS-60 networks are presented. Next, the number of available optical paths in the BT-UK and CONUS-60 networks is computed for different channel launch powers, considering the MB node architectures and PLIs influence on the network performance. Then, the total network capacity and cost-per-bit are computed for the three MB node architectures, baseline, common-band and compact architectures, and a comparison with results obtained in works done by other authors is performed.

In **Chapter 5**, the final conclusions of this work, and considerations for future work are presented.

1.3. Main contributions

This work has the following main contributions:

- Study and comparison of four C+L+S MB ROADM architectures in terms of their internal structure, capacity, total node cost, and cost-per-bit and comparison with the SDM network scenario.
- Implementation of a C+L+S MB RMSA planning tool that considers the impact of the PLIs and node architecture.

- Study and analysis of the impact of the MB node architectures and their PLIs on the total network capacity and cost-per-bit.
- Demonstrating that in the common-band architecture, when considering the impact of the PLIs, the additional noise of the AO-WCs decreases the total network capacity and increases the cost-per-bit in relation to the other MB node architectures.

CHAPTER 2

Node architectures for multi-band optical networks

2.1. Introduction

The main objective of this chapter is to review the MB ROADMs to be used in multi-band networks. In this section, four MB architectures proposed in the literature will be studied: MB baseline architecture [7, 9], MB AO-WC architecture [8], MB common-band architecture [7–9] and MB compact architecture [10, 11].

This chapter starts by reviewing the MB optical transmission and amplification topics in section 2.2. The characteristics and the operation of four MB ROADM architectures, suitable for C+L bands and C+L+S bands transmission are discussed in section 2.3. In section 2.4, the total node cost of C-band, C+L bands, C+L+S-bands are assessed, and the cost-per-bit of C+L+S-bands nodes architecture is computed. For comparison purposes the total node cost and the cost-per-bit of a SDM ROADM architecture is also calculated. In section 2.5, the main conclusions of this chapter are presented.

2.2. Multi-band optical transmission and amplification

The worldwide increasing demand for Internet data traffic and the dramatic growth in the number of users on-line (either person or machines), is pushing for a huge increase in the data capacity of optical networks [4, 13]. The use of the MB solution is seen as short-medium term solution for increasing the networks data capacity [5]. By adding the L-band, a wavelength bandwidth of 95 nm is readily available (instead of only the 35 nm bandwidth of the C-band), allowing to have a cheaper solution to increase capacity, in relation to the SDM solution [5, 14]. Table 2.1 represents the bands of the optical fiber, as defined by the International Telecommunication Union - Telecommunications (ITU-T) [15], as well as their edge wavelengths, supported by a single-mode fiber (SMF).

Table 2.1. ITU-T bands definition for SMF.

Band	**O**	**E**	**S**	**C**	**L**
Wavelength [nm]	1260-1360	1360-1460	1460-1530	1530-1565	1565-1625
C-Band			70 nm	35 nm	60 nm
C+L-Band				95 nm	
S+C+L-Band			165 nm		
All Bands	365 nm				

Using the MB solution instead of SDM, avoids the costly deployment of more fibers in the optical network, allowing also to reduce the costs associated with fewer fibers management and maintenance. However, the main challenge related to the use of the MB solution lies in the fact that the equipment for MB networks has much less maturity [5], than C-band only devices, i.e., it is poorly developed, while the C-band equipment is very common and completely mature [5]. Furthermore, since the different fibers bands have their own features, regarding attenuation and dispersion, as shown in Figure 2.1, the propagation of a large number of wavelength division multiplexing (WDM) channels becomes a critical aspect for network management.

The two types of fibers, considered in Figure 2.1, ITU-T G.652A and ITU-T G.652D, are two of the four subcategories of G.652 fiber [16]. The fiber G.652D was developed to reduce the Water Peak, shown in Figure 2.1 for the ITU-T G.652A fiber, in the E-band region (1360-1460 nm), that leads to a high attenuation in this band. As in the ITU-T G.652D fiber, the attenuation coefficient varies only between 0.38 dB and 0.18 dB over all bands (1260 nm - 1625 nm), this fiber, which is already worldwide deployed, is the most suitable for MB transmission [5].

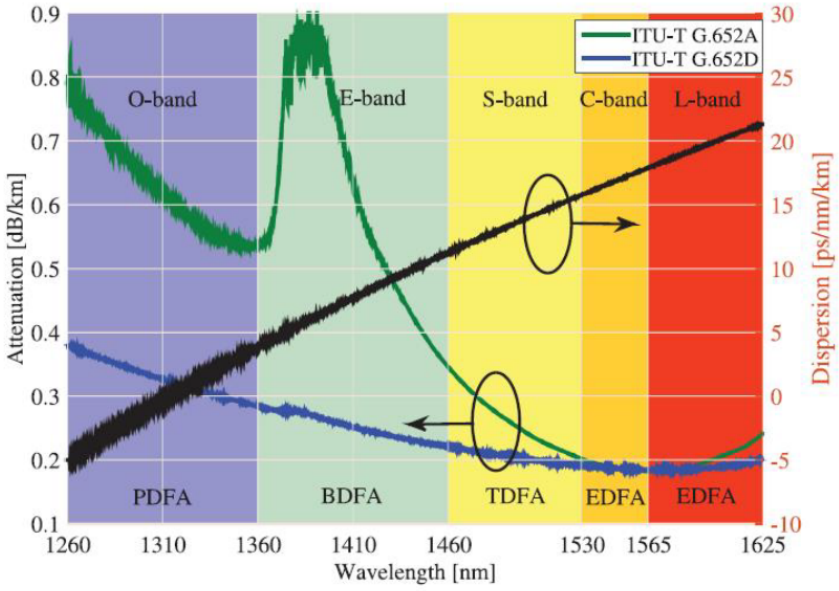

FIGURE 2.1. Measured attenuation (green and blue) and dispersion coefficient (black) for the fibers ITU-T G652.A and ITU-T G652.D.
Figure taken from [5].

For the C- and L-bands, the attenuation coefficient, reaches its lowest measured value of 0.18 dB/km. In addition, for the C- and L-bands presented, the optical amplifier

(OA) used is the same, the Erbium-Doped Fiber Amplifier (EDFA), which is a very mature technology in comparison with the amplifiers that must be used in the other fiber bands [5]: the Praseodymium-Doped Fiber Amplifier for the O-band, the Bismuth Doped Fiber Amplifier for the E-band, and the Thulium-Doped Fiber Amplifier (TDFA) for the S-band. The dispersion parameter $D(\lambda)$, represented in black in Figure 2.1, increases almost linearly with the wavelength and ranges from -5 ps/nm/km (O-Band) to approximately 22 ps/nm/km (L-Band), for both fibers. As a reference, for the C- and L-bands center wavelengths, the dispersion parameter is, respectively, around 18 ps/nm/km and 20 ps/nm/km [17].

In a C+L multi-band network, the optical amplification can be performed using several options, and the most widely used is represented in Figure 2.2 [6]. This option uses two EDFAs to amplify the C- and L-bands simplifying the amplification and allowing to activate bands when necessary. When only C-band signals need to be amplified, only the EDFA in this band is used, if L-band transmission must be also used, the EDFA in this band is activated [6, 11]. The structure of Figure 2.2 consists of two EDFAs, one for each band and composed by two couplers [10]. The two optical bands arriving at the ingress coupler, are selected to its respective branch, and a band dedicated EDFA performs the amplification. After amplification, the two bands are again combiner by a egress coupler and launched into the fiber.

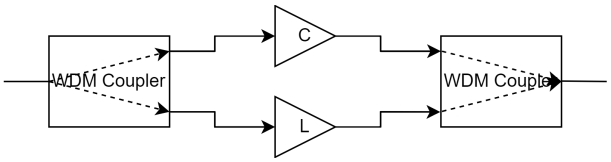

FIGURE 2.2. Structure of a conventional C+L band EDFA.
Figure taken from [10].

There are two more possible MB amplification options that are proposed in [6]: single wide-band amplifier and Hybrid EDFA/Raman with multi-pump Raman amplifiers.

2.3. Multi-band ROADM architectures

This section presents the architectures and main properties of the conventional single-band ROADM in subsection 2.3.1, and introduces four ROADM architectures proposed for MB networking in subsection 2.3.2.

2.3.1. Single-band ROADMs

In an optical network, the main function of the ROADM is to provide connectivity between the network clients [18]. A generic ROADM with R degrees is generally composed by an express structure and an add/drop (A/D) structure, as shown in Figure 2.3.

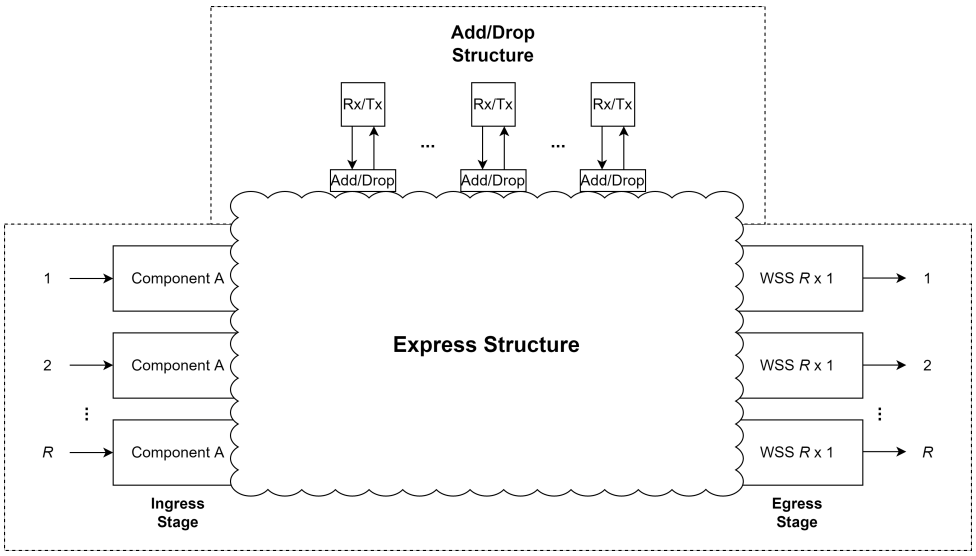

FIGURE 2.3. Generic R-degree ROADM structure.

The express structure routes the incoming wavelengths to other ROADM directions or to the A/D structure. The WSS, represented at the ROADM output stage, is the main responsible for the wavelength selection and routing inside the ROADM nodes and allows dynamic node reconfiguration. A ROADM is built typically with two express architectures: Broadcast and Select (B&S) and Route and Select (R&S).

The B&S architecture, at the ROADM input stage, consists of a splitter (as component A in Figure 2.3) and of a WSS, known as the select WSS, at the ROADM output. At each B&S ROADM node, the wavelengths arriving from one fiber direction are broadcasted by the splitter to all node directions of the ROADM and to the drop structure, and the select WSS receives all the wavelengths broadcasted from all ROADM directions and add structure and switches/blocks them to the corresponding output ROADM direction accordingly with the routing plan.

The R&S architecture consists of two WSSs on the express structure: the WSS at the node input (component A represented in Figure 2.3), which is responsible for the "route" of the incoming wavelengths to the output ports and to the drop structure, and the select WSS at the node output.

The benefits of using the B&S architecture instead of the R&S are the reduced cost and power consumption, due to the use of only one WSS in the architecture [19]. However,

the use of R&S architecture allows for a reduction of the insertion losses, especially in the case of large ROADM degrees, since the B&S architecture would require a large splitting ratio, which leads to high insertion losses [19].

The addition and removal of wavelengths from the optical network, is one of the most important functions of ROADMs [20]. The A/D structure represented in Figure 2.3, which performs these functions, can have different properties, such as Colorless, Directionless and Contentionless.

The Colorless (C) ROADM allows any wavelength to be assigned to any port of the A/D structure. This structure typically consists of a $1\times N$ WSS and a $N\times 1$ coupler, responsible for dropping and adding wavelengths, respectively, where N is the number of wavelengths to be inserted or removed from the ROADM. This number of wavelengths is typically set by the A/D ratio planned for the ROADM node. In this architecture, each direction of the node has a dedicated A/D structure and, hence, adding/dropping a wavelength to/from another degree is not possible. This problem can be solved by using a Colorless and Directionless architecture [21].

In the Colorless and Directionless (CD) ROADM, the directionless feature is added and allows that each wavelength, added or removed at a specific A/D port to be sent/received to/from any ROADM direction. This can be accomplished by adding a $1\times R$ optical coupler in the add structure and another $1\times R$ WSS in the drop structure (R corresponding to the number of node directions), which means that each direction has no longer a dedicated A/D structure, as in the C ROADM case. However, in CD ROADMs, the problem of wavelength contention exists, meaning that incoming signals from different directions with the same wavelength cannot coexist in the same A/D structure. This problem is solved with Colorless, Directionless and Contentionless (CDC) ROADMs.

On the CDC ROADM, the contention problem is surpassed by inserting $R\times N$ WSSs [22] or $R\times N$ Multicast Switches (MCSs) [23] in the A/D structure, as shown in, Figure 2.4, allowing signals with the same wavelength to be added or dropped in the same structure. The MCS A/D structure is composed by an array of optical switches (OSs) and a splitter/coupler (S/C) $1\times N$, denoted as component X in Figure 2.4 [24]. In the $R\times N$ WSS A/D structure, the insertion and removal of wavelengths is done by OSs and $1\times N$ WSSs (which corresponds to component X in Figure 2.4).

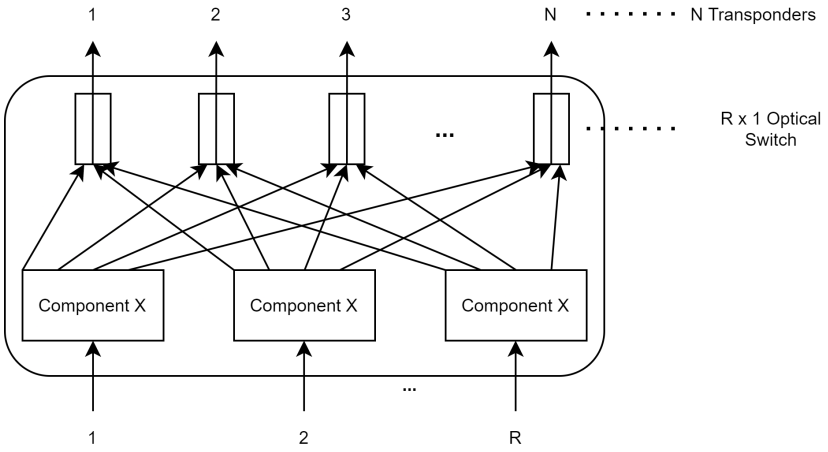

FIGURE 2.4. Generic CDC $R \times N$ drop structure.

2.3.2. Multi-band ROADMs

An optical network is usually divided geographically into several networks with different characteristics and functions: the long-haul, metropolitan, and access networks. The access network distributes/collects traffic provided by the operators and service providers to end-users [25]. The metropolitan network is responsible for handling traffic in the metropolitan area, and aggregates the traffic of several access networks [25]. For MB metropolitan networks, there are already studies proposing nodes architectures, named as Filterless drop and waste and Fixed optical add/drop multiplexer [26, 27]. These node proposals have the advantage of being simpler and cheaper as required by metropolitan networks, in despite of the lower flexibility. Long-haul networks are responsible for handling traffic over long distances, either nationally or globally, hence, requiring larger degree, more complex and flexible ROADMs to handle the much higher traffic volume.

For long-haul networks, several MB ROADM architectures have been proposed in the literature: a node with multiple WSSs dedicated to each fiber band [7, 9], as depicted in Figure 2.5; two ROADM solutions that use all-optical wavelength converters (AO-WCs) [7–9], as shown in Figures 2.6 and 2.7; and a ROADM that uses components that support multiple bands [10, 11], as represented in Figure 2.8.

Figure 2.5 shows a R-degree R&S MB ROADM that supports the C-, L- and S-bands [7, 9], which we consider as our baseline configuration. It consists of a MB multiplexer (MUX) and MB demultiplexer (DEMUX), where the MB-DEMUX separates the three wavelength bands and the MB-MUX is responsible for their aggregation. Following the MB-DEMUX, there is a bank of parallel single-band WSSs, which are connected to output single-band WSSs of the same and other ROADM directions [7]. In addition, the input

WSSs are connected to the drop structure and the output WSSs are connected to the add structure. Hence, the wavelengths can be switched to any direction within each band. However, in this architecture, switching between bands is not possible and the management and maintenance of the ROADM is more difficult due to the large amount of equipment required for each band, compared to the architectures shown in Figures 2.7 and 2.8 [7, 11]. In addition, on the A/D structure, the use of different transponders for each band can be costly [9]. As a main advantage, by using this architecture, the equipment dedicated to other bands may be not be acquired when network traffic is low, especially in the beginning of network operation, i.e., only C-band components are installed, leaving the acquisition of the components for the other bands for the future when network traffic increases [11].

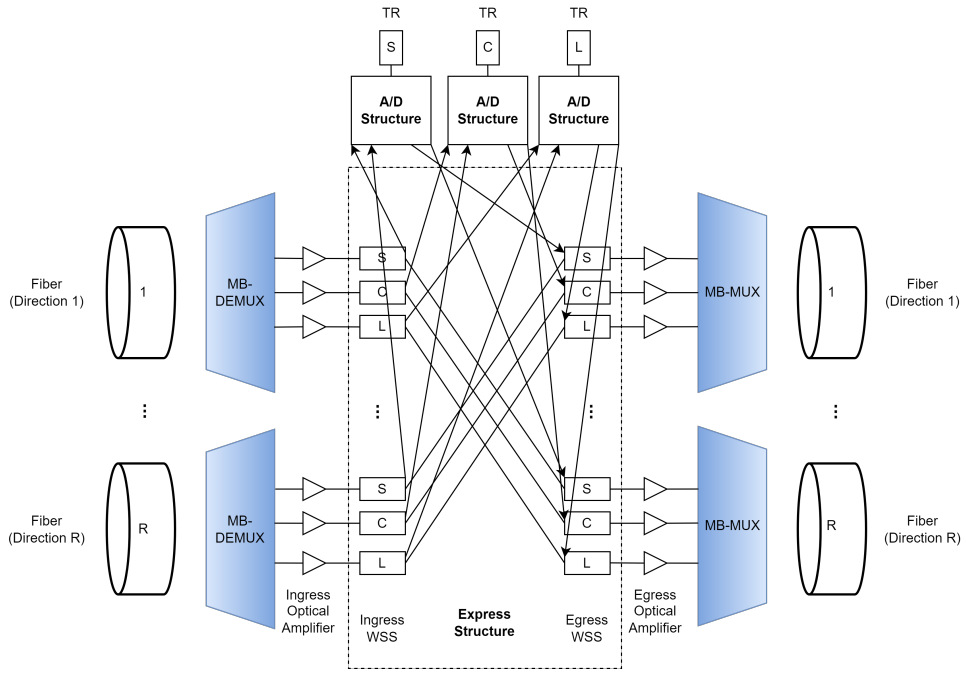

FIGURE 2.5. Baseline R-degree R&S MB ROADM architecture.

To add the possibility of switching wavelengths between bands, the two architectures presented in Figures 2.6 and 2.7 were proposed in [7–9]. Figure 2.6 shows a R-degree R&S MB ROADM that supports the C-, L- and S-bands (not all bands are represented, due to the complexity of the links), with inter-band AO-WCs after the ingress WSSs, which have the function of converting multiple wavelengths to and from all bands. This architecture has the advantage of allowing wavelength switching between all bands [7, 8] and as in the previous architecture, unused components can be spared, when the network traffic is low [11]. In addition, as in the node of Figure 2.5, this architecture requires, in the

A/D structure, dedicated components for each band, as well as dedicated transponders [9]. Also, the number of required AO-WCs per direction becomes very high, especially when all five fiber bands are used, increasing the amount of equipment and complexity of the node.

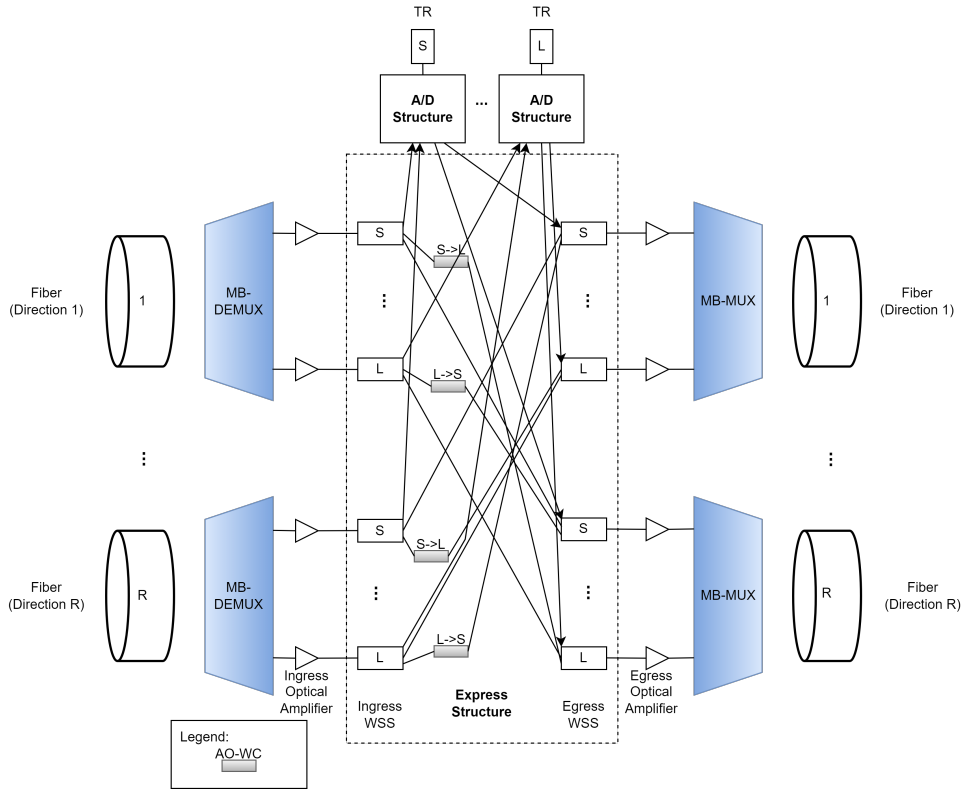

FIGURE 2.6. *R*-Degree R&S MB ROADM architecture with AO-WCs.

To overcome these issues, as depicted in Figure 2.7 a *R*-degree R&S MB ROADM has been proposed that supports the C-, L- and S-bands, with inter-band AO-WCs before and after the C-band WSSs, which have the function of converting multiple wavelengths to and from C-band [7–10]. In this ROADM, the input optical signal passes through the MB-DEMUX at the node input and is split into the several bands. Then, the wavelengths in each band are converted to the C-band by the inter-band AO-WCs, and directed to each ingress C-band WSS, where they are forwarded to all egress C-band WSSs and to drop structure, where are removed from the node. The client signals are added by the add structure and routed by the output WSSs. After that they are converted to the original band by the output inter-band AO-WC, and these wavelengths are combined by the MB-MUX at the output of the ROADM and launched into the fiber. The use of the architecture presented in Figure 2.7 brings several advantages. The wavelengths can be switched to any band and direction; only C-band WSSs and transponders are used,

which are a mature and commercial equipment, instead of using components working on the other bands [9]; the architecture is simpler than the one shown in Figure 2.7 due to the reduced number of AO-WCs; and furthermore, in this architecture, the other bands equipment can be acquired in a phased-way, accordingly with the traffic volume evolution of the network. The main disadvantage of this architecture is the use of AO-WCs, which is a technology that is, currently, not in a commercial phase [9].

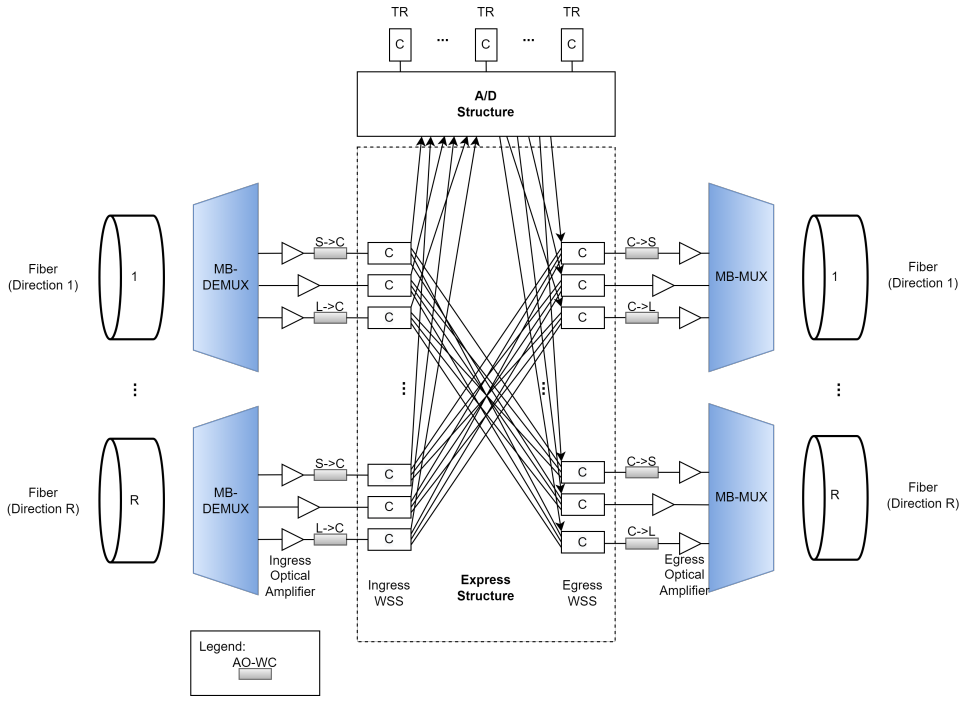

FIGURE 2.7. *R*-degree R&S MB ROADM architecture using a common-band with AO-WCs.

As an alternative for the architectures proposed previously, in Figure 2.8, it is represented a generic *R*-degree R&S MB ROADM suitable for switching wavelengths between all fiber bands [10, 11], which is based on MB WSSs. This architecture is very similar to a R&S C-band node, depicted in subsection 2.3.1. In the node represented in Figure 2.8, the incoming wavelengths arrive at the ingress MB WSSs, which forward these wavelengths to the egress MB WSSs. The egress MB WSSs will select the incoming wavelengths to the corresponding direction.

The architecture shown in Figure 2.8 allows simplifying the maintenance and management of the network, due to the reduction of the number of components, in comparison to previous architectures represented in Figures 2.5-2.7 [11]. Nevertheless, in this node, the use of transponders for each band in the A/D structure is required. In addition, the use of the architecture presented in Figure 2.8, requires the acquisition of MB components at the

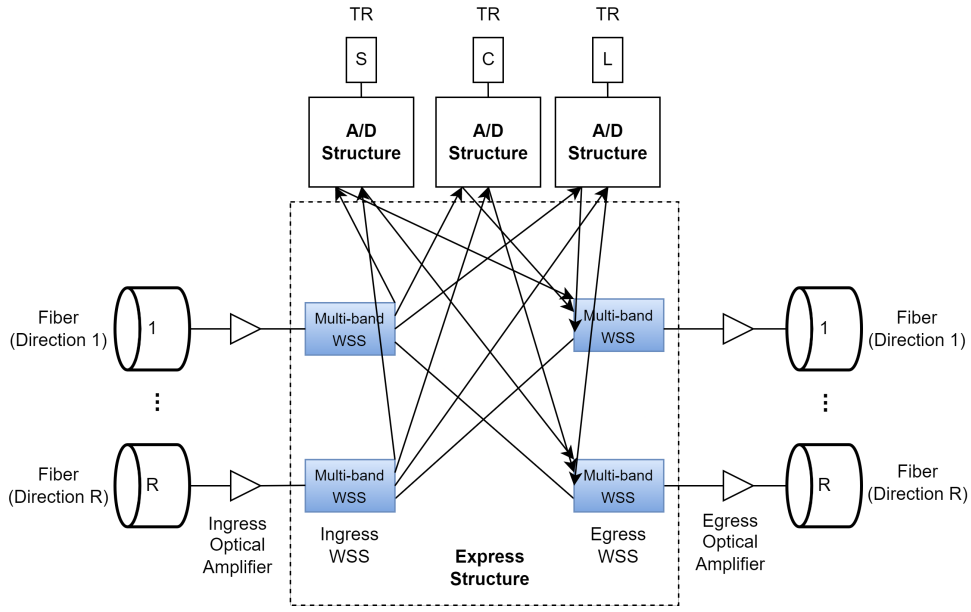

FIGURE 2.8. Compact R-degree MB ROADM architecture.

beginning of the network operation, i.e., leading to a high initial investment. Currently, there are MB WSSs that can operate in C- and L-bands [28]. In [28, 29], two WSSs were proposed and can operate in C- and L-bands, with sizes 1×2 and 1×10, that could be used in the architecture shown in Figure 2.8.

In the case of the A/D structures of the MB ROADMs previously presented in Figures 2.5, 2.6 and 2.8, there is the need to use components dedicated to each band, whereas in the A/D structure of the MB ROADM of Figure 2.7, only C-band components are used, which have the advantage of being a nowadays commercial equipment.

2.4. Multi-band ROADM cost analysis

In this section, the cost analysis of the MB ROADMs architectures presented in section 2.3 will be performed. Firstly, in subsection 2.4.1, the ROADMs cost will be calculated only for the C-band, for the B&S and R&S architectures, considering CD and CDC A/D structures based on both MCSs and WSSs. To compute the cost of the C-band and MB ROADM components, a channel spacing of 50 GHz, and an A/D ratio of 25% and 50%, are considered. Then, in subsection 2.4.2, the cost of the MB architectures presented in subsection 2.3.2 will be performed, first with the C- and L-bands only, and then with the addition of the S-band. Finally, in subsection 2.4.3, a cost comparison study between the MB node solutions presented previously in subsection 2.4.2 and a SDM node solution is performed. In addition, besides the total node cost, is also consider the fiber lease cost. The cost components are extracted from [9, 30–32] and are calculated in relation to the

cost of a C-band EDFA, which has a unitary cost. The cost analysis is performed based on the relative cost of components for C-, L- and S-bands presented in Table 2.2.

TABLE 2.2. Relative cost of components for C-, L- and S-bands.

Component	Cost		
	C-band	**L-band**	**S-band**
EDFA	1	1.2	-
TDFA	-	-	α
EDFA (C+L bands)	2.20667		-
OA (C+L+S bands)	2.2167+α		
1×N_{bands} MB-MUX/DEMUX	0.04		
1×2 S/C	0.00667		
1×N S/C, with $N\geq$4	0.0167×(N/4)		
WSS 1×2	1.25	1.5	1.25α
WSS 1×4	2.5	3	2.5α
WSS 1×9	5	6	5α
WSS 1×20	7.5	9	7.5α
WSS 1×40	15	18	15α
WSS 1×80	30	36	30α
WSS 1×160	60	72	60α
WSS 9×18	20	24	20α
MCS 9×16	20		
TR	36	43.2	36α
AO-WC	36β		
MB WSS 1×2	1.75α		
MB WSS 1×4	3.5α		
MB WSS 1×9	7α		
MB WSS 1×20	10α		
MB WSS 1×40	20α		
MB WSS 1×80	40α		
MB WSS 1×160	80α		

In Table 2.2, it is considered that the L-band components are 20% more expensive than C-band components, and that the cost of the S-band components depends on a multiplicative factor α, which ranges from 1.2 to 1.5 [9, 32]. The C+L EDFA cost is calculated based on the components presented in Figure 2.2, i.e., the cost of 1×2 S/C is added to the cost of the C- and L-band EDFAs. The C+L+S OA cost is determined similarly, but in this case, a 1×4 S/C is used. The S/Cs cost is the same for the three bands because of their broad passband, which covers much more than the three bands considered, from 1260-1650 nm. The AO-WC cost depends on the C-band transponder (TR) cost, with the parameter β ranging from 0.5 to 2. Since in [9], the 1×2 and 1×4 C-band WSSs costs are not given, it is assumed that the cost of the 1×2 WSS is half the 1×4 WSS cost, which, in turn, is half the cost of the 1×9 C-band WSS, which is the smallest size WSS considered in [9]. The cost of 1×40 C-band WSS is twice the 1×20 C-band WSS

cost, and the same reasoning is followed for larger WSSs. The cost of MB WSSs depends on parameter α, since this component works in the S-band simultaneously with the C- and L-bands. The cost of 1×9 and 1×20 MB WSS is assumed to be higher than the WSSs cost operating in the C-, L- and S-bands separately. Hence, the cost of the MB WSSs is approximately 2, 1.7 and 1.3 times more expensive compared, respectively, with the same size dedicated C-, L- and S-band WSSs, for α=1.5. Then, the same reasoning than the one used to obtain the cost of dedicated band WSSs with different sizes is followed to obtain the cost of smaller and larger MB WSSs. The cost of the 9×16 C-band MCSs are assumed to be equal to the cost of the 9×18 C-band WSS, as in [30]. The MCSs are assumed to have the same cost independently of the fiber band, in contrast to the WSSs, where the cost depends on the considered band.

2.4.1. C-band ROADMs

The cost of a C-band CD and CDC ROADM will be analysed next. Figure 2.9 shows a generic R-degree C-band ROADM, where M' is the number of transponders in one A/D card, Y defines the size of the components used in the express structure, and $N_{A/D}$ corresponds to the number of A/D cards. Component B shown in the A/D structure of Figure 2.9, consists of a R×1 WSS followed by a 1×M' WSS (in the drop direction) for the CD A/D structure [30], whereas in the case of a CDC A/D structure, component B is a R×M' MCS or R×M' WSS [30]. Component A refers to the input component of the express structure that could be a 1×Y S/C in the case of a B&S architecture or a 1×Y WSS in the case of a R&S architecture.

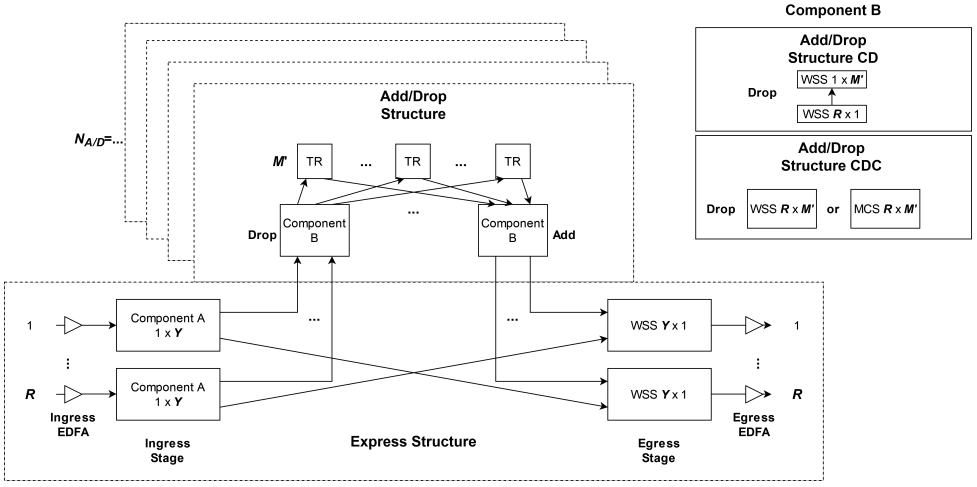

FIGURE 2.9. Generic R-degree C-band ROADM.

The total number of TRs in the A/D structure, M, is given by,

$$M = A/D_{ratio} N_{ch} R \tag{2.1}$$

where A/D_{ratio} defines the ROADM A/D ratio, which, in this work, is considered as 25% or 50%, N_{ch} corresponds to the number of WDM channels arriving to the ROADM node in one direction, which is assumed to be 87 (the calculation of this value is explained in the next subsection), for the C-band, and R is the ROADM degree assuming the values 2, 4, 8 or 16.

The size of the components in the express structure, Y, is given by,

$$Y = R - 1 + N_{A/D} \tag{2.2}$$

The number of A/D cards in the ROADM node is given by,

$$N_{A/D} = \left\lceil \frac{M}{M'} \right\rceil \tag{2.3}$$

Figure 2.10 shows an example of a MCS-based CDC A/D structure with 6 cards, considering R=4 and A/D_{ratio}=25%. In Figure 2.10, the A/D structure is able to connect a maximum of 96 transponders, slightly higher than the number of required TRs, M, obtained with (2.2). These spare connections can be used as a backup in case of malfunction or to upgrade the number of TRs, in case of the network traffic demands a higher A/D ratio. Notice also that the input size of the MCS (drop direction) is higher than the minimum required (R=4), due to the availability of the components that is considered in Table 2.2.

The total cost of the ROADM express structure with R directions is given by

$$Cost_{express} = RCost_{A,1\times Y} + RCost_{WSS,Y\times 1} + 2RCost_{OA} \tag{2.4}$$

where $Cost_{A,1\times Y}$ corresponds to the cost of component A, which is dependent on the type of express structure, $Cost_{WSS,Y\times 1}$ corresponds to cost of the select WSS, and $Cost_{OA}$ represents the cost of the OA (C-band EDFA).
The cost of the CD A/D structure is given by

$$Cost_{A/D,CD,b} = 2N_{A/D}Cost_{WSS,R\times 1} + 2N_{A/D}Cost_{WSS,1\times M'} + MCost_{TR} \tag{2.5}$$

where $Cost_{TR}$ represents the cost of a single transponder. The variable b has been added to (2.5) to identify the bands dependence, with b=C, L or S, since equation (2.5) can be

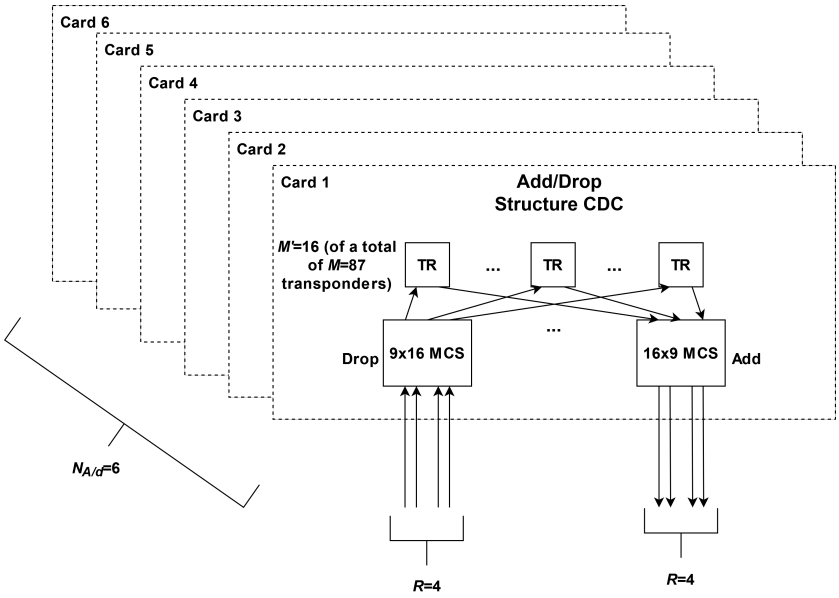

FIGURE 2.10. Example of MCS-based CDC A/D structure with 6 cards, considering R=4 and A/D_{ratio}=25%.

applied to calculate the cost of the CD A/D structure for any of the bands, although only the C-band is being studied in this section.

The cost of CDC A/D structure, either MCS- or WSS-based is given by,

$$Cost_{A/D,CDC,b} = 2N_{A/D}Cost_B + MCost_{TR} \tag{2.6}$$

where $Cost_B$ represents the cost of component B.

Table 2.3 shows the total cost of the ROADM for R=2, 4, 8 and 16, with an A/D ratio of 25% and 50%, considering the CD structure and the CDC structure, for the MCS and WSS scenarios. There are other authors who have performed similar analyses and calculations [33–36]. In this situation, it is not easy to compare the results obtained in Table 2.3 with the results obtained by other authors since different relative cost values and different normalizations were considered. In appendix A, the list and number of components required to build the corresponding C-band ROADMs are presented.

TABLE 2.3. Total cost of C-band ROADMs with an A/D ratio of 25% and 50%.

Add/Drop	Express	A/D ratio of 25%				A/D ratio of 50%			
		R=2	**R=4**	**R=8**	**R=16**	**R=2**	**R=4**	**R=8**	**R=16**
CD	**B&S**	1646	3260	6541	13207	3234	6482	12965	26142
	R&S	1651	3280	6600	13445	3244	6512	13024	26378
CDC MCS	**B&S**	1713	3400	6781	13682	3386	6742	13545	27092
	R&S	1718	3420	6840	13920	3396	6772	13664	27328
CDC WSS	**B&S**	1713	3360	6741	13602	3346	6702	13465	26932
	R&S	1718	3380	6800	13840	3356	6732	13584	27168

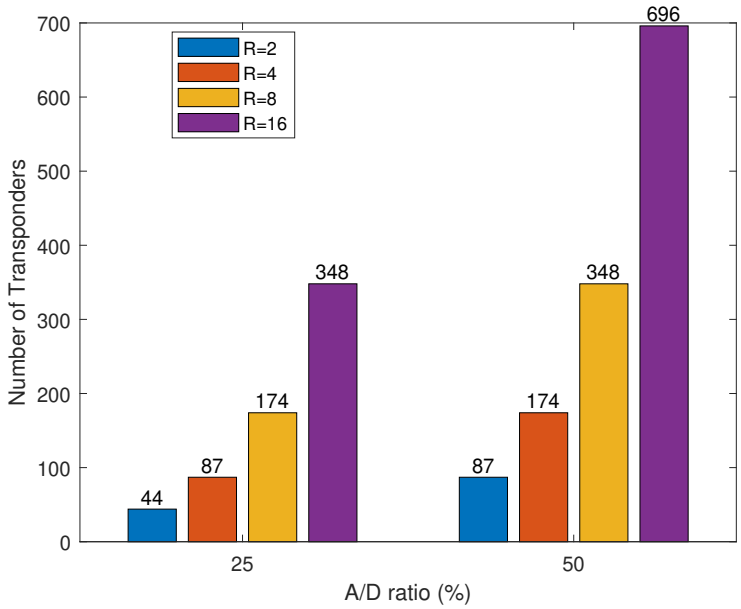

FIGURE 2.11. Number of transponders for an A/D ratio of 25% and 50% considering R=2, 4, 8 and 16.

From Table 2.3, it can be noticed that the CD ROADM has a lower cost than the CDC ROADM, because the A/D structure is more cheaper. The cost of CDC components is about between 2.2 and 4.35 times more expensive than CD components, excluding the TRs. The cost of the CDC ROADM with WSSs-based A/D structure is slightly lower compared to the MCSs-based structure, since each MCS has 16 outputs, in relation to the 18 outputs of each WSS, resulting in a higher number of A/D cards. Only for R=2 and an A/D_{ratio}=25%, the number of cards is the same for both MCS and WSS A/D structures, and the cost is the same in both CDC structures. In addition, the B&S node cost is lower than the R&S architecture due to the lower cost of S/Cs compared to the WSSs cost, although the cost difference is very small, being the R&S less than 1.8% more expensive than the B&S architecture, for both A/D ratios. This occurs because the TRs are the major contribution to the total ROADMs cost. For example, for a B&S node with a CD A/D structure, R=16 and for an A/D ratio of 25%, the total cost of the TRs represents approximately 95% of the total node cost, as noted also in other articles [33–36].

Figure 2.11 represents the number of transponders as a function of the A/D ratio considering R=2, 4, 8 and 16, for the C-band architecture represented in Figure 2.9. As can be seen in Figure 2.11 for a high number of directions and a higher A/D ratio, more TRs are required and, so, the ROADM total cost becomes proportionally higher. Hence, as seen in Table 2.3 and Figure 2.11, when the number of directions is doubled, the number

of TRs is doubled, and the node cost becomes around twice higher. The same happens when we increase the A/D ratio from 25% to 50%.

2.4.2. Multi-band ROADMs

Before analyzing the cost of MB ROADMs, the number of channels used in C-, L- and S-bands, is first computed. Figure 2.12 represents the spectrum occupied by C-, L- and S-bands as well as the number of channels used in each band and its respective bandgaps (the first bandgap is between the C- and L-bands, corresponding to 550 GHz, and the second bandgap between the C- and S-bands, of 1250 GHz), for a channel spacing of 50 GHz [37]. The center frequencies of the WDM channels are chosen accordingly with the ITU-T grid [38]. The number of channels considered in the C-, L- and S-bands are, respectively, 87, 130 and 148 channels and the channel frequencies at the center of the C-, L- and S-bands, are respectively 193.75 THz, 187.7 THz and 200.9 THz, obtained from

$$\nu_m = \nu_{ch} + (m - N_{ch})\Delta\nu_{ch} \tag{2.7}$$

where m refers to the channel number which varies between 1 and the number of channels in each band, N_{ch}, the number of channels associated to the required band, $\Delta\nu_{ch}$, corresponds to the channel spacing, and ν_{ch} corresponds to the frequency of the last channel for the desired band, with ν_{130}=190.95 THz, for the L-band, ν_{87}=195.9 THz, for the C-band and ν_{148}=204.6 THz, for the S-band.

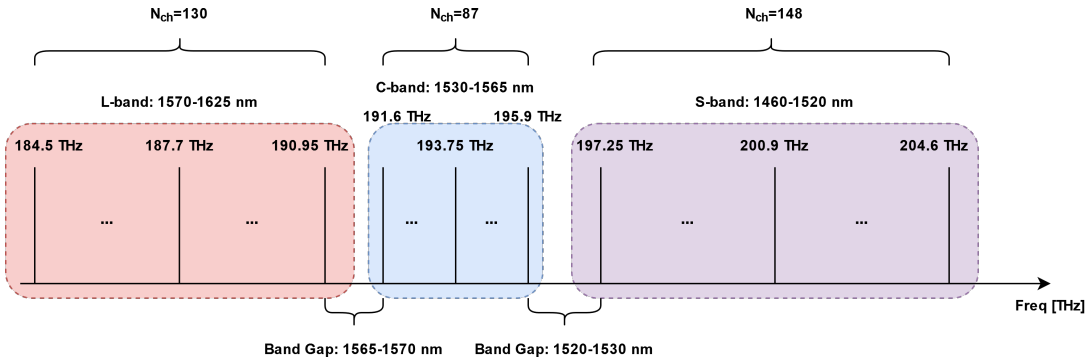

FIGURE 2.12. Spectrum of the C-, L- and S-bands and corresponding ITU-T grid frequencies for a channel spacing of 50 GHz.

Figures 2.13-2.16 show the four MB ROADM architectures considered in this work whose cost is going to be calculated next. Figure 2.13 represents the baseline MB-ROADM architecture, Figure 2.14 represents the MB ROADM architecture with AO-WCs, Figure 2.15 represents the MB ROADM architecture with AO-WC and using the C-band as

a common-band for switching, and finally Figure 2.16 shows a compact MB ROADM architecture, where all components of the express structure are MB devices, i.e., work simultaneously in the C-, L- and S-bands. The MB ROADMs depicted in Figures 2.13, 2.14, and 2.16 have a dedicated A/D structure for each band. The common-band architecture depicted in Figure 2.15 has a unique A/D structure in the C-band. These A/D structures can be CD or CDC, as represented in Figure 2.9 for only one band.

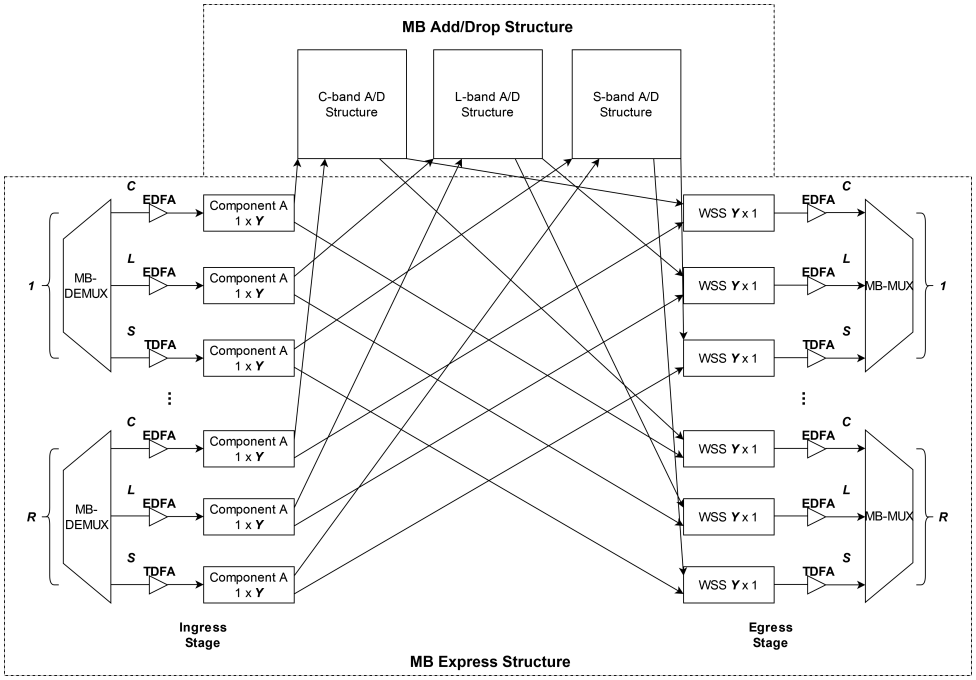

FIGURE 2.13. Baseline R-degree MB ROADM architecture.

Using (2.1), the number of wavelengths to be added/dropped by a MB ROADM node is obtained (note that this number also corresponds to the total number of TRs of the A/D structure, M). The dimension of the components in the express structure depends on the number of directions R and on the number of A/D cards $N_{A/D}$, so Y can be calculated for the architectures of Figures 2.13 and 2.16 with (2.2). For the MB ROADM architectures shown in Figures 2.14 and 2.15, the size of the components presented in the express structure is given by,

$$Y = N_{A/D} + N_{bands}(R-1) \tag{2.8}$$

where N_{bands} corresponds to the number of bands considered in the ROADM. When N_{bands}=1, (2.2) is obtained.

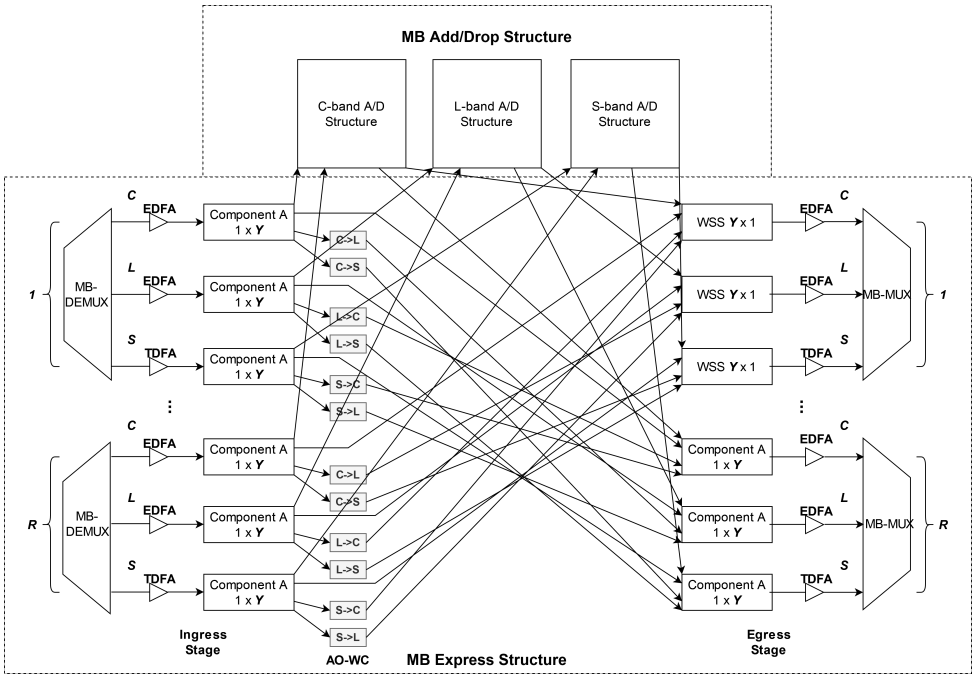

FIGURE 2.14. *R*-degree MB ROADM architecture with AO-WCs.

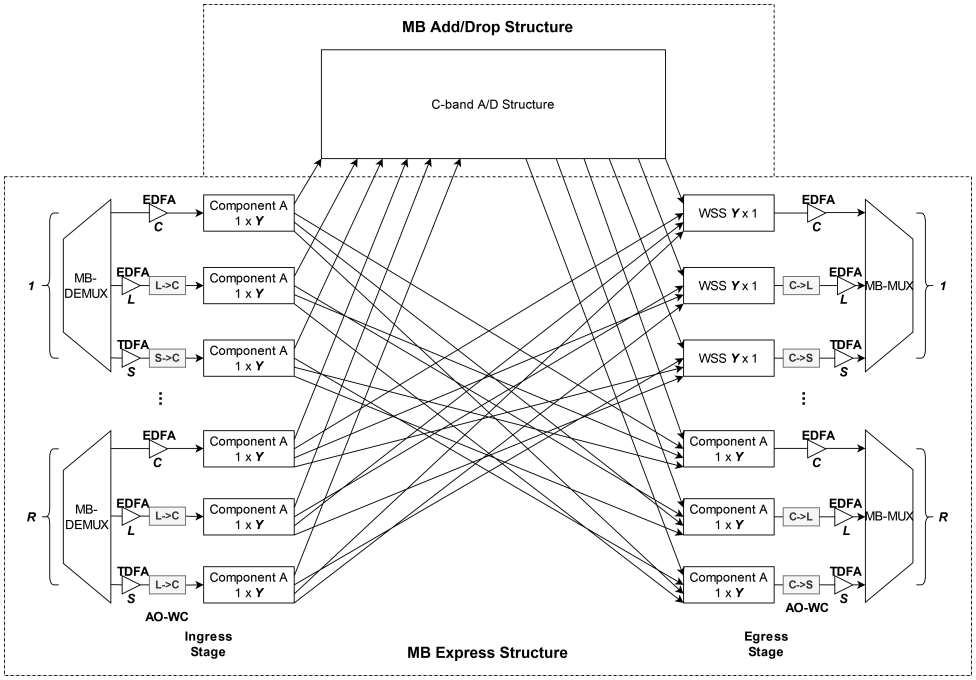

FIGURE 2.15. *R*-degree MB ROADM architecture using a common-band with AO-WCs.

The total cost of the express structure for the baseline architecture shown in Figure 2.13 is

$$Cost_{Baseline,Express} = \sum_{b}^{N_{bands}} (Cost_{Express,b}) + 2RCost_{MB,MUX/DEMUX} \tag{2.9}$$

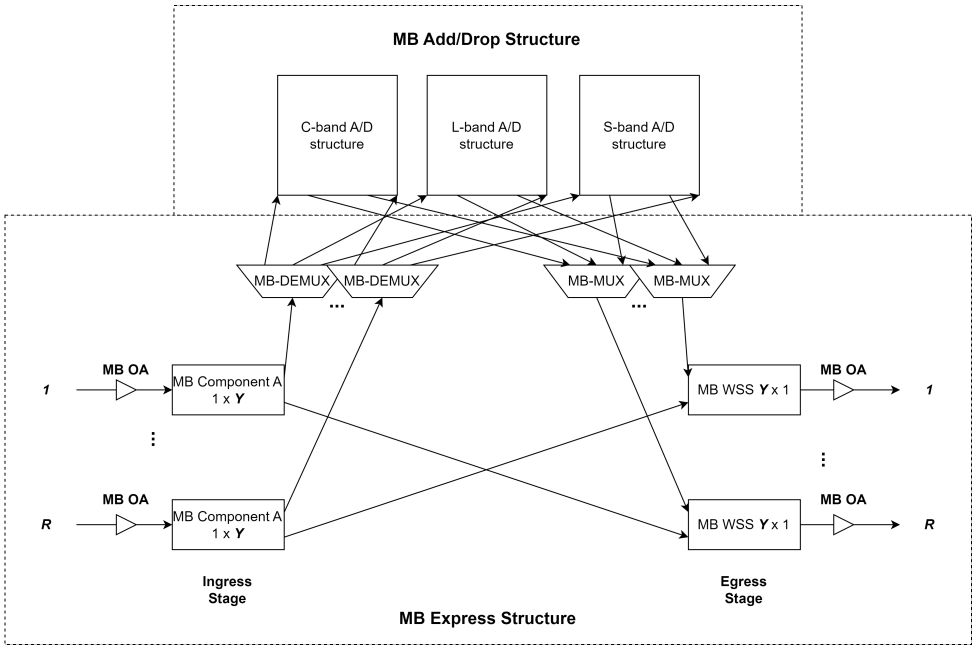

FIGURE 2.16. Compact R-degree MB ROADM architecture.

where $Cost_{express,b}$, corresponds to cost of the express structure in each band, with b=C, L and S, which is given by

$$Cost_{Express,b} = R(Cost_{A,b,1\times Y} + Cost_{WSS,b,Y\times 1} + 2Cost_{OA,b}) \tag{2.10}$$

The total cost of the express structure for the architecture with AO-WCs shown in Figure 2.14 and the common-band architecture with AO-WCs shown in Figure 2.15 is given by,

$$Cost_{AO,Express} = \sum_{b}^{N_{bands}} (Cost_{Express,b}) + N_{AO-WC}Cost_{AO-WC} + 2RCost_{MB,MUX/DEMUX} \tag{2.11}$$

where $Cost_{express,b}$ for the architecture with AO-WCs (Figure 2.14) is given by (2.10), using b=C, L and S, while for the common-band architecture (Figure 2.15), $Cost_{express,b}$ should be computed with b=C, L and S using

$$Cost_{Express,b} = R(Cost_{A,C,1\times Y} + Cost_{WSS,C,Y\times 1} + 2Cost_{OA,b}) \tag{2.12}$$

In (2.11), $Cost_{AO-WC}$ corresponds to the cost of the AO-WC and N_{AO-WC} corresponds to the number of AO-WCs , which is given for Figures 2.14 and 2.15, respectively, by

$$N_{AO-WC} = RN_{bands}(N_{bands} - 1)(R - 1) \tag{2.13}$$

$$N_{AO-WC} = 2R(N_{bands} - 1) \tag{2.14}$$

The total cost of the express structure for the MB compact architecture shown in Figure 2.16 is given by,

$$\begin{aligned} Cost_{Compact,Express} = R(&Cost_{MB,A,1\times Y} + Cost_{MB,WSS,Y\times 1} + 2Cost_{MB,OA,z}) \\ &+2RN_{A/D}Cost_{MB,MUX/DEMUX} \end{aligned} \tag{2.15}$$

where $Cost_{MB,OA,z}$, with z=C+L or C+L+S.

To calculate the total cost of each A/D structure for each band, (2.5) and (2.6), with b=C, L or S, are used. The number of A/D cards is calculated using (2.3). For the architectures of Figures 2.13, 2.14 and 2.16, the number of TRs and the number of A/D cards is computed for each band, by calculating M from (2.1). For example, in a node with 2 directions operating simultaneously in the C-, L- and S-bands, with an A/D ratio of 25%, the value of M is calculated for each band, 44 (C-band), 65 (L-band), 74 (S-band). The number of A/D cards is calculated through (2.3) for each band from the value of M obtained for each band. For the case of common-band architecture (Figure 2.15), the total number of C-band transponders is obtained by summing the number of TRs required in each band. For example, in the case of a node with 2 directions operating in the C-, L- and S-bands, with an A/D ratio of 25%, the value of M is calculated for each band, 44 (C-band), 65 (L-band), 74 (S-band), and a total of 183 TRs is obtained. From this value, the number of A/D cards is calculated through (2.3).

Tables 2.4-2.7 show the total cost of each one of the four MB ROADMs just presented, considering CD and CDC A/D structures based on MCSs or WSSs, B&S or R&S express structures, for an A/D ratio of 25% and 50%, α=1.5 and β=2, which corresponds to a less favourable cost scenario [9]. The costs are obtained for a different number of ROADM directions (R=2, 4, 8 and 16) and considering the C+L and C+L+S MB solutions.

From the results presented in Tables 2.4-2.7, a cost analysis is performed for each MB architecture considering the influence of CD and CDC A/D structures, B&S and R&S architectures, the ROADM degree, the A/D ratio and the number of bands.

The total cost of the baseline and compact architectures represented in Figures 2.4 and 2.7 is strongly impacted by the TRs cost. For both MB architectures, approximately 95%

TABLE 2.4. Total cost of the baseline MB ROADM architecture with an A/D ratio of 25% and 50%, R=2, 4, 8 and 16, considering the MB C+L and the C+L+S scenarios.

Add/Drop	Bands	Express	A/D ratio of 25%				A/D ratio of 50%			
			R=2	**R=4**	**R=8**	**R=16**	**R=2**	**R=4**	**R=8**	**R=16**
CD	C+L	**B&S**	4557	9092	18202	36705	9016	18074	36147	73096
		R&S	4573	9147	18333	37228	9037	18139	36277	73903
	C+L+S	**B&S**	8680	17382	34871	70097	17240	34566	69221	139830
		R&S	8710	17481	35181	70977	17275	34765	69529	141352
CDC	C+L MCS	**B&S**	4740	9424	18858	37838	9387	18703	37497	75282
		R&S	4756	9479	19061	38361	9414	18767	37757	76089
	C+L WSS	**B&S**	4732	9408	18860	37838	9365	18703	37489	75266
		R&S	4748	9463	19061	38361	9386	18767	37749	76073
	C+L+S MCS	**B&S**	8958	17874	35808	71739	17808	35550	71332	142951
		R&S	8988	17973	36189	72617	17857	35703	71949	144473
	C+L+S WSS	**B&S**	9050	17998	36070	72257	17926	35765	71644	143935
		R&S	9080	18907	36449	73137	17969	35873	72081	145457

TABLE 2.5. Total cost of the MB ROADM architecture with AO-WCs, with an A/D ratio of 25% and 50%, R=2, 4, 8 and 16, considering the MB C+L and the C+L+S scenarios.

Add/Drop	Bands	Express	A/D ratio of 25%				A/D ratio of 50%			
			R=2	**R=4**	**R=8**	**R=16**	**R=2**	**R=4**	**R=8**	**R=16**
CD	C+L	**B&S**	4850	10830	26340	71557	9304	19803	44344	107896
		R&S	4871	10895	26487	72364	9325	19867	44551	108943
	C+L+S	**B&S**	9549	22576	59198	174815	18117	39833	93548	243902
		R&S	9584	22685	59637	175729	18166	40021	93985	244808
CDC	C+L MCS	**B&S**	5033	11162	26984	72930	9675	20467	45706	110082
		R&S	5054	11227	27245	73977	9702	20567	46109	111129
	C+L WSS	**B&S**	5025	11146	26984	72690	9659	20467	45698	110066
		R&S	5046	11211	27245	73497	9686	20567	46101	111113
	C+L+S MCS	**B&S**	9827	23069	60061	176310	18672	40770	95789	247603
		R&S	9862	23177	60860	178073	18721	40959	96669	250073
	C+L+S WSS	**B&S**	9919	23193	60321	176831	18796	41030	96281	247867
		R&S	9954	23301	60760	178593	18845	41219	97161	249617

TABLE 2.6. Total cost of the MB ROADM architecture using a common-band, with an A/D ratio of 25% and 50%, R=2, 4, 8 and 16, considering the MB C+L and the C+L+S scenarios.

Add/Drop	Bands	Express	A/D ratio of 25%				A/D ratio of 50%			
			R=2	**R=4**	**R=8**	**R=16**	**R=2**	**R=4**	**R=8**	**R=16**
CD	C+L	**B&S**	4362	8743	17550	35583	8361	16891	33671	67821
		R&S	4382	8802	17788	36535	8390	17009	33907	68773
	C+L+S	**B&S**	7476	15075	30151	61022	14298	28936	57871	117182
		R&S	7520	15253	30505	62449	14387	29293	58585	120049
CDC	C+L MCS	**B&S**	4523	9028	18175	36833	8701	17461	35161	70321
		R&S	4542	9087	18413	37785	8730	17579	35637	71273
	C+L WSS	**B&S**	4523	8988	18095	36673	8661	17340	34681	69841
		R&S	4542	9047	18333	37625	8690	17459	34917	70793
	C+L+S MCS	**B&S**	7706	15465	30931	62582	14743	29485	59371	118754
		R&S	7750	15643	31285	64009	14832	29663	60085	120169
	C+L+S WSS	**B&S**	7666	15295	30691	62102	14663	29325	59011	118034
		R&S	7710	15383	31045	63529	14752	29503	59725	119449

of the total node cost corresponds to TRs cost. In the case of the AO-WC and common-band architectures, the total node cost also depends significantly on the TRs cost, but

TABLE 2.7. Total cost of the MB ROADM compact architecture, with an A/D ratio of 25% and 50%, R=2, 4, 8 and 16, considering the MB C+L and the C+L+S scenarios.

Add/Drop	Bands	Express	A/D ratio of 25%				A/D ratio of 50%			
			R=2	**R=4**	**R=8**	**R=16**	**R=2**	**R=4**	**R=8**	**R=16**
CD	C+L	**B&S**	4560	9097	18162	36669	9015	18071	36084	73267
		R&S	4581	9157	18282	37147	9036	18131	36203	74223
	C+L+S	**B&S**	8667	17341	34651	69702	17223	34518	69097	139282
		R&S	8688	17401	34771	70179	17244	34577	69336	140237
CDC	C+L MCS	**B&S**	4743	9429	18904	37807	9389	18701	37492	75462
		R&S	4764	9489	19143	38285	9419	18760	37730	76418
	C+L WSS	**B&S**	4735	9395	18903	37805	9364	18682	37481	75441
		R&S	4756	9473	19142	38283	9385	18759	37719	76397
	C+L+S MCS	**B&S**	8945	17834	35674	71349	17787	35518	71206	142412
		R&S	8966	17894	35913	71824	17817	35637	71684	143367
	C+L+S WSS	**B&S**	9037	17957	35932	71864	17911	35717	71456	143391
		R&S	9058	18017	36171	72341	17941	35776	71694	144346

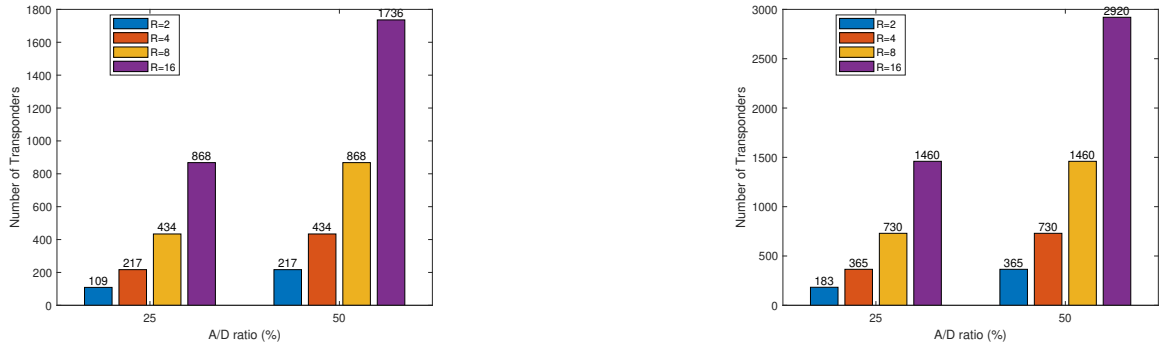

(a) C+L band node.

(b) C+L+S node.

FIGURE 2.17. Number of TRs for C+L and C+L+S nodes for the four MB architectures considered.

also on AO-WCs total cost, as discussed next. Figure 2.17 represents the number of transponders as a function of the A/D ratio considering R=2, 4, 8 and 16, for the four MB architectures represented in Figures 2.13-2.16. As can be observed the number of transponders roughly doubles with the number of directions and the A/D ratio, and also increases with the addition of the S-band. Figure 2.18 shows the number of AO-WCs considering R=2, 4, 8 and 16, for an A/D ratio of 25% and 50%, for the AO-WCs and common-band architectures, as shown in Figures 2.14 and 2.15, respectively. As can be seen for the common-band architecture, the number of AO-WC doubles with the number of directions and with the addition of the S-band. In the case of the AO-WC architecture, the number of AO-WC has a higher impact on the cost for larger node dimensions, since more directions are added to the node, and therefore more AO-WCs are needed to perform the wavelength switching between bands for all directions, see (2.13).

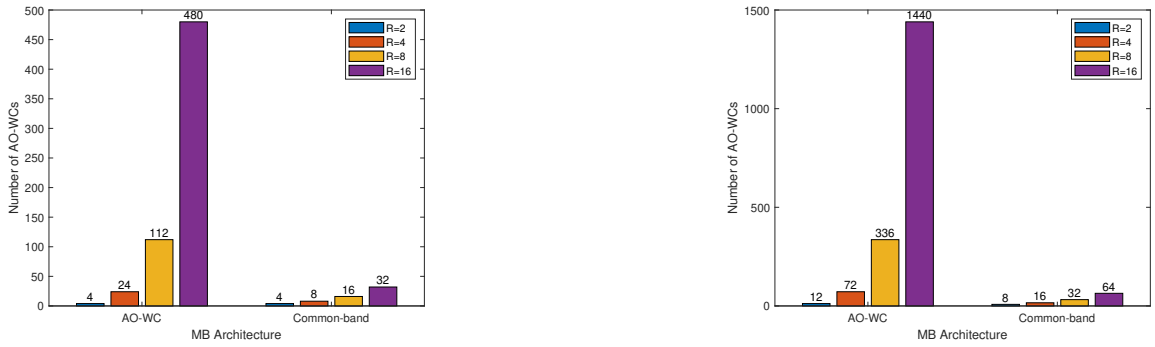

(a) C+L node.

(b) C+L+S node.

FIGURE 2.18. Number of AO-WCs for a C+L and C+L+S nodes for AO-WC and common-band architectures.

Tables 2.8 and 2.9 show the percentage of TRs and AO-WCs cost relative to the total node cost, for the AO-WC architecture, in the case of a C+L and C+L+S nodes and for the A/D ratios of 25% and 50%, respectively. As can be observed in Tables 2.8 and 2.9 in the AO-WC architecture, the cost percentage of TRs ranges approximately between 38% and 89%, for an A/D ratio of 25%, and for an A/D ratio of 50% varies between 55% and 93%. In the case of AO-WCs, the cost percentage varies approximately between 6% and 59%, for an A/D ratio of 25%, and for an A/D ratio of 50%, the range is between 3% and 42%. The cost percentage of the AO-WCs is higher when the A/D ratio is 25% in comparison with an A/D ratio of 50%, since the number of AO-WCs does not increase with the A/D ratio, as also happens in the common-band architecture. From Tables 2.8 and 2.9, it can be concluded that the total cost percentage of TRs plus AO-WCs cost is approximately 96%, and increasing the number of directions increases the number of AO-WCs as well as the total node cost.

TABLE 2.8. Cost percentages of TRs and AO-WCs for AO-WC architecture, with an A/D ratio of 25%.

Bands	AO-WCs				TRs			
	R=2	**R=4**	**R=8**	**R=16**	**R=2**	**R=4**	**R=8**	**R=16**
C+L	6%	16%	31%	48%	89%	79%	65%	48%
C+L+S	9%	23%	41%	59%	86%	73%	56%	38%

TABLE 2.9. Cost percentages of TRs and AO-WCs for AO-WC architecture, with an A/D ratio of 50%.

Bands	AO-WCs				TRs			
	R=2	**R=4**	**R=8**	**R=16**	**R=2**	**R=4**	**R=8**	**R=16**
C+L	3%	9%	18%	32%	93%	87%	78%	64%
C+L+S	4%	13%	26%	42%	91%	83%	70%	55%

In the common-band architecture, the total node cost is also influenced by the TRs and the AO-WCs cost, however, the AO-WCs have a lower impact on the total cost, since their number is smaller, as can be seen in Figure 2.18. The contribution of the TRs cost to the total node cost corresponds approximately to 86% and 91% of the total cost, for an A/D ratio of 25% and 50%, respectively. The cost percentage of AO-WCs is approximately 8% and 4%, for the A/D ratios of 25% and 50%.

When the number of directions is increased by a factor of 2, the number of TRs doubles, for both A/D ratios. In the case of increasing the A/D ratio from 25% to 50%, while maintaining the number of directions, the number of TRs also doubles. In the baseline, common-band and compact architectures, the total node cost is practically twice, when the number of directions doubles. When the A/D ratio is increased from 25% to 50%, the total node cost of the baseline, common-band and compact architectures is also doubled, since the number of TRs is twice as large. In the case of the AO-WC architecture, the total node cost almost doubles when the number of directions is increased from 2 to 4. However, when the number of directions is increased to 8 and 16, the total node cost almost triples due to the greater impact of the number of AO-WCs on the node cost, as shown in Figure 2.18. Regarding the A/D ratio increase from 25% to 50%, the cost doubles when the number of directions is 2 and 4, while when the number of directions is 8 and 16, the cost is approximately 1.5 times more expensive, due to the greater impact of the AO-WCs in the total cost.

From the results presented in Tables 2.4-2.7, it can also be observed that nodes with CD A/D architecture are slightly cheaper in comparison with the nodes with CDC A/D architecture, and nodes with a B&S express structure are cheaper than a R&S node, although the difference is small. For all the four MB architectures studied, the CDC A/D structure is approximately between 1.7 and 2.6 times more expensive than the CD structure, excluding TRs cost.

Table 2.10 represents the average increase of the total node cost in percentage, when the L-band and the L+S-bands are added to the R&S CD C-band, considering the MB baseline, common-band and compact architectures, and an A/D ratio of 25% and 50%. Table 2.11 represents the average increase of the total node cost in percentage, when the S-band is added to the R&S CD C+L node, considering the MB baseline, common-band and compact architectures and an A/D ratio of 25% and 50%. The values presented in Tables 2.10 and 2.11 were determined considering the average of the cost increase for the

four directions (2, 4, 8 and 16) since the values obtained for each direction are similar. The values obtained in Tables 2.10 and 2.11 are also much similar when considering a B&S node or an A/D structure of the CDC type (WSS or MCS).

In appendix B, the values of the cost increase when the L-band and the L+S-bands are added to the R&S CD C-band, for the four directions and an A/D ratio of 25% and 50%, for the AO-WC architecture (Table B1) are calculated. In addition, Table B2 shows the values of the cost increase when the S-band is added to the R&S CD C+L node, for directions 2, 4, 8 and 16 and an A/D ratio of 25% and 50%, for the AO-WC architecture. The values obtained for this architecture are different for each direction, due to the inclusion of a high number of AO-WCs with the increase of the number of directions, impacting the total node cost.

TABLE 2.10. Average cost increase percentages of the additions of the L-band and the L+S bands in an R&S CD C-band node, for the three MB architectures, and an A/D ratio of 25% and 50%.

Architectures	Percentage of node cost increase			
	L-band		L+S-bands	
	A/D ratio of 25%	**A/D ratio of 50%**	**A/D ratio of 25%**	**A/D ratio of 50%**
Baseline	177.6%	178.9%	430.4%	434.0%
Common-band	168.8%	160.2%	361.8%	349.6%
Compact	177.5%	179.1%	426.4%	431.6%

TABLE 2.11. Average cost increase percentages of the addition of the S-band in a R&S CD C+L band node, for the four MB architectures, and an A/D ratio of 25% and 50%.

Architectures	Percentage of node cost increase	
	A/D ratio of 25%	**A/D ratio of 50%**
Baseline	91.0%	91.4%
Common-band	71.8%	72.8%
Compact	89.7%	90.5%

Adding the L- and S-bands to a node working only in the C-band, increases the cost as expected and shown in Tables 2.4-2.7. From Tables 2.10, 2.11, B1 and B2, it can be concluded that the AO-WC architecture shows a higher cost increase compared to the other MB architectures, when the L, S or both bands are added, due to the huge number of AO-WCs required and their higher contribution to the AO-WCs architecture cost. In contrast, the common-band architecture shows a lower cost increase when compared to the other MB architectures due to the use of only C-band components. The baseline and compact architectures show similar behaviors when adding new bands to the node due to the use of the same A/D structure. From these tables, it can also be concluded that,

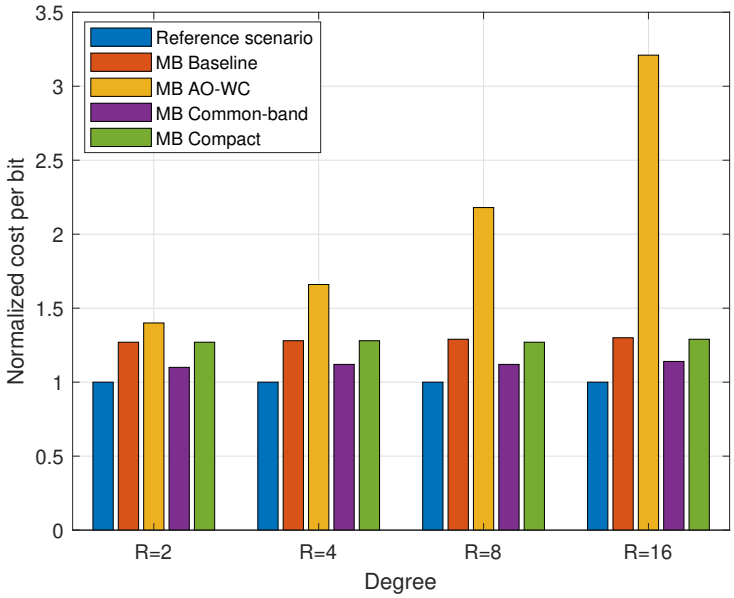

FIGURE 2.19. Cost-per-bit normalized to the R&S CD reference scenario cost with 2 directions, for an A/D ratio of 25%, and for the four C+L+S MB architectures.

it becomes cheaper to add the S-band to an existing node with the C+L bands, than to add the L- and S-bands to a node with only the C-band.

Next, a cost-per-bit analysis will be performed, which appears in several studies [9] and [32]-[36]. This analysis allows us to relate the cost and the respective capacity (in bit/s) of each one of the MB ROADM architectures studied. The cost-per-bit is defined as the ratio between the total node cost and the total node A/D capacity, which depends on each TR bit rate and on the number of TRs. To calculate the cost-per-bit, it is assumed a bit rate of 100 Gbit/s per transponder. The cost-per-bit is normalized to the cost of the reference scenario, i.e., a R&S C-band node with 2 directions, where the total node A/D capacity is 4.4 Tbit/s, for an A/D ratio of 25%. The cost-per-bit of this reference scenario is 3.75×10^{-10} (=1651/4.4 Tbit/s), where the A/D capacity is calculated as 44×100 Gbit/s (the number of transponders, 44, is calculated with (2.1), with A/D_{ratio}=0.25, R=2 and N_{ch}=87). The normalized cost-per-bit in this scenario is 1. For the other MB architectures, the normalized cost-per-bit is obtained in a similar way, having in mind the reference value of the reference scenario.

Figure 2.19 shows the normalized cost-per-bit for each architecture considering 2, 4, 8 and 16 directions, C+L+S band scenario, and an A/D ratio of 25%. From Figure 2.19, it can be observed that the cost-per-bit of the baseline, common-band and compact architecture is practically the same when the number of directions is increased, except

for the AO-WC architecture. For a fixed number of directions, the cost-per-bit is higher about 29%, 12% and 28% respectively, for baseline, common-band and compact architectures, when compared with the reference scenario. These three architectures are highly dependent on the TRs cost, and by doubling the number of directions, the number of TRs and total node cost also double, and, hence, the cost-per-bit remains practically the same. The MB baseline and compact architectures have a similar cost-per-bit due to the use of a similar A/D structure. The common-band architecture presents a lower cost-per-bit, since it uses only C-band components in the express and A/D structures. The AO-WCs architecture shows a higher cost-per-bit due to the high number of AO-WCs and its stronger contribution to the total node cost when increasing the number of directions. For the AO-WC architecture and a fixed number of directions, R=2, 4, 8 and 16, the cost-per-bit is, respectively 40%, 66%, 118% and 221% higher when compared to the reference scenario. The results obtained in Figure 2.19 are similar to ones presented in [9], Figure 3, with α=1.5, β=2 and γ_f=0, where the baseline architecture is named conventional architecture and the common-band is called proposed architecture. In the case of the common-band architecture, the cost-per-bit obtained in this work is 1.12, a slightly lower value when compared with the cost-per-bit of approximately 1.17 in [9].

The cost analysis just presented has assumed that α=1.5 and β=2, which is a worst-case analysis [9]. In appendix C, the cost analysis is also performed a more favourable cost scenario with α=1.2 and β=0.5 [9]. In the baseline and compact architectures, the total node cost in the less favourable scenario is approximately 10.6% (baseline architecture) and 10.7% (compact architecture) more expensive than in the more favourable scenario in the case of an R&S CD C+L+S node with A/D ratios of 25% and 50%. In the case of a C+L node, the cost difference in the baseline and compact architectures between the two scenarios is negligible. In the case of the C+L baseline architecture, S-band and AO-WCs components are not used, whose costs are affected by the parameters α and β. In the case of the C+L compact architecture, it is used in the express structure MB WSSs, whose cost is affected by the parameter α, however, the total node cost is not much impacted, when varying the parameter α from 1.5 to 1.2. In addition, the cost is also lower in AO-WC and common-band architectures due to the use of AO-WCs, because the cost of this component is dependent on parameter β, as the AO-WC cost decreases from 72 (in the less favourable scenario) to 18 (in the more favourable scenario).

In appendix D, the values of the cost increase of the less favourable over the more favourable scenario in a R&S CD node, for the four directions and an A/D ratio of 25% and 50%, for the AO-WC architecture (Table D1) and common-band architecture (Table D2) are calculated. It can be concluded that the parameters α and β influence the total cost of nodes, however, the total cost of C+L+S nodes is the most affected when compared with C+L nodes. In the case of AO-WCs architecture, the cost percentage increases with the number of directions, due to the number of AO-WCs, however, the increase is more pronounced in the case of a C+L+S node, due to the introduction of the S-band in the node. In the case of the common-band architecture, the cost percentage remains more or less constant with the increase in the number of dimensions, due to the number of AO-WCs doubling with the increase in the number of dimensions.

2.4.3. Cost comparison between SDM and MB solutions

In this subsection, a cost comparison study between the MB node solutions presented previously in subsection 2.4.2 and a SDM node solution is performed. In this study, besides the node cost, we also consider the fiber lease cost, since in a SDM scenario multiple fibers are used for transmission as opposed to the single fiber scenario used in the MB solutions.

The analysis starts by presenting in Figure 2.20 the SDM node architecture considered in this study. This architecture has 3 fibers per direction, each fiber working only in the C-band, and has wavelength granularity switching without lane changes [35, 36, 39], so that a fair comparison can be done with the MB solutions nodes studied in subsection 2.4.2, that use 3 bands and do not allow wavelength switching between the different bands.

In Figure 2.20, the size of the express structure components is obtained with (2.2) and the total number of TRs in the A/D structure, M, is calculated with (2.1), considering that each fiber carries 87 wavelengths, with a total of 261 wavelengths for the three fibers. The number of A/D cards is calculated with (2.3). In the SDM architecture, three fibers per direction are considered, so there is one dedicated A/D structure per fiber. In this situation, it is considered that an A/D card is formed by three $R\times M'$ WSSs or by three $R\times M'$ MCSs, in the case of a CDC-type A/D structure, or three $R\times 1$ WSSs followed by three $1\times M'$ WSSs, in the CD-type structure (drop structure).

Figure 2.21 shows an example of a MCS-based CDC A/D structure with 6 cards, considering R=4 and an A/D_{ratio}=25%. In Figure 2.21, the number of A/D cards calculated

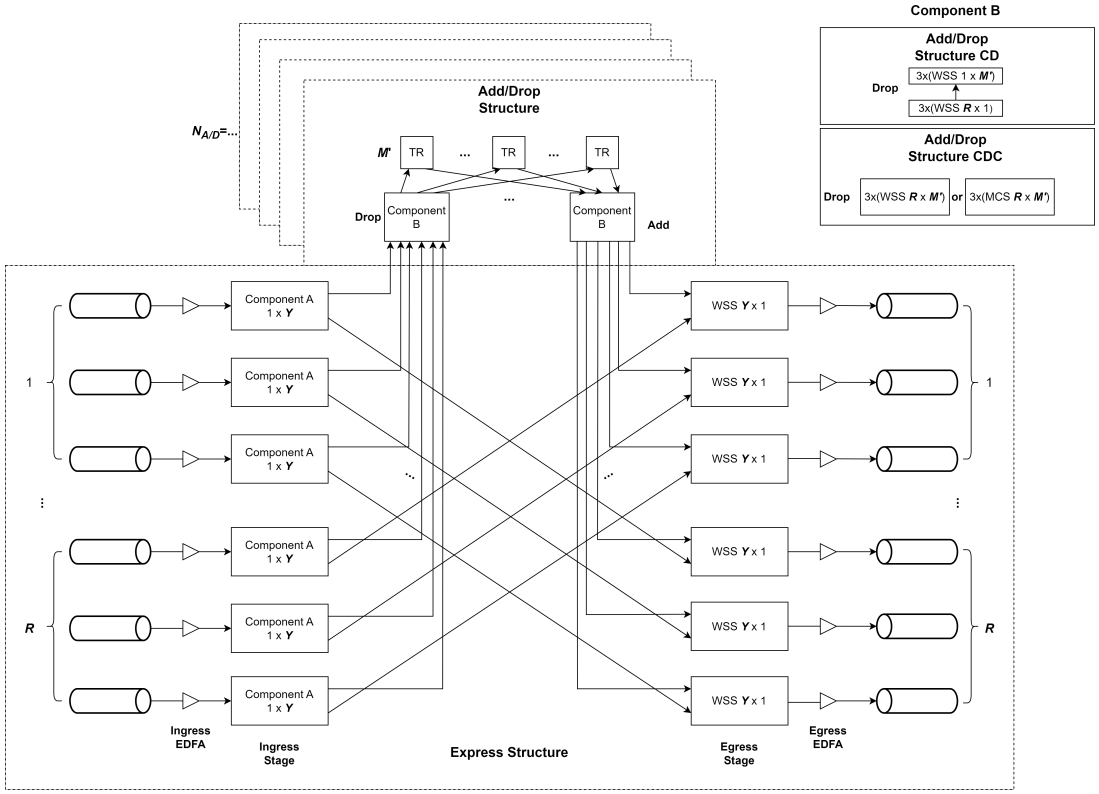

FIGURE 2.20. *R*-degree C-band SDM ROADM architecture with 3 fibers per direction.

as the ratio between the total number of TRs, 261, (M) and the size of the three MCSs (M'), in this case 48 (16×3).

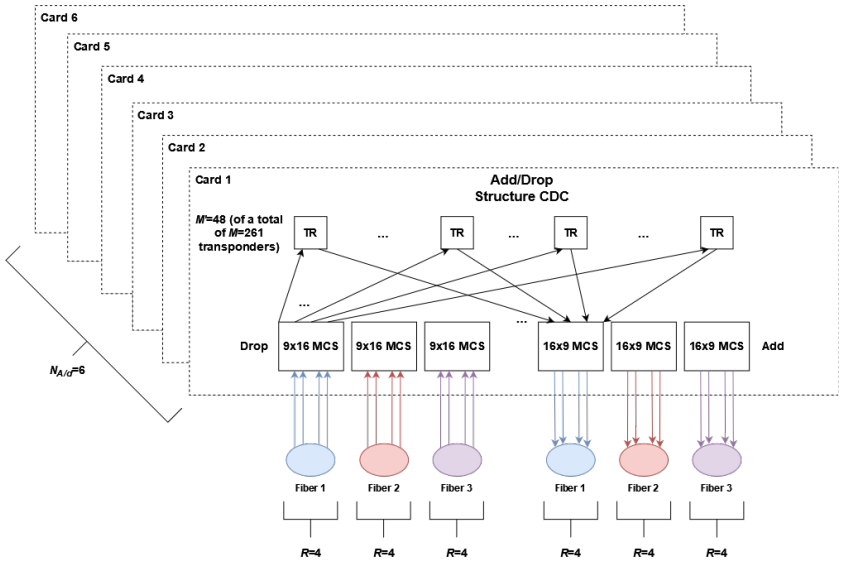

FIGURE 2.21. Example of MCS-based CDC A/D structure with 6 cards, considering R=4 and A/D_{ratio}=25%.

The cost of the SDM ROADM express structure with R directions is given by

$$Cost_{express} = RN_{fibers}Cost_{A,1\times Y} + RN_{fibers}Cost_{WSS,Y\times 1} + 2RN_{fibers}Cost_{EDFA} \quad (2.16)$$

where N_{fibers} corresponds to the number of fibers considered per direction in the node, in our case N_{fibers}=3.

The cost of the CD A/D structure is given by,

$$Cost_{A/D,CD} = 2N_{fibers}N_{A/D}Cost_{WSS,R\times 1}+2N_{fibers}N_{A/D}Cost_{WSS,1\times M'}+MCost_{TR} \quad (2.17)$$

Likewise, the cost of the CDC A/D structure (MCS or WSS based) is given by,

$$Cost_{A/D,CDC} = 2N_{fibers}N_{A/D}Cost_{B} + MCost_{TR} \quad (2.18)$$

where $Cost_B$ represents the cost of component B, that can be a MCS or WSS [9].

Table 2.12 shows the total cost of the C-band SDM architecture, considering the CD and CDC A/D structures, based on MCSs or WSSs and the express structures based on B&S and R&S architectures. The costs are obtained for R=2, 4, 8 and 16, for an A/D ratio of 25% and 50% and considering three fibers per direction. In addition, Figure 2.22 represents the number of TRs required by the SDM and MB C+L+S architectures as a function of the number of directions R=2, 4, 8 and 16 considering two A/D ratios, 25% (Figure 2.22 (a)) and 50% (Figure 2.22 (b)).

TABLE 2.12. Total cost of C-band SDM ROADM with an A/D ratio of 25% and 50% with 3 fibers per direction.

Add/Drop	Express	A/D ratio of 25%				A/D ratio of 50%			
		R=2	**R=4**	**R=8**	**R=16**	**R=2**	**R=4**	**R=8**	**R=16**
CD	**B&S**	4904	9785	19630	39638	9704	19451	38902	78443
	R&S	4918	9844	19808	40351	9733	19540	39080	79150
CDC MCS	**B&S**	5106	10205	20352	40999	10161	20231	40644	81293
	R&S	5120	10264	20528	41776	10190	20320	41000	82000
CDC WSS	**B&S**	5106	10085	20232	40759	10041	20111	40404	79213
	R&S	5120	10144	20408	41536	10070	20200	40760	79920

From Table 2.12 and Figure 2.22 and comparing with Tables 2.4-2.7, it can be concluded that the cost of the four MB C+L+S architectures is higher than the cost obtained for the SDM architecture, since the MB architectures use a greater number of TRs (C-band with 87 channels, L-band with 130 channels and S-band with 148 channels for a total of 365 channels in comparison with $3\times87 = 261$ channels used in the SDM scenario), which is the main contributor to the total node cost. Furthermore, MB architectures use components operating in the L- and S-bands, which are more expensive than C-band

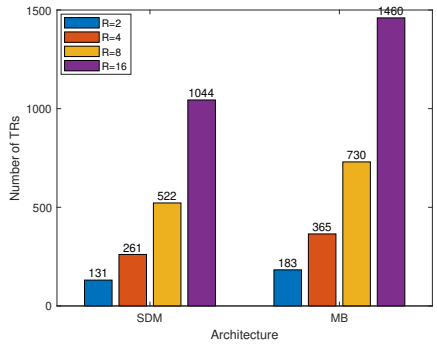

(a) Number of TRs for SDM and C+L+S nodes considering an A/D ratio of 25%.

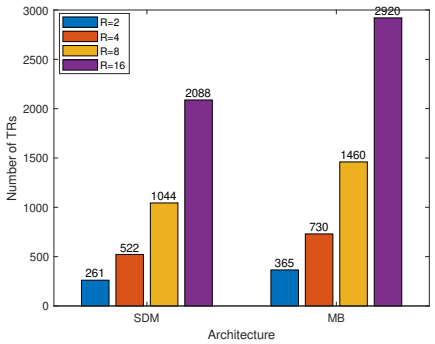

(b) Number of TRs for SDM and C+L+S nodes considering an A/D ratio of 50%.

FIGURE 2.22. Number of TRs for SDM and C+L+S nodes considering an A/D ratio of 25% and 50%.

components. Note that the number of TRs for the MB solution is the same for the four architectures studied.

Table 2.13 represents the average cost increase of the MB baseline, common-band and compact architectures over the SDM ROADM solution, considering a R&S CD node, with an A/D ratio of 25% and 50%. The values presented in Table 2.13 are calculated considering the average of the cost increase for the four directions (2, 4, 8 and 16), since the values obtained for each number of directions are similar. Table 2.14 represents the values of the cost increase of the MB AO-WC architecture over SDM node solutions, considering a R&S CD node, for the directions 2, 4, 8 and 16, with an A/D ratio of 25% and 50%.

TABLE 2.13. Average cost percentages increase of MB nodes over SDM nodes in a R&S CD node, for the three MB architectures, and considering an A/D ratio of 25% and 50%.

Architectures	Percentage of node cost increase	
	A/D ratio of 25%	**A/D ratio of 50%**
Baseline	77.1%	77.9%
Common-band	54.2%	49.8%
Compact	75.7%	77.2%

As can be observed from Tables 2.13 and 2.14, the AO-WC architecture presents a higher cost increase with the increase in the number of directions, in relation to the SDM architecture due to the greater impact of the TRs and AO-WCs on the total node cost. For example, when the number of directions is 16, considering an A/D ratio of 25%, the total cost increase is about 4.3 (335.5%) times higher. In addition, when the number of directions is increased from 2 to 16, the cost percentage increase in the case of

A/D ratios of 25% and 50%, are approximately 1733.6% (18.3 times) and 1247.6% (13.5 times), respectively. Furthermore, as expected, the common-band architecture presents a smaller cost increase, due to the use of only C-band components. The baseline and compact architectures present a similar cost increase due to the use of a very similar A/D structure.

TABLE 2.14. Cost percentages increase of MB nodes over SDM nodes in a R&S CD node, for the AO-WC architecture, and considering an A/D ratio of 25% and 50%.

Degree	Percentage of node cost increase	
	A/D ratio of 25%	**A/D ratio of 50%**
2	94.9%	86.6%
4	130.4%	104.8%
8	201.1%	140.5%
16	335.5%	209.3%

Figure 2.23 shows the cost-per-bit for each R&S CD architecture solution considering 2, 4, 8 and 16 directions and an A/D ratio of 25%. The cost-per-bit is calculated in the same way as in the previous subsection. As can be observed in Figure 2.23, the cost-per-bit of the SDM architecture is quite similar (only approximately 2% higher) compared to the reference scenario cost, since both the total cost of the SDM architecture and the node A/D capacity are greatly dependent on the TRs number. The cost-per-bit of the SDM architecture is lower compared to the four MB architectures due to the smaller cost of the C-band TRs compared with the L- and S-bands TRs. The cost-per-bit of the SDM, baseline, common-band and compact architectures remains unchanged with the increase in the number of directions, since these architectures are strongly dependent on the TRs cost. As previously seen, the cost-per-bit of the AO-WC architecture increases when the number of directions is higher due to the increase of the number of AO-WCs and their greater contribution to the nodes cost.

Comparing the values obtained in Figure 2.23 with the values of Figure 3 of [9], for α=1.5, β=2 and γ_f=0, i.e., without considering the fiber cost, it is observed that the values of the cost-per-bit, for the baseline (conventional architecture in [9]), common-band (proposed architecture in [9]) and SDM architectures, are similar, i.e., for the baseline architecture, 1.29 (our result) and 1.3 (obtained in [9]), for the common-band architecture, 1.12 (our result) and 1.17 (obtained in [9]) and for the SDM architecture, 1.02 and 1 ([9]). Note that in [9], the cost-per-bit was normalized to the cost of the SDM architecture, with 3 fibers per direction.

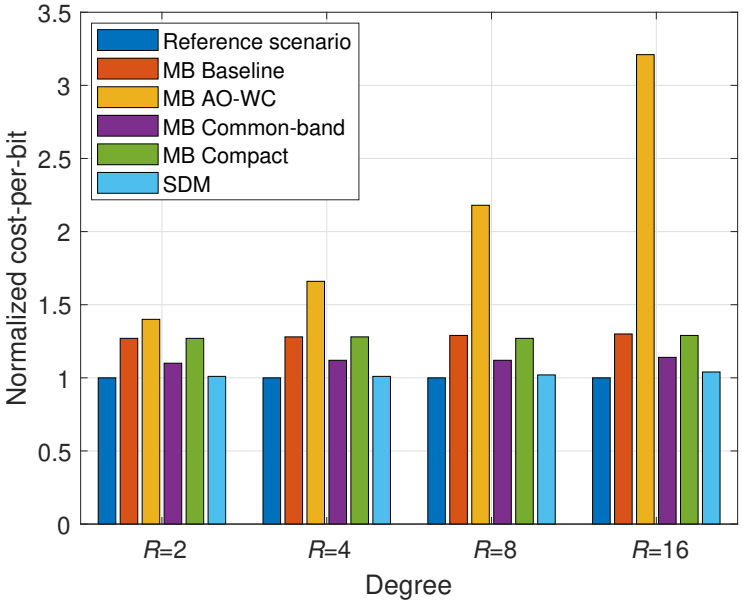

FIGURE 2.23. Cost-per-bit normalized to the R&S CD reference scenario cost with 2 directions, for an A/D ratio of 25% for both MB and SDM ROADM architectures.

Table 2.15 represents the A/D capacity in Tbit/s, for the SDM and MB architectures (the four MB architectures have the same number of TRs), for A/D ratios of 25% and 50%. It is observed that the capacity is higher in the MB nodes, due to the high number of L- and S-bands channels, impacting the number of TRs. The MB nodes have 1.4 higher A/D capacity compared to the SDM architecture presented in Figure 2.20. For example, as shown in Table 2.15, for a node with 2 directions and for an A/D ratio of 25%, for the SDM architecture, the total node A/D capacity is 13.1 Tbit/s against the 18.3 Tbit/s for the four MB architectures.

TABLE 2.15. A/D capacity (Tbit/s) of C-band SDM ROADMs and MB ROADMs with an A/D ratio of 25% and 50%.

Architecture	A/D ratio of 25%				A/D ratio of 50%			
	R=2	**R=4**	**R=8**	**R=16**	**R=2**	**R=4**	**R=8**	**R=16**
SDM	13.1	26.1	52.2	104.4	26.1	52.2	104.4	208.8
MB	18.3	36.5	73	146	36.5	73	146	292

Next, the fiber lease cost is introduced in our cost analysis. Two network scenarios will be considered, a small network - British Telecom (BT-UK), and a large network - CONUS-60 (with both topologies represented in appendix E) [25, 32]. Note that in the SDM network scenario we consider a bidirectional transmission with 3 fibers in each direction, so 6 fibers in both directions have to be considered in our calculations, whereas

in the MB network scenario, there is only one fiber in each direction, so 2 fibers have to be considered.

Table 2.16 shows the network characteristics used in our analysis for both BT-UK and CONUS-60 networks. In particular, Table 2.16 indicates the fiber lease cost parameter, fiber lease duration, the number of nodes, the average node degree (average of all the node degrees in the network), the total network length (sum of the length of all paths in the network), and the number of links and the average link length (average of all link lengths in the network).

TABLE 2.16. Parameters used for BT-UK and CONUS-60 networks.

Parameters	Network	
	BT-UK	**CONUS-60**
Cost per fiber/km/year, $Cost_{fiber}$	0.33	
Lease time duration [years]	5	
Number of nodes, N_{Nodes}	22	60
Average node degree	3.2	2.6
Total network length, $Total_{Length}$ [km]	5148	35388
Number of links	35	79
Average link length [km]	147	445

The total network cost depends on the network topology and node architecture and can be given by,

$$Cost_{Network,a,n} = \sum_{v=1}^{N_{Nodes}} Cost_{node,v} + 2N_{fibers}(Cost_{fiber}Total_{Length}) \tag{2.19}$$

with a=MB baseline, AO-WC, common-band, compact or SDM architecture, and n=BT-UK or CONUS-60 network. In addition, N_{Nodes} corresponds to the number of nodes, $Cost_{node,v}$ to the node cost depending on the architecture considered, N_{fibers} to the number of fibers per direction, which can be 1 (for MB scenario) and 3 (for SDM scenario) fibers, $Cost_{fiber}$ corresponds to the fiber lease cost per km during 5 years and $Total_{Length}$ corresponds to the total length of the network considered in km.

Next, the cost-per-bit is computed for both the BT-UK and CONUS-60 networks considering the MB and SDM node architectures studied previously. Figures 2.24 and 2.25 show the cost-per-bit for the BT-UK and CONUS-60 networks, respectively, as a function of the fiber lease cost per km and year considering the R&S CD ROADM architecture and an A/D ratio of 25%. In this analysis it is assumed that the MB networks are operating simultaneously in the C-, L- and S-bands and 3 fibers per direction are used in the SDM network. Furthermore, the cost-per-bit for both networks is normalized to the same scenario and computed in the same way as considered in Figure 2.23, so that a fair

comparison can be done. Note that the total number of TRs has to be calculated for the MB and SDM networks scenario considering the BT-UK and CONUS-60 topologies.

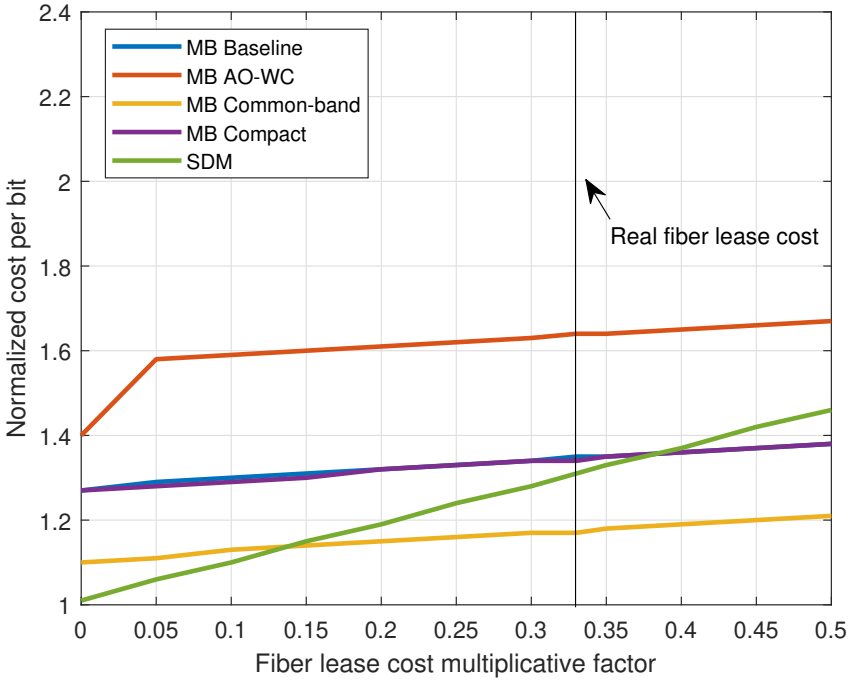

FIGURE 2.24. Cost-per-bit normalized to the R&S ROADM CD reference scenario cost with 2 directions without considering the fiber cost, considering the BT-UK network, for an A/D ratio of 25% for both MB and SDM ROADM architectures with 4 directions.

From Figure 2.24 (BT-UK network), it can be seen that the SDM architecture with null fiber lease cost, has the lowest cost-per-bit compared to the other MB architectures, as explained before (the same scenario occurs for the CONUS-60 network). In addition, the steep slope present in the AO-WC architecture, (between 0 and 0.05), is due to the introduction of the fiber lease cost, and the increase in the number of AO-WCs (this behavior is similar in the CONUS-60 network). Moreover, it is observed that the cost-per-bit of MB architectures has a smooth increase with the fiber lease cost since only one fiber per direction is used, as opposed to the sharp increase in the SDM network scenario where 3 fibers per direction are considered. It is also observed that the cost-per-bit of the MB AO-WC architecture is the highest among the MB architectures studied, due to the high number of AO-WCs, compared to the other MB architectures. In addition, the compact and baseline architectures present a similar cost-per-bit due to the use of a similar A/D structure, as already referred. Furthermore, the common-band architecture presents the lower cost-per-bit compared to the other MB architectures due to the use of

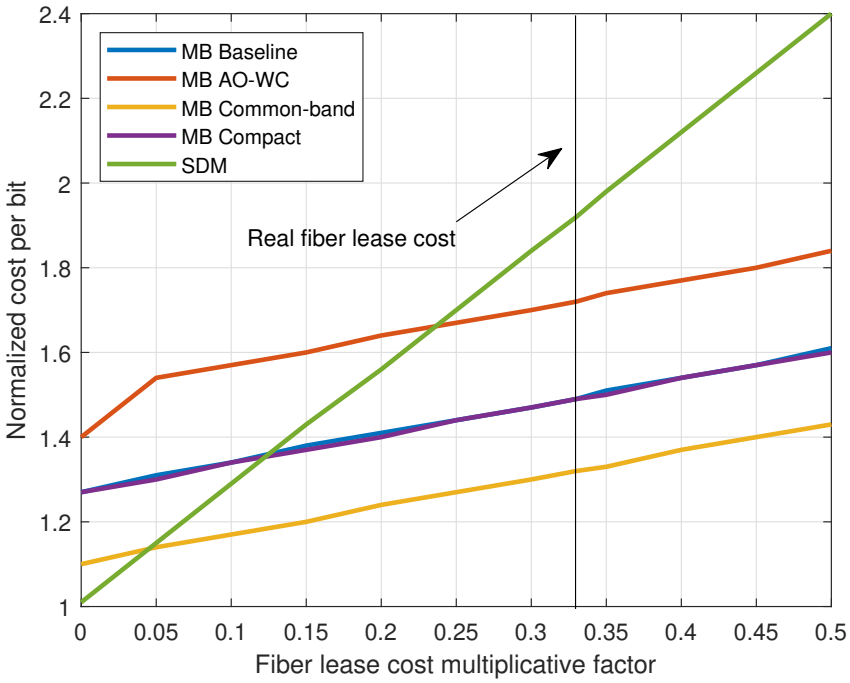

FIGURE 2.25. Cost-per-bit normalized to the R&S ROADM CD reference scenario cost with 2 directions without considering the fiber cost, considering the CONUS-60 network, for an A/D ratio of 25% for both MB and SDM ROADM architectures with 4 directions.

only C-band components. In addition, when the real fiber lease cost is considered (0.33), the AO-WC architecture has the highest cost-per-bit, and common-band architecture presents the lowest cost-per-bit compared to the other architectures. Finally it can be observed that the cost-per-bit of the SDM architecture becomes higher than the MB common-band architecture for a fiber lease cost of 0.15 and becomes higher than the baseline and compact architectures for a fiber lease cost of 0.38.

Similar conclusions to the results of Figure 2.24 can be drawn also from Figure 2.25 where the CONUS-60 network is considered. However, despite the similar behavior of the results of both figures, there are some differences. In particular, it can be noted that the cost-per-bit in Figure 2.24 increases less than in Figure 2.25 for all the architectures, since the CONUS-60 network has a higher number of nodes and needs more fibers (Table 2.16). Furthermore, in the CONUS-60 topology for the real fiber lease cost (0.33), the cost-per-bit of the SDM architecture exceeds the cost-per-bit of the baseline, AO-WC, common-band and compact architectures. Also, it can be observed that, in the CONUS-60 network scenario, the SDM curve surpasses the MB curves for a lower fiber lease cost, 0.05, 0.12 and 0.24, than in the BT-UK network scenario, 0.15 and 0.38, which means that in the CONUS-60 network scenario, the fiber lease cost has a greater impact on

the cost-per-bit of the SDM network than in BT-UK network scenario, due to the higher number of links and total network length (Table 2.16).

Table 2.17 shows the fiber lease cost percentage relatively to the total network cost in BT-UK and CONUS-60 networks, for the SDM architecture. From Table 2.17, it can be seen that the percentage of the total fiber cost increases with the fiber lease cost, as expected, but the cost increase is higher in the CONUS-60 network due to the size of this network. In addition, it can be observed that the cost percentages of the fiber cost of the CONUS-60 network are approximately twice the BT-UK network cost, for all fiber lease costs.

TABLE 2.17. Cost percentages of the fiber lease cost on the total cost of the BT-UK and CONUS-60 networks, for the SDM architecture.

fiber lease per fiber/km/year	Network	
	BT-UK	**CONUS-60**
0.1	9%	22%
0.2	16%	36%
0.3	22%	46%
0.33	23%	48%
0.4	27%	53%
0.5	31%	59%

Comparing the results obtained in Figures 2.24 and 2.25 with the results of Figure 3 of [9], for α=1.5, β=2 and of Figure 3 of [32], when the launch power is -5.25 dBm (to ensure low NLI), it can be observed that the cost-per-bit of the SDM architecture, for both BT-UK and CONUS-60 networks, exhibits the same variation as the one presented in [9, 32], in relation to the fiber lease cost. In addition, it is observed in Figure 3 of [32] that when the launch power is -5.25 dBm and the fiber lease cost is 0.33, the cost-per-bit of the SDM architecture is higher than the cost-per-bit of the MB architecture, as happens when the BT-UK topology is considered (Figure 2.24). However, in this case only the common-band presents a lower cost-per-bit compared to the other architectures. Note that in both [9, 32], different normalizations are considered which may cause the differences in the obtained cost-per-bit values: in [9], the NSFNET topology is considered, and the cost-per-bit values are normalized to the SDM architecture without consideration of the fiber lease cost, and in [32] the BT-UK and Indian topologies are considered, while the cost-per-bit values are normalized to the SDM architecture considering the fiber lease cost of 0.5. In [32], the influence of the PLIs in the cost-per-bit calculation is also taken into account, which potentially can have a greater impact on the MB networks results,

since the ISRS effect has more influence in MB than in SDM scenarios, that only use the C-band [9].

2.5. Conclusions

In this chapter, a review of the MB ROADM node architectures is performed and a comparison with a common SDM node architecture is done in terms of total node cost and cost-per-bit. It has been observed that for all the architectures studied the main contribution to the total node cost is the TRs number and cost. The cost of the other node components is marginal to the total cost. Only for the MB AO-WC architecture, the cost of the AO-WC has a significant contribution to the total node cost. Hence, the MB AO-WC architecture is the most expensive compared to the other architectures due to the use of a large number of AO-WCs and their contribution to the total node cost. The total node cost of the baseline architecture compared with the cost of the compact MB ROADM architecture is very similar, since the A/D structure for these two architectures is very similar. The common-band architecture presents the lowest total node cost, due to the use of only C-band components.

Regarding the cost-per-bit, the SDM architecture presents the lowest cost-per-bit compared to MB architectures, due to the lower total cost of the SDM node since only C-band TRs are used. Thereby, the common-band architecture also presents the lowest cost-per-bit, when compared with the other MB architectures, due to the use of only C-band components. When the fiber lease cost is considered in the BT-UK and CONUS-60 networks, the cost-per-bit of the SDM architecture increases with the fiber lease cost, as expected. For a smaller network size (e.g. BT-UK), the SDM architecture is a good solution, when the fiber lease cost is less than 0.15. Although, when the fiber lease cost is above 0.15, the MB solution with the common-band architecture becomes cheaper. When the network is larger (e.g. CONUS-60), the common-band architecture with a fiber lease cost greater than 0.05 is again a good option, since it presents a lower cost-per-bit in comparison with the remaining architectures.

CHAPTER 3

Physical layer impairments in C+L+S multi-band optical networks

3.1. Introduction

The PLIs in C+L+S MB optical networks have some important differences from the PLIs in C-band-only networks due to the use of more bands of the optical spectrum. The main goal of this chapter is to find out which MB architecture is more robust to PLI impairments in a MB network environment and, as a consequence, the MB network that is capable of transporting more capacity and ultimately leads to a lower cost-per-bit. The use of other bands beyond the C-band has the advantage of increasing the network capacity, however, the impact of the ISRS, which consists of power transfers from high to low-frequency channels has more impact for wideband communications, which is the case of the C+L+S MB scenario considered in this chapter [40, 41]. The study of NLI in such a scenario must consider the ISRS effect. Furthermore, the NLI effect also depends on the modulation format considered [42]. In addition, the noise figure of L- and S-bands OAs is higher than in the C-band, with a higher fiber attenuation coefficient in the L- and S-bands, which leads to higher ASE powers. The impact of all these impairments will be quantified with the OSNR metric for several paths in the BT-UK topology.

Section 3.2 studies and computes the total ILs of the components of each MB architecture studied and analyzed in the previous chapter. Section 3.3 analyzes the impact of the accumulation of ASE noise in a C+L+S MB network. Next, in section 3.4, the NLI noise power is assessed considering different modulation formats for a C+L+S MB network with different MB architectures. Sections 3.5 and 3.6 compute the total OSNR for some candidate paths of the BT-UK topology considering the PIC and LCoS WSS technologies in the MB architectures. Section 3.7 presents the main conclusions of this chapter.

3.2. Insertion losses in C+L+S MB ROADMs

The insertion losses (ILs) introduced by the MB ROADM architectures studied in chapter 2 are assessed in this section. To accomplish this task, the different signal paths

inside the ROADM architecture and the components that belong to those paths must be identified.

In a ROADM, an optical signal can propagate through three possible optical paths - the express, add and drop paths. The express path establishes the connection between the ROADM inputs and outputs. The add path establishes the connection between the client network and the ROADM outputs, whereas the drop path is responsible for the path between the ROADM inputs and the client network.

The optical components inside the MB R&S ROADMs crossed along these paths are typically WSSs, AO-WCs and MB-DEMUX/MUXs as discussed in chapter 2. Next, the ILs of these components are characterized. The most common component used in MB ROADM is the WSS, which can be implemented using micro-electromechanical systems (MEMS) based on micro-mirrors, LCoS, or PIC technologies [43, 44]. MEMS technology has the disadvantage of not supporting the flexible grid and WSSs with high port count (>20) [45] and has typical ILs of approximately 6.5 dB [46]. The LCoS technology supports the flexible grid and WSSs with medium and high port count [45]. Typical ILs of LCoS WSSs range between 2 dB and 8 dB, with around 6 dB being a common value [46, 47]. Recent progresses in LCoS WSSs show that the ILs in the C- and L-bands are similar [45, 48]. From Figure 9 of [45], ILs approximately between 4 dB and 5 dB, can be found in both bands, and between 2.5 dB and 5 dB, for the 15 THz (C+L+S) LCoS WSS proposed in [48]. Other bands are expected to introduce similar ILs [45]. In [49], a 36 THz bandwidth WSS which uses the LCoS technology is proposed. This WSS can be used for the C-, S-, E- and O-bands simultaneously, and the ILs in the C- and S-bands are, respectively, approximately 5 dB and 6 dB, from Figure 6 of [49]. For the future, both MEMS and LCoS technologies are considered complex to manufacture [44] in comparison with the PIC technology [43, 44]. In [43], a C-band PIC-based WSS is implemented, and in [44] a C+L+S MB PIC-based WSS is built. The ILs of the C-band PIC-based WSS are given by [43],

$$IL_{WSS} = \log_2(N_{output} + N + 1) \tag{3.1}$$

where N_{output} corresponds to the number of outputs of the WSS, and N corresponds to the number of wavelength channels handled by the WSS in each fiber direction which is considered to be 64 (C-band), 87 (L-band), 109 (S-band) or 260 channels, in the case of MB WSSs (C+L+S bands), considering a channel spacing of 75 GHz [40, 41], assuming a worst-case full-band loading. In the C-band, 3 nm (1568 nm) was added in relation

to chapter 2 (1565 nm). Table 3.1 shows the insertion losses of the WSSs used in the MB architectures, computed with (3.1) assuming that the ILs of C-, L-, S-bands and MB PIC-based WSSs [44] can be assessed also this expression.

TABLE 3.1. Insertion losses of the WSSs for C-, L- and S-bands with a channel spacing of 75 GHz.

Component	Insertion losses [dB]		
	C-band	**L-band**	**S-band**
WSS 1×2	6.1	6.5	6.8
WSS 1×4	6.1	6.5	6.8
WSS 1×9	6.2	6.6	6.9
WSS 1×20	6.4	6.8	7.0
WSS 1×40	6.7	7.0	7.2
WSS 1×80	7.2	7.4	7.6
MB WSS 1×9	8.1		
MB WSS 1×20	8.1		
MB WSS 1×40	8.2		

From Table 3.1, it can be observed that the WSS ILs show a small variation with the increase of the number of WSS outputs, between 6.1 and 8.2 dB. The higher ILs values correspond to a high number of ROADM directions and/or the usage of a band that allows more WDM channels, e.g. the S-band.

In the AO-WC and common-band architectures, studied in chapter 2, the AO-WC IL must be assessed to find the path ILs. The AO-WCs can be based on periodically poled lithium niobate (PPLN) waveguides or highly-nonlinear fibers (HNLF) [7–9]. The AO-WCs considered in the AO-WC and common-band architectures are based on HNLF, which uses the four-wave mixing (FWM) process to achieve the wavelength conversion [7, 8, 50, 51]. In these studies, the HNLF-based AO-WC converters are already designed to operate in the C-, L- and S-bands [7, 8, 50, 51]. The HNLF-based AO-WC considered has a typical IL (which in the case of wavelength conversion is denoted as conversion loss or also as conversion efficiency between an input signal and a converted signal generated after a nonlinear medium [52]) of approximately 20 dB, which is compensated by an OA that is located inside the AO-WC [50, 51]. In the compact architecture besides the MB WSSs, we also have in the A/D structure, the MB-DEMUX/MUX, which introduces ILs between 1 dB [5] and 3 dB [41]. In the ILs of the compact architecture, it was considered that each MB-DEMUX/MUX introduces 3 dB of ILs (worst-case scenario) [41].

The next step is to calculate the paths insertion losses inside each MB architecture, that are compensated by the post-amplifier at the ROADM output.

Figure 3.1 shows a simplified version of the R&S CD baseline architecture presented in Figure 2.5 with the possible optical paths identified by numbers and colours. The optical paths with the colours red, blue and purple are, respectively, associated to the C-, L- and S-bands, (this color scheme is used next in the other MB architectures).

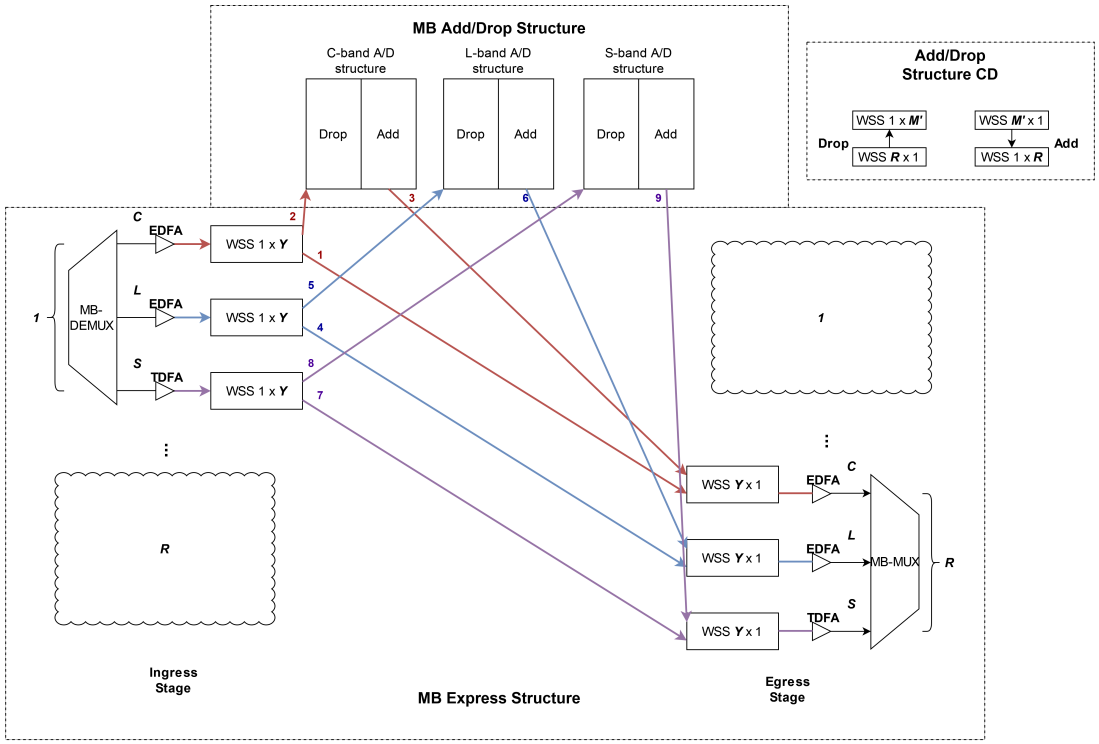

FIGURE 3.1. Baseline R-degree MB ROADM with the possible express, add and drop paths.

In Figure 3.1, the optical paths with the numbers 1, 4 and 7 represent the express paths, respectively, for C-band, L-band and S-band, the paths with the numbers 2, 5 and 8 identify the drop paths, and finally, the paths with the numbers 3, 6 and 9, correspond to the possible add paths.

The ILs of the express path of the baseline architecture are given by

$$IL_{express,b} = IL_{WSS,route,1\times Y,b} + IL_{WSS,select,Y\times 1,b} \tag{3.2}$$

where $IL_{WSS,route,1\times Y,b}$ and $IL_{WSS,select,Y\times 1,b}$, correspond, respectively, to the ILs of the route and select WSSs, and the variable b identifies the band dependence, with b=C, L or S, since (3.2) can be used to calculate the ILs of the express path for any of the bands.

The ILs of the add path of the baseline architecture are given by

$$IL_{add,b} = IL_{WSS,add,M'\times 1,b} + IL_{WSS,add,1\times R,b} + IL_{WSS,select,Y\times 1,b} \tag{3.3}$$

where $IL_{WSS,add,M'\times1,b}$ and $IL_{WSS,add,1\times R,b}$, correspond to ILs of the CD add structure WSSs, and the variable b identifies the band dependence, with b=C, L or S, since (3.3) can be used to calculate the ILs of the add path for any of the bands.

The ILs of the drop path of the baseline architecture are given by

$$IL_{drop,b} = IL_{WSS,route,1\times Y,b} + IL_{WSS,drop,R\times1,b} + IL_{WSS,drop,1\times M',b} \tag{3.4}$$

where $IL_{WSS,drop,R\times1,b}$ and $IL_{WSS,drop,1\times M',b}$, correspond to ILs of the CD drop structure WSSs.

The components of the baseline architecture used for each direction and band for the three possible optical paths are presented in appendix F. To calculate the insertion losses of each optical path, (3.2), (3.3) and (3.4) were used. The ILs of these optical paths are computed in appendix F.

Table 3.2 shows the ILs for the baseline architecture, for each direction and band. The ILs shown in Table 3.2, refer only to the losses of the A/D optical paths since their losses are the highest ones in comparison with the express path ILs given in Table F4 (appendix F), as the optical signal in the A/D path must traverse 3 WSSs, instead of 2 in the express path. Furthermore, it can be seen from Table 3.2 that the band that introduces higher losses is the S-band for each direction, since the optical signal crosses S-band WSSs that are more lossy, due to the high number of S-band channels. In addition, the ILs of the add and drop paths are the same, due to the use of the same components in these optical paths, and the same is observed for the remaining MB architectures. From Table 3.2, the ILs of add and drop paths, have about 1.2 dB (C-band), 0.9 dB (L-band) and 0.7 dB (S-band) of difference between a node with 16 and 2 directions.

TABLE 3.2. Insertion losses of the baseline architecture for the C-, L- and S-bands and R=2, 3, 4, 8 and 16.

Directions	Insertion losses [dB]		
	C-band	**L-band**	**S-band**
2	18.6	19.9	20.7
3	18.7	19.9	20.7
4	18.7	20.1	20.8
8	19.3	20.4	21.1
16	19.8	20.8	21.4

Figure 3.2 shows a simplified version of the R&S CD AO-WC architecture presented in Figure 2.6 with the possible optical paths identified by numbers and colours.

From Figure 3.2, the optical paths with the numbers 1, 2, 3, 6, 7, 8, 11, 12 and 13 refer to the express path. The paths with the numbers 4, 9 and 14 are drop paths, and the

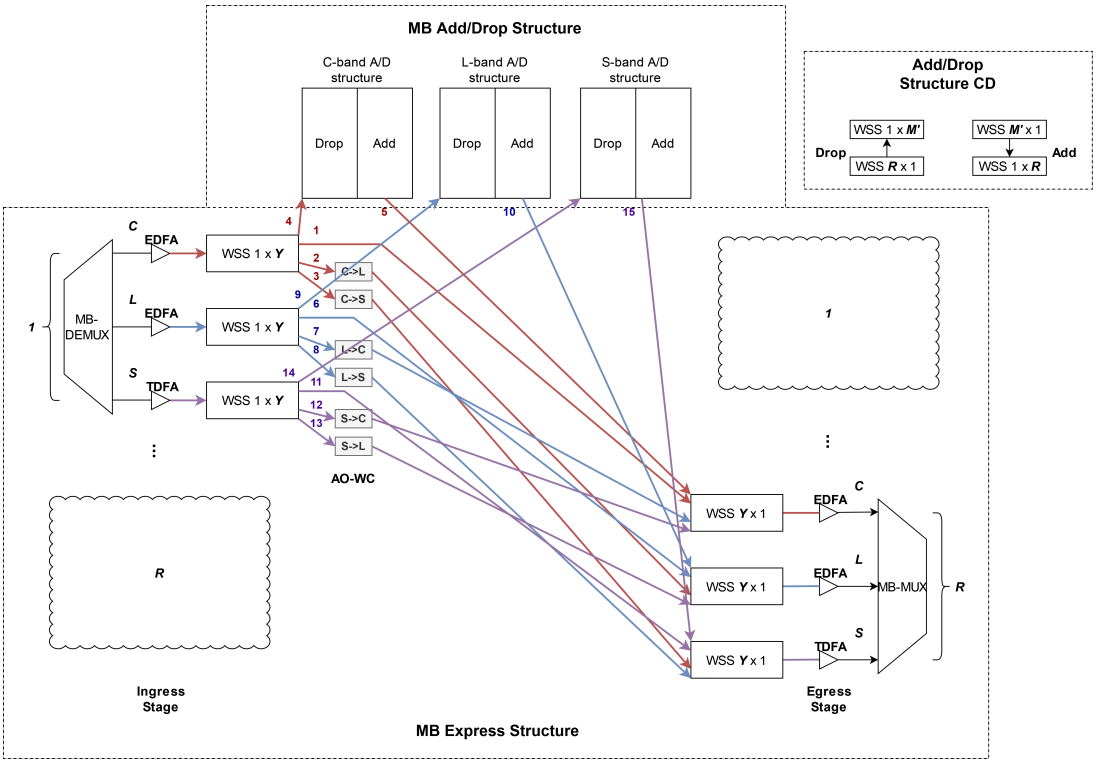

FIGURE 3.2. AO-WC R-degree MB ROADM with the possible express, add and drop paths.

paths 5, 10 and 15 add paths. The components used for each optical path and band and the ILs of the optical paths shown in Figure 3.2, are presented in appendix G. The ILs of the express, add and drop optical paths are computed in the same way as in the baseline architecture, using (3.2), (3.3) and (3.4). Note that the ILs of the AO-WCs are not shown in (3.2), since the losses are compensated by an OA located inside of the AO-WC, as happens also in the common-band architecture [50, 51].

Table 3.3 shows the ILs for the AO-WC architecture, for each direction and band. The ILs shown in Table 3.3 refer only to the losses of the A/D optical paths since they introduce more losses in comparison with the express path as in the baseline architecture. From Tables G4-G8 and 3.3, the optical paths with more ILs are the add and drop paths, since the optical signal crosses 3 WSSs, which introduces more losses for the node. In addition, from Table 3.3, as happens in Table 3.2, the S-band introduces more losses in the node, regardless of the number of directions, due to the high number of S-band channels.

Furthermore, from Table 3.3, the ILs of the add and drop paths for each direction are very similar, with about 1.6 dB (C-band), 1.3 dB (L-band), and 1.1 (S-band) of difference, between a node with 2 and 16 directions.

TABLE 3.3. Insertion losses of the AO-WC architecture for the C-, L- and S-bands and R=2, 3, 4, 8 and 16.

Directions	Insertion losses [dB]		
	C-band	**L-band**	**S-band**
2	18.7	19.9	20.7
3	18.9	20.1	20.8
4	18.9	20.1	20.8
8	19.6	20.6	21.3
16	20.3	21.2	21.8

Figure 3.3 shows a simplified version of the R&S CD common-band architecture presented in Figure 2.7 with the possible optical paths identified by numbers and colours. In this architecture, there are only C-band optical paths between WSSs due to the AO-WCs located before the route WSSs. Note that in the previous chapter, it was considered that the AO-WCs used in the common-band architecture convert all the L- and S-bands channels to the C-band. However, as shown in [50, 51], the AO-WCs used can only switch a number of channels equal to one used in the C-band, due to technology constraints. The AO-WC can only convert 64 out of 87 (L-band) and out of 109 (S-band) channels to the C-band, which restricts the traffic capacity that this node architecture can handle.

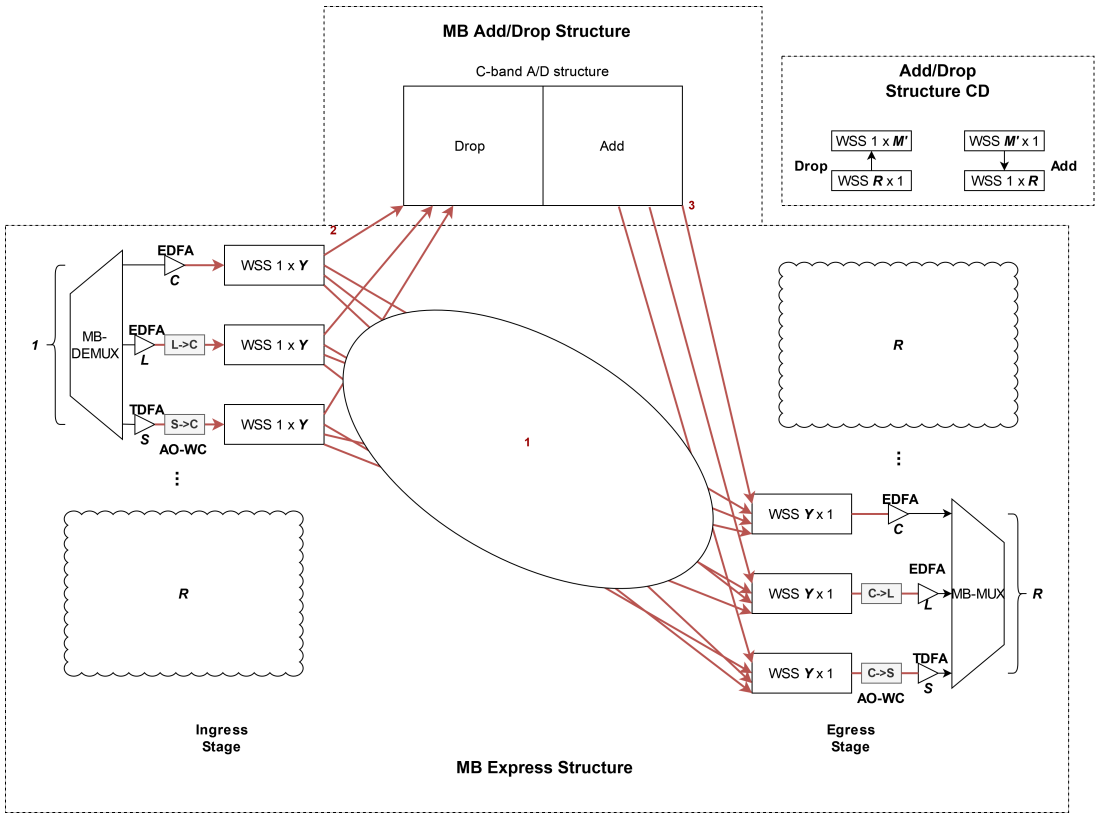

FIGURE 3.3. Common-band R-degree MB ROADM with the possible express, add and drop paths.

From Figure 3.3, the ILs of the optical paths 1, 2 and 3 are computed, respectively, with (3.2), (3.3) and (3.4), although, in this case, the ILs are only calculated for the C-band, with b=C. The components list and corresponding ILs computation are shown in appendix H. Table 3.4 shows only the ILs of the A/D paths, which are the paths with highest losses.

TABLE 3.4. Insertion losses of the common-band architecture for R=2, 3, 4, 8 and 16.

Directions	Insertion losses [dB]
2	19.0
3	19.0
4	19.5
8	20.1
16	21.6

From Table 3.4, the ILs of add and drop paths for each direction are very similar, ranging from 19.0 and 21.6 dB, aproximately 2.6 dB of difference. The ILs of the add and drop paths are higher than the ILs of the express path due to the higher number of WSSs presented in add and drop paths compared to the number of WSSs in the express path (see Tables H1-H3). In addition, the ILs for the common-band architecture for 2 and 3 directions, are the same because of the same components considered in these two directions (see appendix H).

Figure 3.4 shows a simplified version of the R&S CD compact architecture presented in Figure 2.8 with the possible optical paths identified by numbers and colours. In this architecture, the optical path with the colour green indicates a MB path, where optical signals in C-, L- and S-bands are transported in the same optical path. In addition, the remaining colours, red, blue and purple, indicate, respectively, the C-, L- and S-band paths in the A/D structure.

The ILs of the optical paths with the numbers 1-7 are computed with the following equations. The ILs of the express path of the compact architecture (path 1) are given by

$$IL_{express} = IL_{MBWSS,route,1\times Y} + IL_{MBWSS,select,Y\times 1} \tag{3.5}$$

where $IL_{MBWSS,route,1\times Y}$ and $IL_{MBWSS,select,Y\times 1}$ correspond, respectively, to the ILs of the route and select MB WSSs.

The ILs of the add path of the compact architecture (3, 5 and 7 paths) are given by

$$IL_{add,b} = IL_{WSS,add,M'\times 1,b} + IL_{WSS,add,1\times R,b} + IL_{MBWSS,select,Y\times 1} + IL_{MB-MUX} \tag{3.6}$$

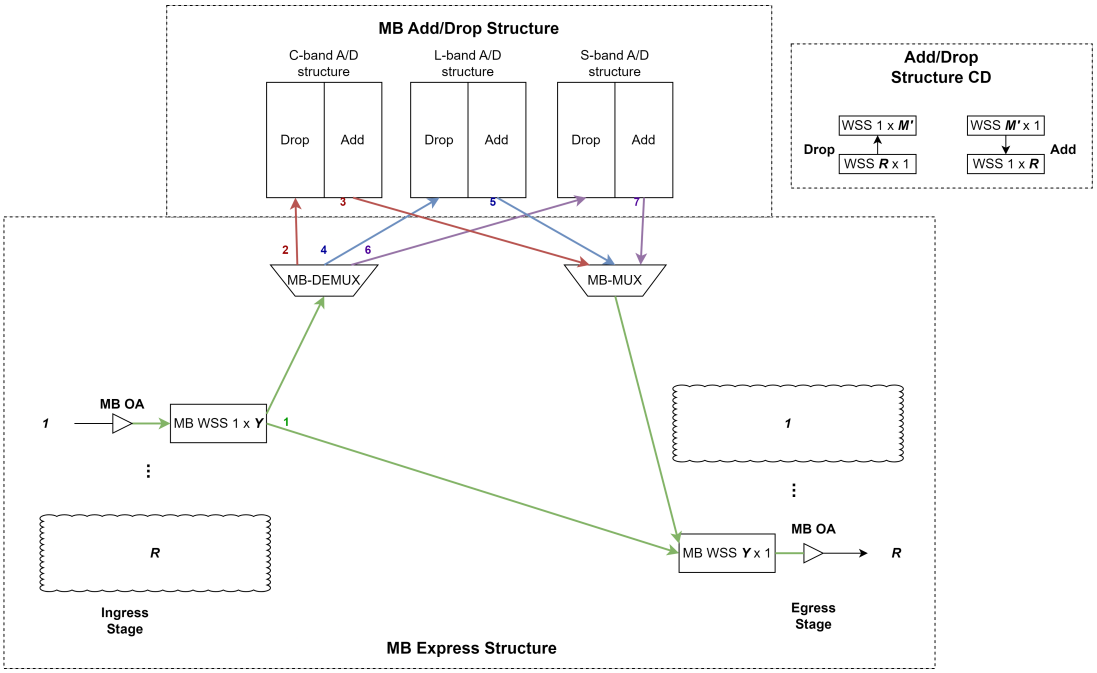

FIGURE 3.4. Compact R-degree MB ROADM with possible express, add and drop paths.

where $IL_{WSS,add,M'\times1,b}$ and $IL_{WSS,add,1\times R,b}$, correspond to ILs of the CD add structure WSSs, and IL_{MB-MUX} corresponds to the ILs of MB-MUX.

The ILs of the drop path of the compact architecture (2, 4 and 6 paths) are given by

$$IL_{drop,b} = IL_{MBWSS,route,1\times Y} + IL_{MB-DEMUX} + IL_{WSS,drop,R\times1,b} + IL_{WSS,drop,1\times M',b} \quad (3.7)$$

where $IL_{WSS,drop,R\times1,b}$ and $IL_{WSS,drop,1\times M',b}$ correspond to the insertion losses of the CD drop structure WSSs, and $IL_{MB-DEMUX}$ corresponds to the ILs of MB-DEMUX. Eqs. (3.6) and (3.7) can be used to calculate the ILs, respectively of the add and drop paths for any of the bands.

TABLE 3.5. Insertion losses of the compact architecture for the C-, L- and S-bands and R=2, 3, 4, 8 and 16.

Directions	Insertion losses [dB]		
	C-band	**L-band**	**S-band**
2	23.6	24.4	24.9
3	23.6	24.4	24.9
4	23.6	24.4	24.9
8	24.0	24.7	25.2
16	24.3	25.0	25.4

The components list used for each direction and band for the possible optical paths, shown in Figure 3.4, and corresponding ILs are presented in appendix I. To calculate the

ILs of each optical path, (3.5), (3.6) and (3.7) are used. Table 3.5 shows the ILs of the A/D paths, for each band and direction of the compact architecture.

From Table 3.5, it can be seen that the band that introduces higher losses for any number of ROADM directions is the S-band, due to the high number of channels in the S-band, as occurs for the baseline and AO-WC architectures. In addition, the ILs of the add and drop paths for each direction are very similar, with about 0.7 dB (C-band), 0.6 dB (L-band) and 0.5 dB (S-band) of difference, between a node with 2 and 16 directions. Comparing the values from Tables I4 and 3.5, the ILs of the add and drop path are higher than the ILs of the express path due to the number of WSSs (3) and MB-DEMUX/MUX, which increases the ILs of the node.

In summary, as observed, through Tables 3.2-3.5, the compact architecture introduces more ILs compared with the remaining MB architectures mostly due to the higher ILs of the MB WSSs, which must route the total number of channels (260) of the 3 bands, but also due to the MB-DEMUX/MUX considered in the A/D structure. The baseline and AO-WC architectures have similar losses since the same components are used in the A/D structure. The main difference in the value of the ILs of these two MB architectures is due to the size of the WSSs used in the express structure. Furthermore, the common-band architecture, as expected, shows the lowest ILs of all MB architectures studied. The use of only C-band components, which introduces less ILs in the node, reduces slightly the common-band architecture ILs in comparison with the ILs of the baseline and AO-WC architectures.

With the results obtained in Tables 3.2-3.5 it was also found that the losses of the MB nodes studied are higher than the ILs of a typically C-band ROADM, with, typically, 18 dB of ILs [53]. The main reason is the higher ILs of the components present in the MB architectures in comparison with C-band ROADM nodes. In the case of this work, it was considered a CD ROADM, where the A/D structure is formed by 2 WSSs in cascade [30, 54]. The ILs of the A/D structure are the sum of the ILs of the 2 WSSs.

In the following sections of this chapter, that further analyze the PLIs impact on MB networks, it was decided to perform this study only for the baseline, common-band and compact architectures. The AO-WC architecture has been discarded from this study due to their disadvantages: very high total node cost and cost-per-bit, as shown in the chapter 2, with no advantages regarding to its ILs, as observed in this chapter.

3.3. Accumulated amplified spontaneous noise power in a C+L+S MB ROADM-based network

The ASE introduced by the OAs along the optical paths in an optical network (named in-line amplifiers) and at the ROADM nodes input/output, respectively, pre- and post-amplifiers needs to be assessed as it degrades the system performance. The in-line and pre-amplifiers are used to compensate the fiber losses, whereas the post-amplifier is used to compensate the ROADM insertion losses. In this section, as an example, the accumulated ASE noise power in some paths of the BT-UK network is calculated, considering the baseline, common-band and compact ROADM node architectures. We perform the analysis by computing the OAs gain, the corresponding ASE noise power contribution generated by each OA and the accumulated ASE noise along the chosen optical paths of the BT-UK network.

In a C+L+S MB network scenario, a typical lightpath with several spans and the respective MB amplifiers is represented in Figure 3.5, where the MB ROADM architecture can be the baseline, common-band or compact architectures. Each MB amplifier consists of independent amplifiers for each band, EDFAs for the C- and L-bands and TDFAs for the S-band. Hence, the MB signal must be separated for amplification with a MB-DEMUX and the reverse operation should be done after amplification using a MB-MUX, as represented in Figure 3.5 [40, 41, 55]. Note that, in the common-band architecture, besides the pre-, in-line and post-amplifiers, OAs inside each AO-WC are considered to compensate the losses introduced by the wavelength-conversion process.

We have assumed in the following analysis that the MB network transports 64 Gbaud signals (value used in most recent systems) using a 75 GHz channel spacing [40, 41]. In this scenario, 64 channels can be transmitted in each band, as depicted in Figure 3.6, which represents the spectrum occupied by the WDM channels in each band and its respective bandgaps (the first bandgap between the C- and L-bands, has 450 GHz, and the second bandgap between the C- and S-bands, 675 GHz). From Figure 3.6, the channel center frequency of the C-, L- and S-bands (channel 32, considering that channel 1 has the lower frequency in each band) is respectively 193.550 THz, 188.300 THz and 199.025 THz, obtained using (2.7).

The pre-amplification gain in dB is given by,

$$G_{pre,b} = L_{sec}\alpha_b + 2IL_{MB-DEMUX/MUX} \tag{3.8}$$

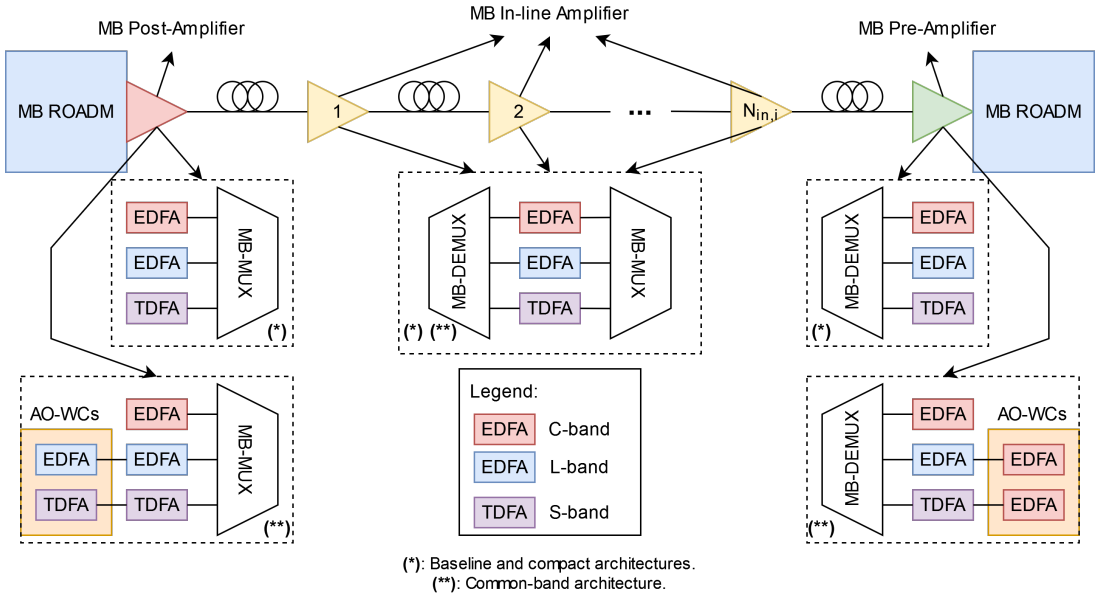

FIGURE 3.5. Amplification scheme in a generic link i with j spans for the baseline, common-band and compact architectures.

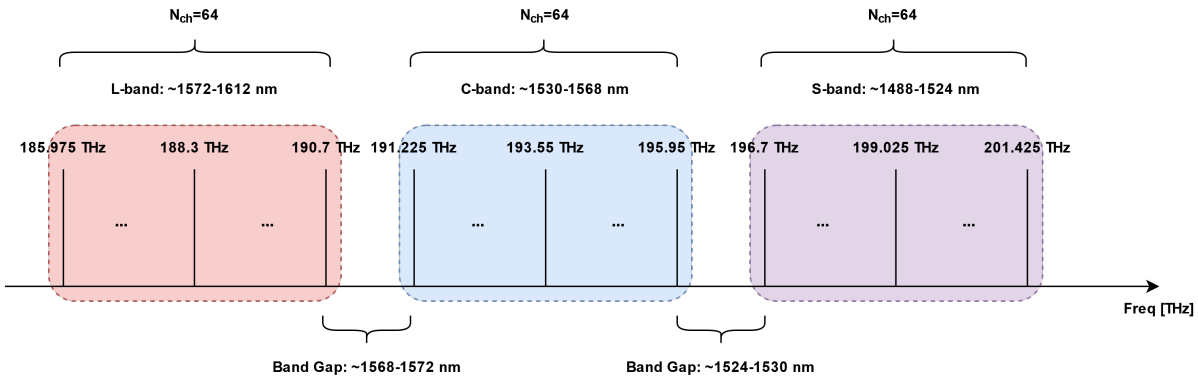

FIGURE 3.6. WDM signal spectrum considered in the C-, L- and S-bands and corresponding ITU-T grid frequencies for a channel spacing of 75 GHz.

where L_{sec} corresponds to the length of each link in km, $IL_{MB-DEMUX/MUX}$ corresponds to the ILs of the MB-DEMUX/MUX and α_b is the fiber attenuation coefficient in dB/km with b=C, L or S, since (3.8) can be used to calculate the pre-amplification gain for any of the bands. If the pre-amplifier gain is greater than the maximum gain of the amplifier, in-line amplifiers must be used in that link. The number of in-line amplifiers in link i is given by,

$$N_{in,i} = \left\lceil \frac{G_{pre,S}}{G_{max}} \right\rceil - 1 \tag{3.9}$$

where G_{max} (dB) is the maximum gain considered for each OA and is assumed equal for all bands. The number of in-line amplifiers computed for the S-band scenario is also used for the other two bands since fiber attenuation coefficient of the S-band is higher than

the ones of the C- and L-bands. It is assumed that each in-line amplifier's characteristics (gain and noise figure) are the same ones used in the pre-amplifier. The gain of each in-line amplifier is given by,

$$G_{in,i,b} = \left\lceil \frac{G_{pre,b}}{N_{in,i}+1} \right\rceil - 1 \tag{3.10}$$

The gain of each post-amplifier for the C-, L- and S-bands is set to 19.8 dB, 20.8 dB and 21.4 dB, respectively, to exactly compensate the path with the worst ILs as calculated in the previous subsection for the baseline architecture (see Table 3.2) and the same reasoning is followed for the common-band and compact architectures. The gain of each post-amplifier of the common-band architecture for the C-, L- and S-bands is set to 21.6 dB (see Table 3.4), and finally, for the compact architecture (see Table 3.5) for the C-, L- and S-bands is set, respectively, to 24.3 dB, 25.0 dB and 25.4 dB.

The next step is to compute the ASE noise power of each OA in each band for each link i and in the case of in-line amplifiers for each j-th span, with the following equations,

$$p_{ASE,m,pre,i,b} = f_{m,b}(g_{pre,i,b} - 1)h\nu_{m,b}B_0 \tag{3.11}$$

$$p_{ASE,m,pos,i,b} = f_{m,b}(g_{pos,i,b} - 1)h\nu_{m,b}B_0 \tag{3.12}$$

$$p_{ASE,m,in,i,j,b} = f_{m,b}(g_{in,i,j,b} - 1)h\nu_{m,b}B_0 \tag{3.13}$$

where $g_{pre,i,b}$, $g_{pos,i,b}$ and $g_{in,i,j,b}$, correspond respectively, to the pre-amplifier, post-amplifier and in-line amplifier gains in linear units for each band, h is the Planck constant, 6.626×10^{-34} J/s, $\nu_{m,b}$ is the nominal frequency of the central WDM channel (m represents the channel number) within each band, B_0 is the optical bandwidth, which we assume equal to the symbol rate, R_s [40, 41], and finally $f_{m,b}$ corresponds to the noise figure of each OA which depends on the band. From Figure 2 of [40], the average noise figure for the C-, L- and S-bands is, respectively, 4.25 dB, 4.68 dB and 6.40 dB.

To further compute the accumulated ASE noise power in a particular optical path of the BT-UK network, it must be observed that the accumulated ASE noise power depends on the chosen path in the common-band and compact architectures. In the baseline architecture, the accumulated ASE noise power is the same for all paths inside the node. In the compact architecture, as switching between bands is possible, the signal amplification can be performed with different noise figures and amplifier gains along the

optical path, which may lead to several possibilities of noise accumulation inside the node. In the common-band architecture, besides the switching between bands, there are also additional amplifiers due to AO-WC losses and the accumulated ASE noise power will depend even more on the chosen path, as it is analyzed next. Figures 3.7 and 3.8 show the possible optical paths inside the common-band architecture node, respectively, for the add/drop and express paths. The numbers shown in Figures 3.7 and 3.8 are only used to designate and distinguish each possible optical path.

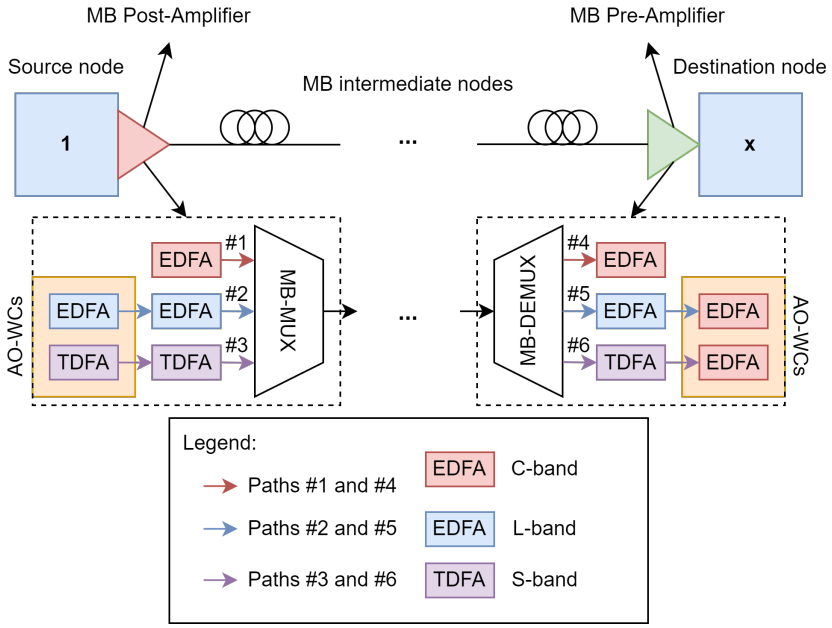

FIGURE 3.7. Add and drop optical paths #1−#6 of the common-band architecture.

From Figure 3.7, it is possible to see that only the L- and S-bands add and drop paths require one additional OA, due to the required wavelength conversion of the optical signals from the L- and S-bands to the C-band and vice versa. In the express paths (Figure 3.8), there are more possibilities for routing the optical signal. For an express path crossing the node in the C-band, there is no need for additional optical amplification. When the signal enters (or leaves) the node in the C-band, coming from the other bands, one additional amplification is required. In all the other cases, two additional OAs must be used to compensate for the wavelength conversion losses. All cases of possible add, drop and express paths and the required additional optical amplification are shown in Table 3.6.

In the following ASE noise power calculations, for the common-band and compact architectures, for simplicity and also because this is the most common scenario in today's

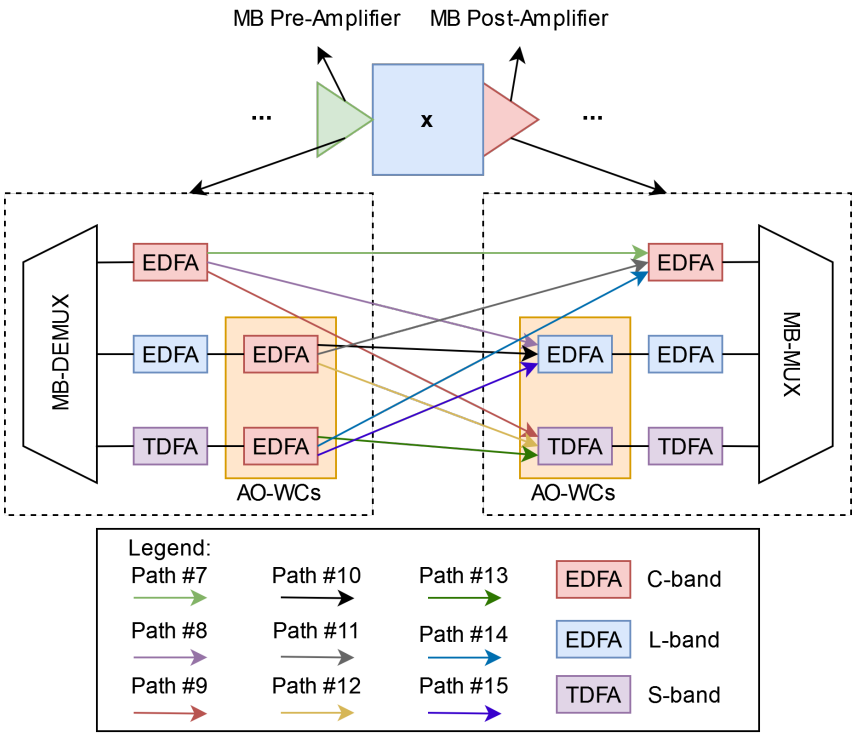

FIGURE 3.8. Express optical paths #7−#15 of the common-band architecture.

TABLE 3.6. Number of AO-WCs crossed for each possible add, drop and express paths in the common-band architecture (Figures 3.7 and 3.8).

Optical path inside the node		**Additional optical amplifiers**
Add paths	Path #1 (C-band only)	-
	Path #2 (L-band only)	1 (L-band EDFA)
	Path #3 (S-band only)	1 (S-band TDFA)
Drop paths	Path #4 (C-band only)	-
	Path #5 (L-band only)	1 (C-band EDFA)
	Path #6 (S-band only)	1 (C-band EDFA)
Express paths	Path #7 (C-band only)	-
	Path #8 (C-band to L-band conversion)	1 (L-band EDFA)
	Path #9 (C-band to S-band conversion)	1 (S-band TDFA)
	Path #10 (L-band only)	2 (L-band EDFA and C-band EDFA)
	Path #11 (L-band to C-band conversion)	1 (C-band EDFA)
	Path #12 (L-band to S-band conversion)	2 (C-band EDFA and S-band TDFA)
	Path #13 (S-band only)	2 (S-band TDFA and C-band EDFA)
	Path #14 (S-band to C-band conversion)	1 (C-band EDFA)
	Path #15 (S-band to L-band conversion)	2(C-band EDFA and L-band EDFA)

optical networks, it is considered that the optical signal enters and leaves the node in the same band, i.e., no switching between bands inside the node is assumed. Hence, only the optical paths #1−#7, #10 and #13 inside the common-band architecture are considered

to perform the ASE noise power calculation. The additional ASE noise power due to the AO-WC losses compensation in link i of the add-drop paths (the path where the signal is inserted in the source node (add) and removed at the destination node (drop)), #2→#5, and #3→#6, and express paths, #10 and #13, is given by,

$$p_{ASE,m,AO-WC,i,b} = f_{m,b}(g_{AO-WC} - 1)h\nu_{m,b}B_0 + f_{m,C}(g_{AO-WC} - 1)h\nu_{m,C}B_0 \qquad (3.14)$$

where g_{AO-WC} corresponds to the conversion gain of AO-WC in linear units, considered 100 (20 dB) [50, 51]. Notice that paths #1, #4 and #7 (C-band paths) do not require additional amplification.

Table 3.7 resumes the parameters considered to compute the ASE noise power for each band and for each link of the BT-UK topology (Figure E1), considering the baseline, common-band and compact architectures. The maximum gain of the OAs presented in Table 3.7 correspond to the maximum gain of the C-, L- and S-bands OAs reported in [56] for commercial devices.

TABLE 3.7. Parameters used to compute the accumulation of ASE noise power for some links of the BT-UK topology.

Parameters	Values		
	C-band	**L-band**	**S-band**
Channel spacing ($\Delta\nu_{ch}$) [GHz] [40, 41]	75		
Fiber attenuation (α_b) [dB/km] [40]	0.185	0.185	0.200
Maximum amplifier gain ($G_{max,b}$) [dB] [56]	30		
AO-WC gain (G_{AO-WC}) [dB] [50, 51]	20		
MB-DEMUX/MUX ILs ($IL_{MB-DEMUX/MUX}$) [dB] [5]	3		
Optical bandwidth (B_0) [GHz] [40, 41]	64		
Post-amplifier gain of baseline node ($G_{pos,i,b}$) [dB]	19.8	20.8	21.4
Post-amplifier gain of common-band node ($G_{pos,i,b}$) [dB]	21.6		
Post-amplifier gain of compact node ($G_{pos,i,b}$) [dB]	24.3	25.0	25.4
Noise figure ($F_{m,b}$) [dB] [40]	4.25	4.68	6.40
Number of channels (N_{ch}) [40, 41]	64	64	64
Central channel	32	32	32
Nominal frequency of the central channel ($\nu_{32,b}$) [THz]	193.550	188.300	199.025

After computing the ASE noise power for each amplifier present in link i, the total ASE noise power of that link, for channel m, for the baseline and compact architectures, is given by,

$$p_{ASE,m,total,i,b} = p_{ASE,pos,i,b} + \sum_{j=1}^{N_{in,i}} p_{ASE,in,i,j,b} + p_{ASE,pre,i,b} \qquad (3.15)$$

To compute the total ASE noise power for the common-band architecture, the ASE noise power from the OAs inside the AO-WC must be considered and, hence,

$$p_{ASE,m,total,i,b} = p_{ASE,pos,i,b} + \sum_{j=1}^{N_{in,i}} p_{ASE,in,i,j,b} + p_{ASE,AO-WC,i,b} + p_{ASE,pre,i,b} \qquad (3.16)$$

where $p_{ASE,AO-WC,i,b}$ is given by (3.14). If the optical path enters and leaves the node in the C-band, $p_{ASE,AO-WC,i,b}$ is zero, and different from zero if the optical path is using the L- or S-band.

Now, the total ASE noise power is going to be computed for three demands in the BT-UK network - demands 1−2, 1−3 and 1−7. Table 3.8 represents for each demand (d), the 5 candidate paths of the BT-UK topology used to compute the accumulation of ASE noise power. Note that the shortest path of demand d=1 has two nodes 20 km apart (and one link, i.e., i=1) and its longest path ($P_{1,5}$), with a 427 km distance, passes through 6 nodes, whereas the shortest path of demand d=3 has 7 nodes 901 km apart (and 6 links, i.e., i=1,...,6) and its longest path ($P_{3,5}$), with a 956 km distance, has 10 nodes, where it is expected to be measured the highest total ASE noise power, due to the total length and number of OAs.

TABLE 3.8. Candidate paths for demand pairs 1−2, 1−3 and 1−7 considered in the BT-UK topology.

Demand *d*	**Candidate Path**
***d*=1**	$P_{1,1}$=[1,2], $P_{1,2}$=[1,9,2], $P_{1,3}$=[1,19,9,2], $P_{1,4}$=[1,19,6,14,2] and $P_{1,5}$=[1,9,19,6,14,2]
***d*=2**	$P_{2,1}$=[1,18,3], $P_{2,2}$=[1,19,17,18,3], $P_{2,3}$=[1,9,19,17,18,3], $P_{2,4}$=[1,2,14,5,3] and $P_{2,5}$=[1,9,2,14,5,3]
***d*=3**	$P_{3,1}$=[1,2,14,5,13,11,7], $P_{3,2}$=[1,9,2,14,5,13,11,7], $P_{3,3}$=[1,19,9,2,14,5,13,11,7], $P_{3,4}$=[1,18,3,5,13,11,7] and $P_{3,5}$=[1,9,19,1,18,3,5,13,11,7]

After defining the candidate paths, the ASE noise power is computed for each band, using the parameters in Table 3.7 and (3.15) or (3.16), depending on the MB architecture considered. In appendix J, the number of in-line amplifiers, the pre-amplifier gain and the ASE noise power for each link used in the chosen candidate paths of the BT-UK network presented in Table 3.8, for the baseline, common-band and compact architectures and for the C-, L- and S-bands are calculated and presented in Tables J1-J3. In addition, appendix J details, as an example, the total ASE noise power calculation steps for path $P_{3,4}$ considering the common-band architecture in the L-band scenario.

Table 3.9 shows the total number of amplifiers used in each candidate path, and the ASE noise power calculated at the end of each candidate path for the C-, L- and S-bands for the baseline and compact architectures, whereas Table 3.10 shows the same results for the common-band architecture.

From Table 3.9, it can be concluded that the total ASE noise power in the baseline architecture, in the C-, L- and S-bands, is lower than the total ASE noise power of the compact architecture due to the lower post-amplifier gains, as expected. The increase

TABLE 3.9. Total ASE noise power for the candidate paths considering the baseline and compact architectures and for C-, L- and S-bands.

Paths	Distance [km]	No. of amplifiers	ASE noise [μW]					
			Baseline			**Compact**		
			C-band	**L-band**	**S-band**	**C-band**	**L-band**	**S-band**
$\boldsymbol{P}_{1,1}$	20	2	2.25	2.99	5.38	6.04	7.59	13.07
$\boldsymbol{P}_{1,2}$	28	4	4.42	5.91	10.63	12.01	15.11	26.01
$\boldsymbol{P}_{1,3}$	32	6	6.57	8.80	15.82	17.95	22.59	38.89
$\boldsymbol{P}_{1,4}$	417	10	21.43	25.34	51.28	36.60	43.73	82.03
$\boldsymbol{P}_{1,5}$	427	12	23.61	28.26	56.52	42.57	51.24	94.96
$\boldsymbol{P}_{2,1}$	262	5	11.71	13.74	27.96	19.30	22.94	43.34
$\boldsymbol{P}_{2,2}$	375	9	27.38	31.73	67.04	42.55	50.12	97.79
$\boldsymbol{P}_{2,3}$	385	11	29.56	34.65	72.27	48.52	57.64	110.72
$\boldsymbol{P}_{2,4}$	399	10	16.29	19.82	38.19	31.46	38.21	68.94
$\boldsymbol{P}_{2,5}$	407	12	18.47	22.74	43.44	37.43	45.72	81.88
$\boldsymbol{P}_{3,1}$	901	16	64.15	72.39	166.38	86.91	99.97	212.51
$\boldsymbol{P}_{3,2}$	909	18	66.33	75.31	171.63	92.88	107.49	225.45
$\boldsymbol{P}_{3,3}$	913	20	68.47	78.19	176.82	98.81	114.97	238.33
$\boldsymbol{P}_{3,4}$	942	15	71.36	80.13	183.85	94.12	107.72	229.98
$\boldsymbol{P}_{3,5}$	956	21	77.81	88.80	199.44	111.94	130.18	268.64

of ASE noise power with distance and within the same fiber band, when comparing the compact architecture with the baseline architecture is practically the same, regardless of the band being C, L or S, and depends essentially on the path chosen. The ASE noise power increases between 1.3 and 2.7 times for all paths presented in Table 3.9. For both architectures, it is also observed that the accumulation of the ASE noise power in the S-band is higher than the ASE noise power accumulated in the other bands due mainly to the higher amplifier noise figure in the S-band, $F_{m,S}$=6.4 dB and the higher central channel frequency, 199.025 THz. Also from Table 3.9, the total ASE noise power in the L-band is approximately between 1.1 and 1.3 times higher than the one calculated in the C-band, and between 2.2 and 2.6 times higher in the S-band compared with C-band, being this behavior practically independent of the node architecture.

In the common-band architecture, there are additional amplifiers in the L- and S-bands due to AO-WCs, which increases the total ASE noise power in these bands. From Table 3.10, it can be concluded that the noise from the additional amplifiers has more impact on paths with shorter length (shorter than 32 km, like paths $P_{1,1}$, $P_{1,2}$ and $P_{1,3}$), than on longer length paths (all remaining paths, which are longer than 250 km), due to the lower pre-amplifier gain compared to the AO-WC gain (20 dB), see appendix J. For the shorter links, when comparing the common-band architecture with the baseline architecture results, the total ASE noise power increases about 1.5, 2.7 and 2.1 times, respectively, in the C-, L- and S-bands. For the longer links, this increase in the C-, L- and S-bands is, respectively, less than 1.3, 2.1 and 1.7, as the additional OAs have less influence.

TABLE 3.10. Total ASE noise power for the candidate paths considering the common-band architecture and for C-, L- and S-bands.

Paths	Distance [km]	No. of amplifiers		ASE noise [μW]		
		C-band	**L- and S-band**	**C-band**	**L-band**	**S-band**
$\boldsymbol{P}_{1,1}$	20	2	4	3.32	8.05	11.43
$\boldsymbol{P}_{1,2}$	28	4	8	6.57	16.02	22.73
$\boldsymbol{P}_{1,3}$	32	6	12	9.78	23.96	33.97
$\boldsymbol{P}_{1,4}$	417	10	18	25.72	45.56	75.47
$\boldsymbol{P}_{1,5}$	427	12	22	28.96	53.53	86.76
$\boldsymbol{P}_{2,1}$	262	5	9	13.85	23.85	40.06
$\boldsymbol{P}_{2,2}$	375	9	17	31.67	51.95	91.23
$\boldsymbol{P}_{2,3}$	385	11	21	34.91	59.92	102.52
$\boldsymbol{P}_{2,4}$	399	10	18	20.57	40.04	62.39
$\boldsymbol{P}_{2,5}$	407	12	22	23.82	48.01	73.69
$\boldsymbol{P}_{3,1}$	901	16	28	70.58	102.72	202.68
$\boldsymbol{P}_{3,2}$	909	18	32	73.83	110.69	213.98
$\boldsymbol{P}_{3,3}$	913	20	36	77.04	118.63	225.22
$\boldsymbol{P}_{3,4}$	942	15	27	77.79	110.46	220.15
$\boldsymbol{P}_{3,5}$	956	21	39	87.45	134.29	253.88

Another observation that comes from the results of Tables 3.9 and 3.10 is that the total ASE noise power obtained for the common-band and compact architectures are quite similar for the L- or S-bands. The common-band architecture has some advantages due to using the C-band, since the ASE noise power is lower than the one found for the compact architecture - less than 0.8 times. In addition, it can be also observed that paths $P_{1,5}$, $P_{2,3}$ and $P_{3,5}$, have the highest ASE noise power accumulated due to the higher number of OAs crossed.

3.4. Nonlinear interference and stimulated Raman scattering in a C+L+S MB ROADM-based network

This section studies the impact of the NLI in a C+L+S MB network, considering the BT-UK topology with the baseline, common-band or compact node architectures and 64 Gbaud signals with different modulation formats, namely, quadrature phase-shift keying (QPSK), 16- and 64- quadrature amplitude modulation (QAM). The calculations of the NLI noise power shown in this section are based on a closed-form approximation of the inter-channel stimulated Raman scattering-Gaussian Noise (ISRS-GN) model that includes the modulation format correction, which is presented in [42, 57]. The NLI formulation presented in [42] corrects the formulation based on the Gaussian modulation proposed in [57], by adding a modulation format correction, which allows to include the influence of the transmitted modulation format on the NLI. The ISRS-GN-model with the modulation format correction formulation allows computing the NLI noise power up to a 15 THz optical bandwidth [37]. The NLI is mainly dependent on the optical fiber

and link characteristics, and independent of the node architecture. The NLI is dependent on the type of fiber chosen, link length, the chosen band (C- or L- or S-band) and mostly on the launch power at the fiber link input [57].

Following [57], the NLI power in μW of channel m in band b and link i is given by,

$$p_{NLI,m,i,b} = \eta_{N_{spans}}(f_m) \cdot p_m^3 \tag{3.17}$$

where $\eta_{N_{spans}}(f_m)$ is the NLI coefficient accounting for the modulation correction and p_m is the launch power of the channel m (with m=1,..., N_{ch}) in link i. The channel m at the nominal central frequency f_m (in lowpass equivalent definition) is typically named the channel of interest (COI) [57]. The NLI coefficient at the end of an optical link at the frequency f_m is computed with [42],

$$\eta_{N_{spans}}(f_m) \approx \sum_{j=1}^{N_{spans}} \left[\frac{p_{m,j}}{p_m}\right]^2 \times [\eta_{SPM,j}(f_m) N_{spans}^{\varepsilon} + \eta_{XPM,j}(f_m)] + \eta_{corr}(f_m) \tag{3.18}$$

where $p_{m,j}$ represents the launch power of channel m in the j-th span and ε is the coherence factor. In this analysis, we have considered, for simplicity, incoherent accumulation of NLI along multiple fiber spans corresponding to ε=0. The coefficient $\eta_{SPM,j}$ computes the self-phase modulation (SPM) contribution to NLI and the coefficient $\eta_{XPM,j}$ deals with the cross-phase modulation (XPM) contribution to NLI in span j, and are given, respectively by [57],

$$\begin{aligned} \eta_{SPM,j}(f_m) \approx \frac{4}{9}\frac{\gamma^2}{B_m^2}\frac{\pi}{\phi_m \overline{\alpha}(2\alpha+\overline{\alpha})} \\ \left[\frac{T_m-\alpha^2}{\alpha}\operatorname{asinh}\left(\frac{\phi_m B_m^2}{\pi\alpha}\right) + \frac{A^2-T_m}{A}\operatorname{asinh}\left(\frac{\phi_m B_m^2}{\pi A}\right)\right] \end{aligned} \tag{3.19}$$

$$\begin{aligned} \eta_{XPM,j}(f_m) \approx \frac{32}{27}\sum_{k=1,k\neq m}^{N_{ch}}\left(\frac{p_{k,j}}{p_{m,j}}\right)^2 \frac{\gamma^2}{B_k \phi_{m,k}\overline{\alpha}(2\alpha+\overline{\alpha})} \\ \left[\frac{T_k-\alpha^2}{\alpha}\operatorname{atan}\left(\frac{\phi_{m,k}B_m}{\alpha}\right) + \frac{A^2-T_k}{A}\operatorname{atan}\left(\frac{\phi_{m,k}B_m}{A}\right)\right] \end{aligned} \tag{3.20}$$

where ϕ_m=$\frac{3}{2}\pi^2(\beta_2 + 2\pi\beta_3 f_m)$, T_m=$(\alpha + \overline{\alpha} - p_{tot}C_r f_m)^2$, A=$\alpha + \overline{\alpha}$, and $\phi_{m,k}$=$2\pi^2(f_k - f_m)[\beta_2 + \pi\beta_3(f_k + f_m)]$. The parameter $\overline{\alpha}$ is a generic attenuation coefficient used to compute the NLI parameter in more general cases, such as the extension to optical bandwidths larger than 15 THz [42]. As in our calculations, we are considering an optical bandwidth of around 15 THz, we set α=$\overline{\alpha}$ in (3.19) and (3.20). Channel m bandwidth is represented by B_m, B_k is the bandwidth of k-th interfering channel, p_{tot} is the total power transmitted at the link input in linear units, C_r represents the Raman gain slope,

and γ is the fiber nonlinear coefficient. Note that in (3.20) and (3.19), the attenuation coefficient (α) should be in converted linear units [Np/m] using,

$$\alpha[\text{Np/m}] = \frac{\alpha[\text{dB/m}]}{4.343} \times 10^{-3} \tag{3.21}$$

The group velocity dispersion parameter β_2 and third order dispersion parameter β_3 are calculated, respectively, with

$$\beta_2 = -\frac{D_{\lambda_0}\lambda_0^2}{2\pi c} \tag{3.22}$$

$$\beta_3 = \frac{\lambda_0^2}{(2\pi c)^2} \times (\lambda_0^2 S_0 + 2\lambda_0 D_{\lambda_0}) \tag{3.23}$$

where c corresponds to the speed of light, D_{λ_0} is the fiber dispersion parameter at the reference wavelength (λ_0) and S_0 corresponds to the dispersion slope at the same reference wavelength.

Equations (3.20) and (3.19) are not dependent on the modulation format, being an approximation that assumes that the transmitted signal follows a Gaussian modulation [57]. The modulation correction factor $\eta_{corr}(f_m)$, shown in (3.18), is given by [42, 58],

$$\eta_{corr,N_{spans}}(f_m) \approx \frac{80}{81}\Phi \sum_{k=1,k\neq m}^{N_{ch}} \left(\frac{p_k}{p_m}\right)^2 \frac{\gamma^2}{B_k} \left\{ \frac{1}{\phi_{m,k}\overline{\alpha}(2\alpha+\overline{\alpha})} \times \left[\frac{T_k - \alpha^2}{\alpha} \operatorname{atan}\left(\frac{\phi_{m,k}B_m}{\alpha}\right) + \frac{A^2 - T_k}{A} \operatorname{atan}\left(\frac{\phi_{m,k}B_m}{A}\right) \right] + \frac{2\pi\tilde{n}T_k}{|\Psi|B_k^2\alpha^2A^2} \left[(2|\Delta f| - B_k)\log\left(\frac{2|\Delta f| - B_k}{2|\Delta f| + B_k}\right) + 2B_k \right] \right\} \tag{3.24}$$

where $\eta_{corr}(f_m)$ corresponds to the correction of the NLI coefficient that is dependent on the channel modulation format [42, 58], with $\Delta f = f_k - f_m$, $\Psi = -4\pi^2[\beta_2 + \pi\beta_3(f_i + f_k)]\overline{L}_{span}$, where $\overline{L}_{span}$ is the average span length of the j-th spans that belong to link i, and $\tilde{n}=0$, if $n=1$, otherwise $\tilde{n}=n$. The excess kurtosis Φ is dependent on the modulation format and its value is shown in Table 3.11 for different modulation formats [42, 58].

TABLE 3.11. Excess kurtosis parameter for various modulation formats.

Modulation format (M)	**Excess kurtosis (Φ)**
QPSK	-1
16-QAM	-0.6800
64-QAM	-0.6190
Gaussian modulation	0

The next step is to compute the NLI noise power for each link, modulation format and band using eqs. (3.18)-(3.24), for the same candidate paths considered in section 3.3. Table 3.12 resumes the parameters considered to compute the NLI power for each

candidate path of the BT-UK topology (Figure E1), considering the baseline, common-band and compact architectures.

TABLE 3.12. Parameters used to compute the NLI noise power along some links of the BT-UK topology.

Parameters	Values
Channel spacing ($\Delta\nu_{ch}$) [GHz]	75
Channel launch power (P_m) [dBm]	0
Total channel launch power (P_{total}) [dBm]	22.83
Dispersion ($D_{\lambda 0}$) [ps/nm/km]	17
Dispersion slope (S_0) [fs/nm^2/km]	67
Reference wavelength (λ_0) [nm]	1550
Raman gain slope (C_r) [1/W/km/THz]	0.028
Nonlinear coefficient (γ) [1/W/km]	1.30
Coherent factor (ε)	0
Fiber attenuation (α) [dB/km] and [Np/m]	0.185 and 4.26×10^{-5}
Group velocity (β_2) [s^2/m]	-2.17×10^{-26}
Third order dispersion parameter (β_3) [s^3/m]	1.45×10^{-40}
Number of channels (N_{ch})	207 (192 data channels)
Optical bandwidth [THz]	15.525
Nominal frequency of the central channel (f_m) [THz]	193.550 (C-band), 188.300 (L-band) and 199.025 (S-band)

The COI considered to calculate the NLI noise power for the C-, L- and S-bands is the central channel of each band, respectively, m=102 (193.550 THz), m=32 (188.300 THz) and m=175 (199.025 THz). Note that the bandgaps between C- and L-bands (6 channels with m=65,...,70) and C- and S-bands (9 channels m=135,...,143) must be considered (as shown in Figure 3.6). To apply eqs. (3.18)-(3.24), considering the bandgap, the launched optical powers in these 15 channels are set to zero. Appendix K details the NLI coefficient with correction factor and NLI noise power computations for each link of the BT-UK topology, for the C-, L- and S-bands and for the modulation formats, QPSK, 16-QAM and 64-QAM, see Tables K1-K3. In appendix K, after computing the NLI power in each link of the candidate paths, as we are considering incoherent accumulation, the total NLI power for each candidate path is simply obtained by summing the NLI powers computed for each link of that candidate path. The total NLI noise power with and without the modulation format correction is computed for the three demand pairs of the BT-UK network, 1−2, 1−3 and 1−7 considered in Table 3.8.

Table 3.13 shows the total number of spans in each candidate path of the three demands considered previously (1−2, 1−3 and 1−7) and the total NLI noise power calculated at the end of each candidate path for the C-, L- and S-bands, calculated with (3.17)

considering the 64-QAM, 16-QAM and QPSK modulation formats. At the end of appendix K, details regarding the NLI calculation steps for path $P_{3,4}$ are given, considering the QPSK modulation format and the L-band scenario.

TABLE 3.13. Total NLI noise power for the candidate paths considering the 64-QAM, 16-QAM and QPSK modulation formats and for the C-, L- and S-bands.

Paths	Distance [km]	Total number of spans	Total NLI noise power [μW] (p_{NLI})								
			64-QAM			**16-QAM**			**QPSK**		
			C-band	**L-band**	**S-band**	**C-band**	**L-band**	**S-band**	**C-band**	**L-band**	**S-band**
$\boldsymbol{P_{1,1}}$	20	1	0.303	0.376	0.222	0.284	0.356	0.207	0.188	0.248	0.128
$\boldsymbol{P_{1,2}}$	28	2	0.606	0.753	0.444	0.569	0.711	0.414	0.375	0.495	0.257
$\boldsymbol{P_{1,3}}$	32	3	0.909	1.129	0.666	0.853	1.067	0.621	0.563	0.743	0.385
$\boldsymbol{P_{1,4}}$	417	6	1.733	2.095	1.346	1.614	1.956	1.258	0.989	1.224	0.793
$\boldsymbol{P_{1,5}}$	427	7	2.036	2.472	1.568	1.898	2.311	1.465	1.176	1.471	0.921
$\boldsymbol{P_{2,1}}$	262	3	0.927	1.124	0.711	0.873	1.061	0.671	0.591	0.734	0.458
$\boldsymbol{P_{2,2}}$	375	5	1.532	1.876	1.155	1.442	1.773	1.085	0.967	1.230	0.714
$\boldsymbol{P_{2,3}}$	385	6	1.835	2.252	1.377	1.726	2.128	1.292	1.154	1.477	0.843
$\boldsymbol{P_{2,4}}$	399	6	1.710	2.066	1.332	1.589	1.924	1.242	0.951	1.176	0.769
$\boldsymbol{P_{2,5}}$	407	7	2.013	2.442	1.554	1.873	2.279	1.449	1.139	1.424	0.897
$\boldsymbol{P_{3,1}}$	901	10	3.112	3.756	2.407	2.935	3.549	2.276	2.009	2.465	1.585
$\boldsymbol{P_{3,2}}$	909	11	3.415	4.132	2.629	3.220	3.905	2.483	2.196	2.712	1.714
$\boldsymbol{P_{3,3}}$	913	12	3.718	4.508	2.851	3.504	4.260	2.690	2.384	2.960	1.842
$\boldsymbol{P_{3,4}}$	942	9	2.934	3.566	2.231	2.788	3.398	2.119	2.024	2.518	1.531
$\boldsymbol{P_{3,5}}$	956	12	3.843	4.694	2.897	3.642	4.465	2.740	2.586	3.261	1.915

From Table 3.13, it is observed that the total NLI noise power in the L-band is higher than in the C- and S-bands due to the ISRS effect, that origins power transfers from high to low frequency channels. For all modulation formats tested, we find out that the total NLI noise power in the L-band increases between 1.2 and 1.3 times when compared to the C-band NLI noise power, and 1.5 and 1.9 times when compared to the NLI noise power in the S-band. In addition, the total NLI noise power is higher when the 64-QAM modulation format is considered, with values closer (about 1.5 times lower) to the Gaussian modulation (see Table L1 in appendix L that shows the total NLI noise power for each candidate path considering the Gaussian modulation), when compared with the other lower modulation formats [42]. The total NLI noise power for the C-, L- and S-bands, increases about 1.1 and 1.4 times when changing the modulation format from, respectively, 16-QAM to 64-QAM and QPSK to 64-QAM, for all paths considered in Table 3.13.

It is observed from Table 3.13 that the candidate path $P_{1,1}$, with only one span, has the lowest total NLI noise power. Paths $P_{1,5}$, and $P_{3,5}$, have the highest total NLI noise power accumulated compared with the other candidate paths, due to the higher number of spans crossed, for all bands and modulation formats. Regarding demand d=2, the path $P_{2,5}$ has the highest total NLI noise power accumulated for the 64-QAM and 16-QAM in

all bands and for the QPSK in the S-band. In the C- and L-bands, for the QPSK, the candidate path $P_{2,3}$ has the highest total NLI noise power accumulated.

Comparing Tables 3.9 and 3.10 with Table 3.13, it is found that in general, the total ASE noise power is much higher when compared to the total NLI noise power, due to the consideration of high gain OAs, with a 30 dB maximum gain, that degrade the candidate paths performance much more significantly than NLI. The total ASE noise power is above between 11.7 and 120.1, 17.4 and 143.8, and 30.4 and 150.2 times the total NLI noise power, respectively for the baseline, common-band and compact architectures, for the QPSK format.

3.5. Optical signal-to-noise ratio in a C+L+S MB ROADM-based network

This section studies the OSNR in a C+L+S MB network, considering the BT-UK topology with the baseline, common-band or compact node architectures and 64 Gbaud QPSK, 16-QAM and 64-QAM signals. The OSNR at the end of a path for channel m, candidate path p and band b is calculated considering the ASE noise and the NLI noise powers, and is given in linear units by,

$$osnr_{total,m,p,b} = \frac{p_m}{\sum_{i=1}^{N_{i,p}} (p_{ASE,m,total,i,b} + p_{NLI,m,i,b})} \tag{3.25}$$

where $N_{i,p}$ corresponds to the number of links in candidate path p, $p_{NLI,m,i,b}$ is computed with (3.17), and the ASE noise power, $p_{ASE,m,total,i,b}$, is computed with (3.15) or (3.16), depending on the MB architecture considered. Note that (3.25) considers exact loss compensation, for channel m, along the candidate path p.

The OSNR calculations presented in Table 3.14 are performed considering a channel launch power of 1 mW (i.e. p_m=1 mW), for the channel frequencies of f_m=193.550 THz (C-band), f_m=188.300 THz (L-band), f_m=193.025 THz (S-band), the 64-QAM, 16-QAM and QPSK modulation formats and the baseline, common-band and compact architectures, for paths $P_{1,1}$, $P_{2,1}$ and $P_{3,1}$.

Table 3.14 shows that the total OSNR is practically independent of the modulation format for each considered path since the OSNR depends essentially on the ASE noise power (since we are using PIC-based WSSs that has higher insertion losses and so the OAs must have higher gains and consequently higher noise) and the ASE noise is the independent of the modulation format as we are using the same symbol rate (64 Gbaud). Regarding the MB node architectures, the total OSNR is higher in the baseline architecture compared with the remaining architectures due to lower total ASE noise power

TABLE 3.14. Total OSNR of the candidate paths $P_{1,1}$, $P_{2,1}$ and $P_{3,1}$, for the C-, L- and S-bands, considering the 64-QAM, 16-QAM and QPSK modulation formats and PIC-based WSSs.

Modulation Format	Paths	Distance [km]	Total optical signal-to-noise ratio [dB] ($OSNR_{total,m,p,b}$)								
			Baseline			**Common-band**			**Compact**		
			C-band	**L-band**	**S-band**	**C-band**	**L-band**	**S-band**	**C-band**	**L-band**	**S-band**
64-QAM	$\boldsymbol{P}_{1,1}$	20	25.94	24.73	22.52	24.41	20.75	19.34	21.98	20.99	18.76
	$\boldsymbol{P}_{2,1}$	262	18.98	18.28	15.43	18.30	16.03	13.90	16.94	16.19	13.56
	$\boldsymbol{P}_{3,1}$	901	11.72	11.18	7.73	11.33	9.73	6.88	10.46	9.84	6.68
16-QAM	$\boldsymbol{P}_{1,1}$	20	25.97	24.75	22.53	24.44	20.76	19.34	21.99	21.00	18.77
	$\boldsymbol{P}_{2,1}$	262	19.00	18.30	15.43	18.32	16.04	13.90	16.95	16.20	13.56
	$\boldsymbol{P}_{3,1}$	901	11.73	11.20	7.73	11.34	9.74	6.88	10.47	9.85	6.68
QPSK	$\boldsymbol{P}_{1,1}$	20	26.14	24.89	22.59	24.55	20.81	19.37	22.06	21.06	18.80
	$\boldsymbol{P}_{2,1}$	262	19.10	18.39	15.46	18.40	16.09	13.92	17.01	16.26	13.59
	$\boldsymbol{P}_{3,1}$	901	11.79	11.26	7.75	11.39	9.78	6.90	10.51	9.90	6.69

in each candidate path (see Tables 3.9 and 3.10). In the C-band, the total OSNR of the baseline architecture is at least 0.4 dB higher compared with the common-band architecture in the C-band. For the L- and S-bands, the total OSNR difference between baseline and common-band architectures is at least approximately higher, respectively, 1.5 dB and 0.9 dB. These lower OSNR differences occur always for the longer path $P_{3,1}$. The minimum difference of the total OSNR of the baseline and compact architectures in C-, L- and S-bands, is at least 1.0 dB. The maximum OSNR difference between the latter architectures reaches 4 dB for path $P_{1,1}$ in the C-band. The total OSNRs of the common-band and compact architectures are quite similar (less than 0.6 dB difference) in the L- and S-bands due to the additional ASE noise coming from the OAs within the AO-WCs in the common-band architecture. Without this additional amplification in the AO-WCs, the common-band architecture in the L- and S- bands should have total OSNRs closer to the ones obtained for the baseline architecture, since the ILs of the baseline and common-band nodes are similar, and are much lower than compact node architecture ILs. As expected, the total OSNR is much higher for the shorter length candidate path $P_{1,1}$, lower for the longer candidate path $P_{2,1}$, and much reduced for the 901 km path $P_{3,1}$. In particular, the total OSNRs difference between the OSNR obtained for $P_{1,1}$ and $P_{3,1}$, is at least 11 dB.

Next, the performance of an optical channel used for a specific modulation format is assessed using the RM computed in dB, with [53, 59],

$$RM_p = OSNR_{total,m,p,b} - ROSNR - SM_p \tag{3.26}$$

where $ROSNR$ is the required OSNR (ROSNR) and SM_p is the safety margin. Table 3.15 shows the practical ROSNR in dB, for the 64-QAM, 16-QAM and QPSK modulation

formats, a pre-forward error correction (FEC) bit error rate (BER) of 2×10^{-2} considering a bandwidth equal to the symbol rate [59, 60]. Note that the ROSNRs presented in [59, 60] are for the reference optical bandwidth of 12.5 GHz, so there is a difference of 7.1 dB ($10\log_{10}(\frac{64}{12.5})$) to the values presented in Table 3.15 (taken from [59, 60]), for the signal bandwidth.

TABLE 3.15. Practical ROSNR for QPSK, 16-QAM and 64-QAM modulation formats.

Modulation format (M)	Practical ROSNR in the reference bandwidth of 12.5 GHz [dB]	Practical ROSNR in the signal bandwidth [dB]
QPSK	16	8.9
16-QAM	24	16.9
64-QAM	30	22.9

The safety margin (SM) takes into account the additional OSNR degradations resulting from aging, optical filtering, crosstalk, and other performance degrading effects and is given by [53, 59],

$$SM_p = 0.05 \times (N_{OLAs} + N_{ROADMs}) + P_{filt} + P_{xtalk} \tag{3.27}$$

where N_{OLAs} and N_{ROADMs} are, respectively, the number of OAs and the number of ROADMs, in the candidate path p considered. This safety margin also considers the optical filtering penalty (P_{filt}) and the crosstalk penalty (P_{xtalk}). The crosstalk penalty is usually between 0 and 0.5 dB, and depends on the carrier spacing [53]. In this work, a worst-case crosstalk penalty of 0.5 dB is considered. The optical filtering penalty depends on the number of WSSs traversed by the optical signal in candidate path p. Hence, the number of PIC-based WSSs present in a candidate path is given by,

$$N_{WSS} = 2 \times N_{ROADMs} + 2 \tag{3.28}$$

It is assumed that the optical filtering penalty values presented in [61] (Figure 4) for the 16-QAM and QPSK modulation formats can be used in this work, since the ratio $\Delta\nu_{ch}/B_0$ is similar ([61] use 33 GHz and 28 Gbaud and we use 75 GHz and 64 Gbaud). The candidate paths $P_{1,1}$, $P_{2,1}$ and $P_{3,1}$ have respectively, N_{WSS}=6, N_{WSS}=8 and N_{WSS}=16. The corresponding filtering penalties are 1 dB for paths $P_{1,1}$ and $P_{2,1}$ for all modulation formats and by 3 dB (QPSK) and 4 dB (16-QAM and 64-QAM) for path $P_{3,1}$ [59, 61]. In these results, we have considered that the filtering penalties of the 64-QAM are equal to the penalties observed for the 16-QAM and QPSK, for less than 10 cascaded WSSs [59].

Table 3.16 shows the modulation formats assigned for the three candidate paths $P_{1,1}$, $P_{2,1}$ and $P_{3,1}$ considered in the BT-UK network, for the C-, L-, and S-bands, as well as the number of nodes and amplifiers crossed, the safety margin, the total OSNR and the residual margin computed for each of these candidate paths. In order to assign the modulation format to a particular candidate path, the highest modulation format is tried first. If the respective residual margin is less than zero, then a lower modulation format is used; if none of the modulation formats leads to a positive residual margin, that candidate path cannot be used. Note that the larger the modulation format, the more capacity can be transported, and the lower cost-per-bit is attained. The values of total OSNR and residual margin, which do not accomplish the 0 dB residual margin, are obtained for the lower modulation format, the QPSK, and are shown in red in Table 3.16.

TABLE 3.16. Residual margin of the optical paths for the three candidate paths considered in the BT-UK network, for the C-, L-, and S-bands, considering PIC-based WSSs.

Band	Architecture	Candidate Path	Number of optical amplifiers (N_{OLAs})	Number of ROADMs (N_{ROADMs})	Safety Margin (SM) [dB]	Total OSNR [dB]	Residual Margin (RM) [dB]	Modulation format
C-band	**Baseline**	$P_{1,1}$	2	2	1.70	25.94	1.34	64-QAM
		$P_{2,1}$	5	3	1.90	19.00	0.20	16-QAM
		$P_{3,1}$	16	7	4.65	11.79	-1.76	QPSK
	Common-band	$P_{1,1}$	2	2	1.70	24.44	5.84	16-QAM
		$P_{2,1}$	5	3	1.90	18.40	7.60	QPSK
		$P_{3,1}$	16	7	4.65	11.39	-2.16	QPSK
	Compact	$P_{1,1}$	2	2	1.70	21.99	3.39	16-QAM
		$P_{2,1}$	5	3	1.90	17.01	6.21	QPSK
		$P_{3,1}$	16	7	4.65	10.51	-3.04	QPSK
L-band	**Baseline**	$P_{1,1}$	2	2	1.70	24.73	0.13	64-QAM
		$P_{2,1}$	5	3	1.90	18.39	7.59	QPSK
		$P_{3,1}$	16	7	4.65	11.26	-2.29	QPSK
	Common-band	$P_{1,1}$	4	2	1.80	20.76	2.06	16-QAM
		$P_{2,1}$	9	3	2.10	16.09	5.09	QPSK
		$P_{3,1}$	28	7	5.25	9.78	-4.37	QPSK
	Compact	$P_{1,1}$	2	2	1.70	21.00	2.40	16-QAM
		$P_{2,1}$	5	3	1.90	16.26	5.46	QPSK
		$P_{3,1}$	16	7	4.65	9.90	-3.65	QPSK
S-band	**Baseline**	$P_{1,1}$	2	2	1.70	22.53	3.93	16-QAM
		$P_{2,1}$	5	3	1.90	15.46	4.66	QPSK
		$P_{3,1}$	16	7	4.65	7.75	-5.80	QPSK
	Common-band	$P_{1,1}$	4	2	1.80	19.34	0.64	16-QAM
		$P_{2,1}$	9	3	2.10	13.92	2.92	QPSK
		$P_{3,1}$	28	7	5.25	6.90	-7.25	QPSK
	Compact	$P_{1,1}$	2	2	1.70	18.77	0.17	16-QAM
		$P_{2,1}$	5	3	1.90	13.59	2.79	QPSK
		$P_{3,1}$	16	7	4.65	6.69	-6.86	QPSK

From Table 3.16, for the candidate path $P_{3,1}$, as the residual margin is negative due to the lower total OSNR, it is not possible to assign a modulation format in any of the bands and with any node architecture. The candidate path $P_{3,1}$ is 901 km long, and due to the

high number of OAs and ROADMs, the PLIs degradation is enhanced in this path and the residual margin is not met. Signal transmission in this path would only be possible if optical regeneration is placed along the path [41]. Regarding the node architectures, the baseline architecture for the candidate paths $P_{1,1}$ and $P_{2,1}$ has higher modulation formats assigned than the common-band and compact architectures due to higher total OSNR. In particular, for candidate path $P_{1,1}$ in C- and L-bands, the highest modulation format, 64-QAM is assigned, allowing to increase the transport capacity and decrease the cost-per-bit in this link. The common-band and compact architectures have the same modulation formats assigned for the candidate paths $P_{1,1}$ and $P_{2,1}$.

Finally, the optimal power per channel that maximizes the OSNR for each band and MB node architecture is computed and compared with other works [40, 41]. The optimal power, in W, for channel m in band b and link i is given by [62],

$$p_{ch,opt,m,i,b} = \sqrt[3]{\frac{p_{ASE,total,i,b}}{2\eta_{N_{spans}}}} \tag{3.29}$$

where $p_{ASE,total,i,b}$ is given by (3.15) or (3.16) and $\eta_{N_{spans}}$ is given by (3.18). Note that the optimal channel power is obtained when $p_{ASE,total,i,b} = 2p_{NLI,m,i,b}$. The optimal power per channel is going to be computed, as an example, for the (2−14) link of BT-UK topology with 127 km, considering the baseline, common-band and compact architectures, the C-, L- and S-bands, and the QPSK, 16-QAM and 64-QAM modulation formats. This link (2−14) belongs to some of the candidate paths of demands d=1, d=2, and d=3. Table 3.17 presents the optimal power for the center channel in each band in dBm, for the baseline, common-band and compact architectures and the QPSK, 16-QAM and 64-QAM modulation formats, considering link (2−14).

TABLE 3.17. Optimal power per channel for the baseline, common-band and compact architectures, the C-, L- and S-bands and the link (2−14), considering PIC-based WSSs.

Architecture	Optimal power per channel [dBm] ($P_{ch,opt,m,i,b}$)								
	C-band			**L-band**			**S-band**		
	64-QAM	16-QAM	QPSK	64-QAM	16-QAM	QPSK	64-QAM	16-QAM	QPSK
Baseline	1.68	1.81	2.80	1.75	1.88	2.90	3.19	3.31	4.11
Common-band	2.08	2.21	3.21	2.90	3.04	4.06	4.03	4.14	4.95
Compact	2.78	2.91	3.90	2.83	2.96	3.98	4.19	4.31	5.11

Table 3.17 shows that the optimal channel power in the S-band is at least 1 dB higher than the remaining bands due to the higher ASE noise power and lower NLI noise power in this band, in relation to the other bands. In addition, the baseline architecture needs less optimal channel power to achieve the best OSNR compared with the remaining MB

architectures. The compact architecture requires a slightly higher optimal channel power compared with the remaining node architectures in C-band due to higher post-amplifier gain which that enhances ASE noise power. Table 3.17 also shows that the optimal channel powers of the compact and common-band architectures in the L- and S-bands are quite similar.

Comparing the values from Table 3.17 with the optimal channel powers obtained in other works [40, 41], it is possible to see that the values obtained in this work are higher: -1 dBm (C-, L- and S-bands) [40], and 0.6 dBm (C-band), 1 dBm (L-band) and 1.4 dBm and 1.7 dBm (for S1 and S2 within the S-band, respectively) [41]. This behavior happens because in this work the ASE noise power is much higher than the NLI noise power, due to higher ILs of the components present inside of each MB architecture and to the maximum gain considered for the OAs.

3.6. C+L+S MB ROADM-based network with LCoS technology

In this section, we consider the LCoS technology, instead of the PIC technology considered in the previous sections, for building the WSSs in the A/D structure and in the express structure of the MB ROADM architectures. The main difference is that the CD A/D structure with the LCoS technology is based on a single $N \times R$ WSS [63], instead of a cascade of two WSSs used in the PIC technology, reducing the insertion losses of the A/D structure. In this way, the reference values considered for the ILs of each MB LCoS WSS for the C-, L- and S-bands are, respectively, 5 dB, 5 dB and 6 dB, and the ILs of the C+L+S MB WSS are 6 dB [45, 49]. Table 3.18 shows the ILs computed for the baseline, common-band and compact architectures nodes, for each band, considering a R&S architecture and a CD A/D structure. Note that, for LCoS WSSs, we are assuming that the ILs are independent of the node degree and that the ILs of the A/D and express paths are the same, since the ILs of the $N \times R$ WSS of the CD A/D structure are the same as the ILs of the $1 \times Y$ WSSs and $Y \times 1$ WSSs of the R&S stages.

TABLE 3.18. Insertion losses of the baseline, common-band and compact architectures for the C-, L- and S-bands, considering LCoS WSSs.

Architecture	Insertion losses [dB]		
	C-band	**L-band**	**S-band**
Baseline	10	10	12
Common-band	10		
Compact	14	14	15

From Table 3.18, it can be observed that the ILs of the baseline, common-band and compact architectures, are the same for the C- and L-bands and show a small increase

for the S-band (2 dB for the baseline and 1 dB for the compact architectures). The compact architecture has higher ILs due to the extra loss of the MB-DEMUX/MUX (3 dB) and the common-band architecture has less ILs due to the use of only C-band WSSs. Comparing the ILs obtained in Tables 3.2-3.5 with Table 3.18, it is possible to see that the ILs for all the studied architectures using LCoS WSSs are at least 8.6 dB lower than the corresponding ILs considered for the PIC WSSs.

The next step is to compute the total OSNR considering a channel launch power of 1 mW (i.e. p_m=1 mW), for the LCoS technology-based WSS, for the baseline, common-band and compact architectures, the QPSK, 16-QAM and 64-QAM modulation formats and the C-, L- and S-bands. The corresponding OSNRs are shown in Table 3.19.

TABLE 3.19. Total OSNR of the candidate paths, for the C-, L- and S-bands, considering the 64-QAM, 16-QAM and QPSK modulation formats and LCoS-based WSSs.

Modulation Format	Paths	Distance [km]	Total optical signal-to-noise ratio [dB] ($OSNR_{total,m,p,b}$)								
			Baseline			**Common-band**			**Compact**		
			C-band	**L-band**	**S-band**	**C-band**	**L-band**	**S-band**	**C-band**	**L-band**	**S-band**
64-QAM	$P_{1,1}$	20	31.67	31.06	29.58	31.67	22.78	21.74	29.95	29.44	27.74
	$P_{2,1}$	262	20.50	20.14	17.06	20.50	17.29	15.11	20.19	19.83	16.81
	$P_{3,1}$	901	12.51	12.17	8.48	12.51	10.58	7.56	12.36	12.02	8.38
16-QAM	$P_{1,1}$	20	31.78	31.18	29.64	31.78	22.80	21.75	30.03	29.52	27.78
	$P_{2,1}$	262	20.53	20.16	17.07	20.53	17.31	15.11	20.22	19.86	16.82
	$P_{3,1}$	901	12.53	12.19	8.49	12.53	10.59	7.56	12.38	12.04	8.38
QPSK	$P_{1,1}$	20	32.47	31.84	29.97	32.47	22.89	21.80	30.48	29.96	27.99
	$P_{2,1}$	262	20.67	20.31	17.12	20.67	17.38	15.14	20.35	19.99	16.87
	$P_{3,1}$	901	12.60	12.27	8.51	12.60	10.64	7.58	12.45	12.11	8.40

Comparing Tables 3.19 and 3.14, it is possible to see that the total OSNR is much higher when considering LCoS WSSs in the MB nodes, due to their much lower ILs. In this case, the baseline architecture considering LCoS WSSs, has at most a 7.4 dB difference, compared with the total OSNR obtained for the same architecture considering PIC WSSs. In the common-band architecture, the difference is slightly higher, 7.9 dB, when comparing the LCoS WSS with PIC-based WSSs. For the compact architecture, the difference reaches a 9.2 dB maximum for the three modulation formats. Another conclusion is that the additional noise from the OAs inside the AO-WCs has a higher impact on the OSNR degradation since the post-amplifier gain is reduced with the LCoS WSSs. In the LCoS WSS scenario, for path $P_{1,1}$, the total OSNR for the common-band architecture in C-band is at least 8.9 dB higher than the OSNRs obtained in the L-band. When changing from the C- to S-band, the total OSNR difference becomes at least 9.9 dB higher, for this 20 km path. For path $P_{1,1}$, for the common-band architecture using

PIC WSSs, the total OSNR in C-band is only 3.7 dB and 5.2 dB higher, when compared to, respectively, the L- and S-bands OSNR.

As in Table 3.16, Table 3.20 shows the safety margin, the total OSNR, residual margin and the modulation formats assignment obtained for the candidate paths $P_{1,1}$, $P_{2,1}$ and $P_{3,1}$, but, in this case, considering LCoS-based WSSs, instead of PIC-based WSSs. For LCoS WSSs, the number of WSSs present in each candidate path is twice the number of crossed ROADMs.

TABLE 3.20. Residual margin of the optical paths for the three candidate paths considered in the BT-UK network, for the C-, L-, and S-bands, considering LCoS-based WSSs.

Band	Architecture	Candidate Path	Number of optical amplifiers (N_{OLAs})	Number of ROADMs (N_{ROADMs})	Safety Margin (SM) [dB]	Total OSNR [dB]	Residual Margin (RM) [dB]	Modulation format
C-band	**Baseline**	$P_{1,1}$	2	2	1.70	31.67	7.07	64-QAM
		$P_{2,1}$	5	3	1.90	20.53	1.73	16-QAM
		$P_{3,1}$	16	7	4.65	12.60	-0.95	QPSK
	Common-band	$P_{1,1}$	2	2	1.70	31.67	7.07	64-QAM
		$P_{2,1}$	5	3	1.90	20.53	1.73	16-QAM
		$P_{3,1}$	16	7	4.65	12.60	-0.95	QPSK
	Compact	$P_{1,1}$	2	2	1.70	29.95	5.35	64-QAM
		$P_{2,1}$	5	3	1.90	20.22	1.42	16-QAM
		$P_{3,1}$	16	7	4.65	12.45	-1.10	QPSK
L-band	**Baseline**	$P_{1,1}$	2	2	1.70	31.06	6.46	64-QAM
		$P_{2,1}$	5	3	1.90	20.16	1.36	16-QAM
		$P_{3,1}$	16	7	4.65	12.27	-1.28	QPSK
	Common-band	$P_{1,1}$	4	2	1.80	22.80	4.10	16-QAM
		$P_{2,1}$	9	3	2.10	17.38	6.38	QPSK
		$P_{3,1}$	28	7	5.25	10.64	-3.51	QPSK
	Compact	$P_{1,1}$	2	2	1.70	29.44	4.84	64-QAM
		$P_{2,1}$	5	3	1.90	19.86	1.06	16-QAM
		$P_{3,1}$	16	7	4.65	12.11	-1.44	QPSK
S-band	**Baseline**	$P_{1,1}$	2	2	1.70	29.58	4.98	64-QAM
		$P_{2,1}$	5	3	1.90	17.12	6.32	QPSK
		$P_{3,1}$	16	7	4.65	8.51	-5.04	QPSK
	Common-band	$P_{1,1}$	4	2	1.80	21.75	3.05	16-QAM
		$P_{2,1}$	9	3	2.10	15.14	4.14	QPSK
		$P_{3,1}$	28	7	5.25	7.58	-6.57	QPSK
	Compact	$P_{1,1}$	2	2	1.70	27.74	3.14	64-QAM
		$P_{2,1}$	5	3	1.90	16.87	6.07	QPSK
		$P_{3,1}$	16	7	4.65	8.40	-5.15	QPSK

By comparing Tables 3.20 with 3.16, it is possible to see that with higher OSNR (due to lower ILs of LCoS WSSs), higher modulation formats can be assigned to more candidate paths, which increases the transport capacity, and reduces the cost-per-bit. In particular, it is possible to see that the higher modulation format (64-QAM) can be assigned to node architectures other than the baseline architecture when considering LCoS WSSs. For the candidate path $P_{1,1}$, the 64-QAM can also be assigned, in the baseline (S-band), common-band (C-band) and compact (C-, L- and S-bands) architectures, due

to higher total OSNR that can be achieved with the lower ILs of LCoS WSS, while with PIC-based WSSs, only for the baseline architecture in the C- and L-bands, it was possible to assign the 64-QAM. Furthermore, with LCoS WSSs, the candidate path $P_{2,1}$, for baseline (L-band), common-band (C-band) and compact architectures (C-, L-bands), has the 16-QAM modulation format assigned, instead of the QPSK obtained with PIC WSSs in Table 3.16. The candidate path $P_{3,1}$ still cannot be assigned due to the severe PLIs degradation along this path.

Similarly to what is done in Table 3.17, the optimal channel power for the link (2−14) of the BT-UK topology is computed considering LCoS WSSs in the MBs architectures, and the results are shown in Table 3.21.

TABLE 3.21. Optimal power per channel for the baseline, common-band and compact architectures, for C-, L- and S-bands and for the link (2−14), considering LCoS-based WSSs.

Architecture	Optimal power per channel [dBm] ($P_{ch,opt,m,i,b}$)								
	C-band			**L-band**			**S-band**		
	64-QAM	16-QAM	QPSK	64-QAM	16-QAM	QPSK	64-QAM	16-QAM	QPSK
Baseline	0.48	0.61	1.61	0.34	0.47	1.49	1.92	2.04	2.84
Common-band	0.48	0.61	1.61	2.30	2.43	3.45	3.38	3.50	4.30
Compact	0.78	0.91	1.90	0.63	0.77	1.79	2.17	2.28	3.08

Comparing the values of Table 3.21 with the optimal channel power obtained in Table 3.17, it is possible to see that the optimal channel power, considering LCoS WSSs, is significantly lower than the one obtained with PIC-based WSSs, due to their higher ILs. For example, the optimal channel power considering LCoS WSSs is at least 1.2 dB lower, for all architectures and modulation formats considered when compared to the optimal channel power obtained with PIC-based WSSs. The only exception is obtained for the common-band architecture in the L- and S-bands, where the optimal power reduction is only 0.6 dB due to the additional amplifiers present in the AO-WCs.

Comparing the values from Table 3.21 with the optimal channel power obtained in other works [40, 41], it is possible to see that with LCoS-based WSSs, the values obtained are closer to the optimal channel powers presented in other works (shown in the previous section).

3.7. Conclusions

This chapter has assessed and analyzed the impact of several PLIs in a C+L+S MB ROADM-based network, considering the three different MB ROADM architectures: baseline, common-band and compact architectures. A detailed analysis of the total OSNR,

including the total ASE and NLI noise powers was performed for three demands in the BT-UK topology, with five possible candidate paths in each demand and a discussion concerning the most robust node architecture is presented. Finally, the total OSNR was recomputed for the three MB ROADM architectures, considering the LCoS technology for the WSSs, instead of the PIC technology.

It has been shown that the total ASE noise power is higher in candidate paths with a higher number of OAs and longer length, as obtained for path $P_{3,5}$. The common-band architecture seems a better option in relation to the compact architecture, when considering the C-band due to the lower ASE noise power generated by C-band components. However, when the L- and S-bands are considered, the common-band architecture has the disadvantage of using additional OAs due to AO-WCs losses, leading to a similar accumulation of ASE noise power to the compact architecture. The baseline architecture due to a lower post-amplifier gain is the best option in terms of lower ASE noise power.

The total NLI noise power is higher in the L-band, when compared with the C- and S-bands due to the ISRS effect and is independent of the node architecture. For the QPSK modulation format, the total NLI noise power is lower than the one obtained for the other modulation formats. For all studies performed, the total ASE noise power obtained for each architecture and band, is much higher than the total NLI noise power, due to the use of high-gain OAs considered.

Finally, the total OSNR was computed for the three MB architectures and bands, considering PIC and LCoS-based WSSs. It has been shown that the total OSNR considering only PIC WSSs is much lower than the total OSNR obtained with LCoS WSSs due to the higher ILs of the PIC WSSs. The common-band and compact architectures lead to a lower total OSNR than the OSNR calculated for the baseline architecture, considering both PIC and LCoS WSSs, requiring the assignment of lower modulation formats, lower transport capacity and higher cost-per-bit. The baseline architecture allows higher modulation formats to be assigned, ensuring more transport capacity and lower cost-per-bit, but at the expense of reduced switching capability.

CHAPTER 4

C+L+S multi-band network design considering the impact of physical layer impairments and node architecture

4.1. Introduction

The use of the L- and S-bands, beyond the C-band, in network planning tools is a challenge due to the effects of PLIs, in particular, the ISRS effect [7–9]. The main goal of this chapter is to develop a simulator able to design a C+L+S network taking into account, not only the impact of the PLIs but also the impact of the node architecture. This topic has been analyzed in [32], but the authors explore only the use of the C+L bands and consider only the baseline node architecture to analyze the BT-UK and Indian networks performance. In [9], the authors study the use of the C+L+S bands with two node architectures (baseline and common-band), considering only the NSFNET topology. In this chapter, we extend these analyses, not only in the number of different node architectures - we consider three, baseline, common-band and compact, but also in the number of network topologies studied - we consider two, a large network (CONUS-60) and a small network (BT-UK). The analysis in this chapter is focused on the network capacity and also on the cost-per-bit and it is our goal to find out what is the most cost-effective node, as well as the node that provides the higher network capacity.

Firstly, section 4.2 presents the main physical and logical characteristics of the network topologies considered, BT-UK and CONUS-60 networks. Next, in section 4.3, it is presented the C+L+S MB network simulator developed in Matlab to solve the RMSA problem with the impact of PLIs and node architecture. This simulator follows the statistical network assessment process (SNAP) model [41, 64]. Section 4.4 studies the impact of the PLIs on the number of available optical paths in the BT-UK and CONUS-60 topologies. Section 4.5 presents and discusses the RMSA results obtained using the simulator described in section 4.3. The total network capacity and cost-per-bit are computed for the baseline, common-band and compact architectures for several channel launched powers. The obtained results are also compared with other works in the literature. Section 4.6 presents the main conclusions of this chapter.

4.2. Network physical and logical characteristics

In this section, we will present the main physical and logical characteristics of each network topology considered, namely the BT-UK and CONUS-60 networks. The respective physical topologies are presented in Figures 4.1 and 4.2.

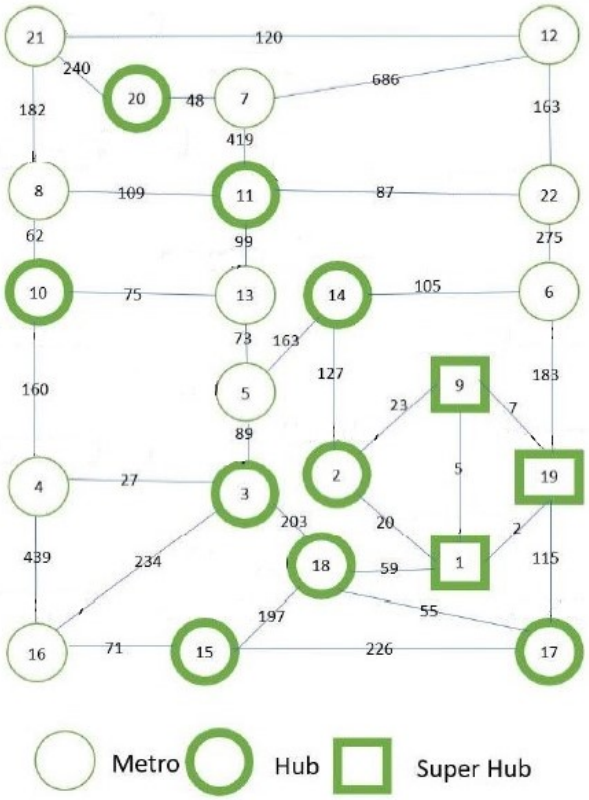

FIGURE 4.1. Physical topology of the BT-UK network.
Figure taken from [32].

Table 4.1 shows the maximum number of node connections that can be established for a full-mesh logical topology, the number of nodes and links, the average node degree and average link length, the shortest and longest links in the network and the total network length for the BT-UK and CONUS-60 topologies [25, 32]. Note that Table 4.1 complements Table 2.16 with the logical characteristics of the BT-UK and CONUS-60 networks.

From Table 4.1, it is possible to see that the CONUS-60 topology has a higher number of node connections compared to the BT-UK network, due to the larger network size (higher number of nodes and longer average link length). The BT-UK network is a smaller size network (lower number of network nodes and link length), but it has a higher average node degree indicating that is more meshed.

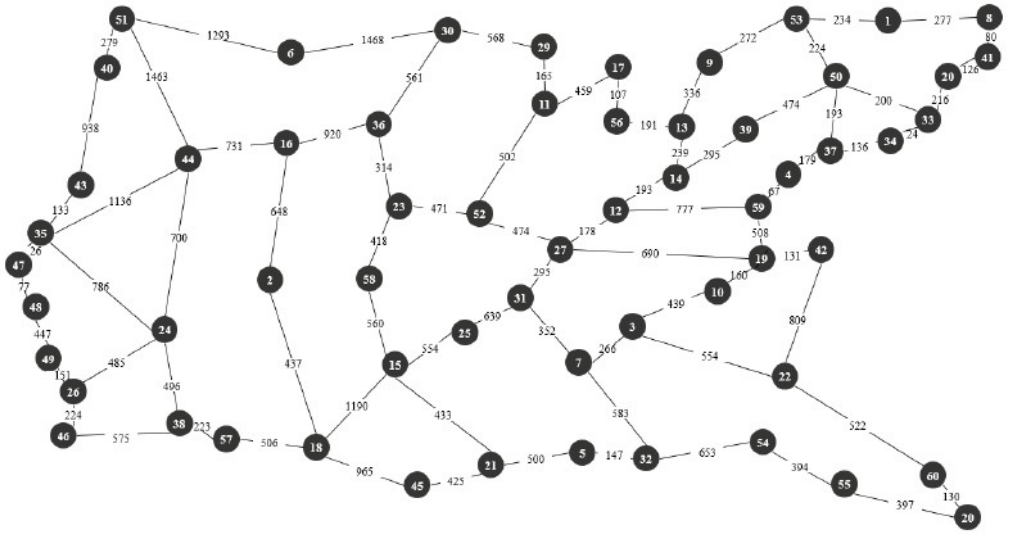

FIGURE 4.2. Physical topology of the CONUS-60 network.
Figure taken from [25].

TABLE 4.1. Physical and logical characteristics of the network topologies BT-UK and CONUS-60.

Parameters	Network	
	BT-UK	**CONUS-60**
Maximum no. of node connections	231	1770
Number of nodes	22	60
Number of links	35	79
Average node degree	3.2	2.6
Average link length [km]	147	445
Shortest link [km]	2	24
Longest link [km]	686	1468
Total network length [km]	5148	35388

4.3. Multi-band optical network simulator

In this section, we present and discuss the flowchart of the C+L+S multi-band network simulator developed in Matlab, used to compute the total network capacity and the cost-per-bit for the BT-UK and CONUS-60 topologies considering the PLIs and also the node architectures presented in chapter 2. The simulator solves a RMSA problem following the SNAP model for dynamic traffic considering a flexible grid C+L+S multi-band scenario [41, 64]. SNAP uses a Monte Carlo (MC) simulation method, wherein in each MC iteration a high number of progressive random traffic demands is generated. Demands are then allocated according to the defined RMSA algorithm, and for each MC iteration, the blocking probability, the network capacity and link saturation can be computed [41, 64].

Figure 4.3 shows the flowchart of the C+L+S multi-band network simulator. This simulator has three main steps: offline computation of the available optical paths, routing

and modulation format assignment and spectrum assignment. The simulator inputs are the network topology (CONUS-60 and BT-UK), channel launch power, target blocking probability (from 1% to 10%), MB node architecture (baseline, common-band, and compact architectures), and the maximum number of demands randomly generated ($N_{gen,max}$) in each MC iteration, whereas the simulation outputs are the total network capacity and cost-per-bit. Furthermore, if for a specific demand, it is not possible to assign modulation formats to all candidate paths, this demand is not used and regeneration must be used.

In the first step of the simulator, the offline computation of the available optical paths, the k-th shortest candidate paths for each demand are computed with the Yen's k-shortest path algorithm [65], using the distance in km, as a metric. For each one of all the possible candidate paths, the ASE noise (computed with (3.15) or (3.16)) and NLI noise (computed with (3.17)) contributions are computed per band and modulation format (QPSK, 8-QAM, and 16-QAM). The total OSNR is calculated for all candidate paths with (3.25), from the highest modulation format to the lowest, and it is checked if the residual margin (3.26) is above a minimum residual margin. Note that, if the residual margin is satisfied for a specific modulation format, the simulator does not compute the total OSNR for the remaining lower modulation formats, and the valid candidate path is saved in a list of available candidate paths. If none of the modulation formats satisfies the minimum residual margin, the corresponding candidate path is not used. Moreover, if no candidate paths of a specific demand satisfy the residual margin, that path is not used, which means that regeneration should be used for this path. Some simplifications are considered in this computation: the coherent factor is assumed zero in the NLI noise power computation, which means that we are assuming an incoherent accumulation of NLI along multiple fiber spans and the PLIs are calculated for the central channel in each band. In this situation, all the optical channels have the same NLI and OSNR for a particular link. After performing the modulation format assignment for all k-candidate paths, the k-candidate paths of each demand are sorted based on the OSNR in descending order.

In the second step, the routing and modulation format assignment, a demand is randomly chosen from the list of the available paths, assuming a uniform distribution. Notice that, for the chosen demand, the candidate paths available, the corresponding total OSNR, and modulation format assignment have been already computed in step 1. For each randomly chosen demand, the candidate path with the highest OSNR (highest modulation

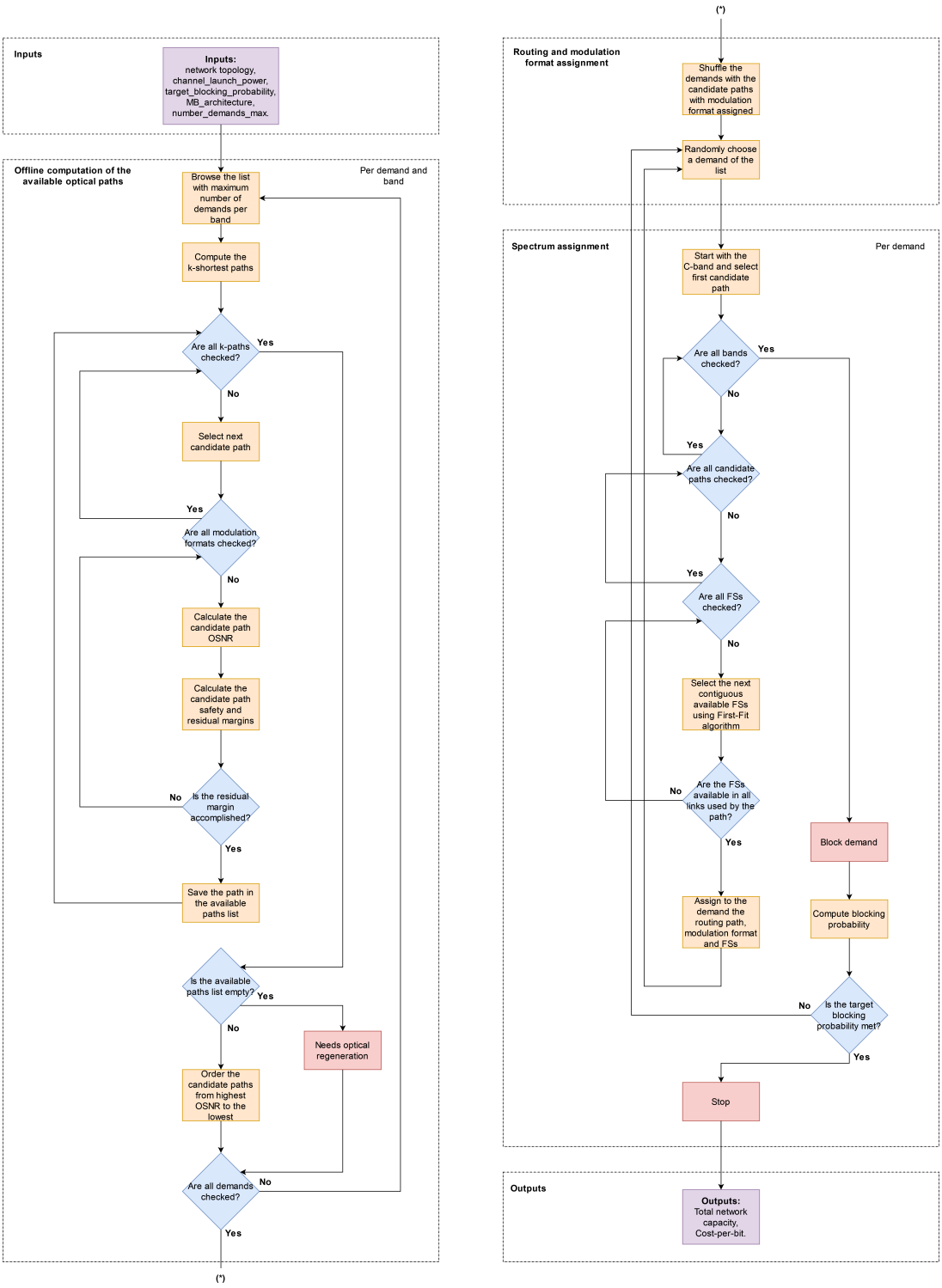

FIGURE 4.3. Flowchart of the Matlab simulator used to solve the RMSA problem in a flexible grid C+L+S multi-band network aware of the PLIs and node architecture.

format) is selected, which means that, in our simulator, the highest possible capacity is always used for each demand.

The third and final step tries to assign FSs to the candidate path with the highest OSNR (i.e. highest modulation format) using the First-Fit (FF) algorithm. The FF algorithm starts looking for available FSs from the lower frequency channels of the C-band towards the L- and S-bands. The number of FSs (each FS has 12.5 GHz) allocated for each demand is always six, independently of the modulation format assigned, because the symbol rate is the same for all modulations considered (64 Gbaud). The FF algorithm tries to assign six contiguous FSs in every link along the optical path. Note that for each band, if the FSs cannot be assigned for a particular candidate path, then the next candidate path must be chosen within each band. The FSs assignment is firstly performed for the C-band, and if it is not possible to assign FSs in the C-band, the L-band is checked and afterwards the S-band (note that if the FSs assignment were performed first for the S-band, where the OSNR is typically low, probably less paths will be blocked). If there are no available FSs in any of the bands and in any of the candidate paths, that demand is blocked, and the network blocking probability is computed. If the blocking probability is below the target blocking probability, the FF algorithm tries to allocate FSs for the next randomly generated demand. If the computed blocking probability is above the target, the total network capacity and cost-per-bit are computed and the simulator ends the present MC iteration and enters in the next MC iteration (not shown in Figure 4.3). A maximum number of demands randomly generated, $N_{gen,max}$, is set for each MC iteration. The simulation ends when a specific number of MC iterations (N_{sim}) is reached.

The blocking probability (BP) is computed by averaging the blocking probabilities obtained for all the N_{sim} MC iterations, given by [8, 9, 32, 41],

$$BP = \frac{\sum_{i=1}^{N_{sim}} \left(\frac{N_{blocked,demands}}{N_{total,demands}} \right)}{N_{sim}} \tag{4.1}$$

where $N_{blocked,demands}$ and $N_{total,demands}$ correspond, respectively, to the number of blocked demands and the total number of demands (including the blocked demands and the demands with FSs assigned) generated in the i-th iteration of the MC simulator.

The total network capacity ($Ctotal$) is given by [41],

$$Ctotal = \frac{\sum_{i=1}^{N_{sim}} (C_{network,capacity,i})}{N_{sim}} \tag{4.2}$$

where $C_{network,capacity,i}$ is the total network capacity obtained in the i-th iteration of the MC simulator.

The cost-per-bit, ($Costperbit$) is computed with [8, 9, 32],

$$Costperbit = \frac{C_{total}}{Cost_{Network,a,n}} \tag{4.3}$$

where $Cost_{Network,a,n}$, corresponds to the total cost of the network given by (2.19).

4.4. Physical layer impairments impact on the number of available optical paths

In this section, the impact of the PLIs, studied in chapter 3, on the number of available optical paths in the BT-UK and CONUS-60 networks is assessed as a function of the channel launch power. The system parameters are given in Table 4.2, whereas the practical OSNR is given in Table 4.3 for the three modulation formats considered [41, 59, 60]. Note that the residual margin is set to 2 dB (instead of 0 dB considered in chapter 3) and the 8-QAM modulation format is used instead of the 64-QAM format used in chapter 3, as it is a less demanding OSNR format than the 64-QAM [40, 41, 60].

TABLE 4.2. System parameters considered for the RMSA tool considering a C+L+S optical network.

Parameters	Values		
	C-band	**L-band**	**S-band**
Number of candidate paths (k_{paths})	5		
Number of MC simulations (N_{sim})	50		
Max. number of demands randomly generated ($N_{gen,max}$)	5000		
Target blocking probability [%]	1, ..., 10		
BER (pre-FEC)	2×10^{-2}		
Channel spacing ($\Delta\nu_{ch}$) [GHz]	75		
Total number of channels (N_{ch})	192		
Number of channels per band	64		
Central channel per band	32		
Nominal frequency of the central channel ($\nu_{m,b}$) [THz]	193.550	188.300	199.025
Channel FSs spacing [GHz]	12.5		
Total number of FSs	1152		
Number of FSs per band	384		
Fiber attenuation (α_b) [dB/km]	0.185	0.185	0.2
Maximum amplifier gain ($G_{max,b}$) [dB]	30		
AO-WC gain (G_{AO-WC}) [dB]	20		
MB-DEMUX/MUX ILs ($IL_{MB-DEMUX/MUX}$) [dB]	3		
Channel bandwidth (B_0) [GHz]	64		
Post-amplifier gain of baseline node ($G_{pos,i,b}$) [dB]	10	10	12
Post-amplifier gain of common-band node ($G_{pos,i,b}$) [dB]	10		
Post-amplifier gain of compact node ($G_{pos,i,b}$) [dB]	14	14	15
Noise figure ($F_{m,b}$) [dB]	4.25	4.68	6.40
Dispersion ($D_{\lambda0}$) [ps/nm/km]	17		
Dispersion slope (S_0) [fs/nm^2/km]	67		
Reference wavelength (λ_0) [nm]	1550		
Raman gain slope (C_r) [1/W/km/THz]	0.028		
Nonlinear coefficient (γ) [1/W/km]	1.30		
Coherence factor (ε)	0		

TABLE 4.3. Practical OSNR and transport capacity of each modulation format.

Parameters	**16-QAM**	**8-QAM**	**QPSK**
Practical OSNR [dB]	16.9	13.9	8.9
Capacity [Gbit/s]	400	300	200

The maximum number of available paths is computed for each band, MB architecture, and several channel launch powers, and it is represented in Figures 4.4 and 4.5, respectively for the BT-UK and CONUS-60 networks.

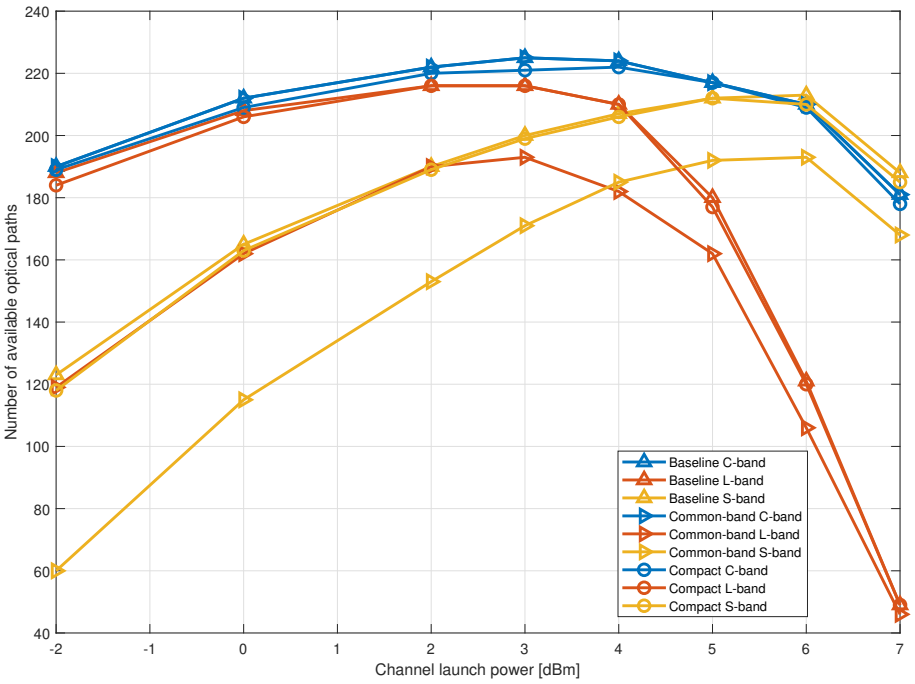

FIGURE 4.4. Number of available paths as a function of the channel launched power, for the BT-UK topology and for each MB node architecture.

Some general behaviours can be observed from Figures 4.4 and 4.5, namely the number of available optical paths increases to a maximum value and, then, decreases with the increase of the channel launch power, due to the impact of the ASE noise for low channel launch powers and, then, the influence of the NLI noise for higher channel launch powers. Also, the number of available optical paths in the C- and L-bands is higher compared to the S-band for lower channel launch powers. However, for higher channel launch powers, the number of available optical paths is higher for the C- and S-bands due to the higher NLI noise power in the L-band compared to the C- and S-bands due to the ISRS effect, which origins power transfers from high to low frequency channels [40]. Moreover, for

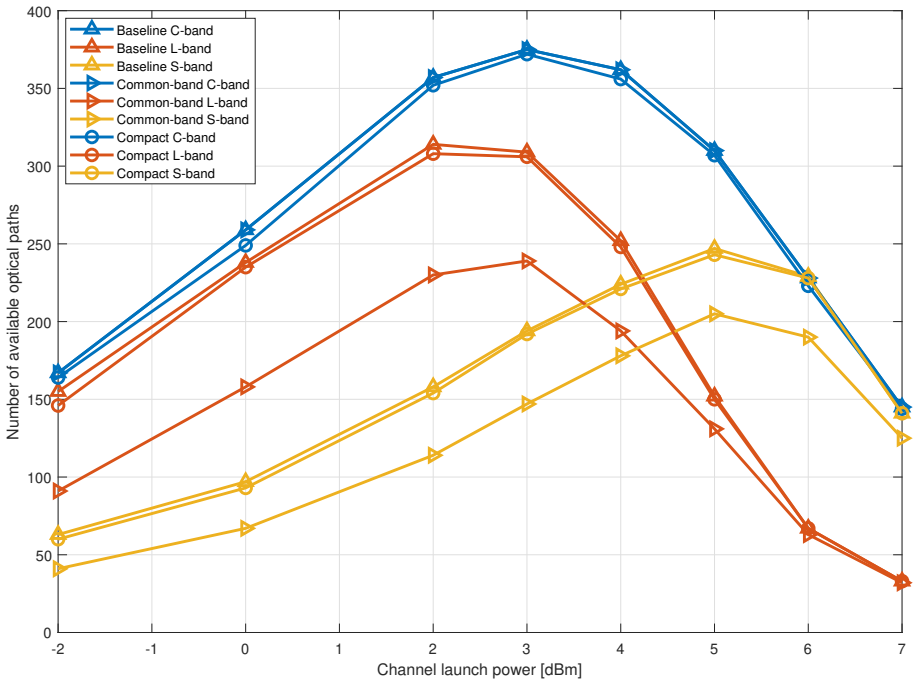

FIGURE 4.5. Number of available paths as a function of the channel launched power, for the CONUS-60 topology and for each MB node architecture.

the highest channel launch power (7 dBm), the number of available optical paths for the three bands and architectures is very similar within each network topology due to the dominance of the NLI noise (which does not depend on the architecture), over the ASE noise.

Regarding the MB architectures, as can be observed in Figures 4.4 and 4.5, the number of available paths that can be assigned for the baseline and compact architectures is very similar due to the high ASE noise introduced by the optical pre-amplifiers along the optical path (which is similar for both architectures). As the noise power from the pre-amplifiers surpasses significantly the ASE noise power introduced by the post-amplifiers, the network performance becomes almost MB node architecture independent. Furthermore, the number of available paths in the C-band is the same for the baseline and common-band architectures, since both nodes have equal ILs in this band (as can be extracted from Table 4.2 from the post-amplifiers gain). In the common-band architecture, for the L- and S-bands, the number of available optical paths is generally much lower compared with the other node architectures due to additional noise coming from the AO-WCs. For example, for the BT-UK topology and a channel launch power of -2 dBm, the number of available optical paths for the common-band architecture is 36.7% and 51.2% lower, respectively,

for the L- and S-bands, compared to baseline architecture. In the case of the CONUS-60 network, the number of available optical paths is 41.3% and 34.9% lower, respectively, for the L- and S-bands. Figures 4.4 and 4.5 also show that the optimum channel launch powers (that lead to a higher number of available optical paths) are roughly between 3 and 4 dBm for the C-band, between 2 and 3 dBm, for the L-band and between 5 and 6 dBm for the S-band, for both networks studied. For the optimal channel power, the maximum number of available optical paths for the BT-UK network is 225, 216 and 212 and, for the CONUS-60 network, 375, 314 and 247, respectively, in the C-, L- and S-bands, and it is obtained for the baseline architecture. Comparing the maximum number of available optical paths obtained for both network topologies, it is possible to see that with the BT-UK topology, the number of optical paths is much closer to the maximum (231) than in the CONUS-60 network (1770) due to the lower average link length of the BT-UK topology, which allows that optical paths meet the residual margin. In the CONUS-60 network, most of the optical paths require optical regeneration. For example, for the baseline architecture and a channel launch power of -2 dBm, the number of candidate paths that do not meet the minimum residual margin are 1603, 1615 and 1707, respectively, for the C-, L- and S-bands.

4.5. RMSA results and discussion

This section presents and discusses the RMSA results obtained using the Matlab simulator described in section 4.3, considering the parameters presented in Tables 4.2 and 4.3, for the C+L+S MB scenario in the BT-UK and CONUS-60 networks. Firstly, in subsection 4.5.1, the total network capacity for each network topology (BT-UK and CONUS-60), MB architecture (baseline, common-band and compact architectures), and channel launch power (-2, 0 and 2 dBm) is computed as a function of the target blocking probability. In subsection 4.5.2, the total cost-per-bit for a typical blocking probability of 1% is computed and compared with the values obtained in chapter 2 without the impact of the PLIs.

4.5.1. Total network capacity

In this subsection, we present the total network capacity calculated with (4.2), for the target blocking probabilities ranging from 1% to 10%.

To check the correctness of the blocking probability and the total network capacity computation, Figures 4.6 and 4.7 show the variation of the blocking probability and total

network capacity as a function of the number of MC iterations, respectively, for the target blocking probabilities of 1% and 10%, considering the baseline architecture and a channel launch power of -2 dBm, as well as the average of the blocking probability and the average of the total network capacity (red line) as a function of the number of MC iterations.

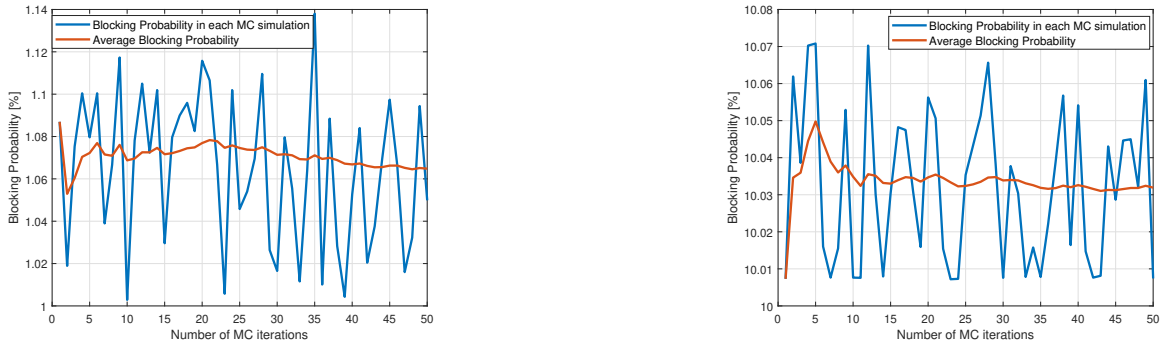

(a) (b)

FIGURE 4.6. Blocking probability (blue line) in each iteration of the MC simulation and its average (red line) as a function of the number of MC iterations for the target blocking probabilities of a) 1% and b) 10%, considering the baseline architecture and a channel launch power of -2 dBm.

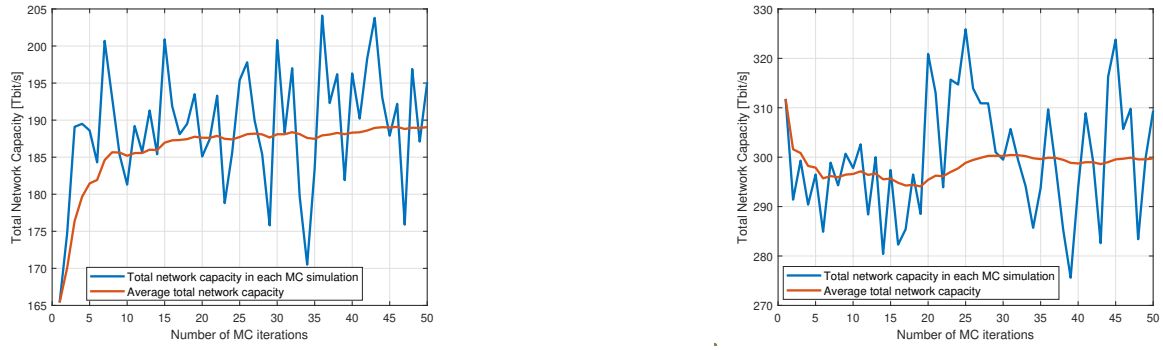

(a) (b)

FIGURE 4.7. Total network capacity (blue line) in each iteration of the MC iterations and its average (red line) as a function of the number of MC iterations for the target blocking probabilities of a) 1% and b) 10%, considering the baseline architecture and a channel launch power of -2 dBm.

Figure 4.6 shows that the blocking probability estimated using the average over the number of iterations becomes more stable with the increase of the number of MC iterations. After 50 MC iterations, the average of the blocking probability varies less than 1% around the target value (1% and 10%), which ensures the correctness of its computation. The same behavior with the number of iterations happens also with the total network capacity estimation, as shown in Figure 4.7. The estimation of the total network capacity

stabilizes with the increasing number of iterations, being its variation less than 1% after 50 iterations.

Figures 4.8 and 4.9, show the total network capacity as a function of the blocking probability for the baseline, common-band and compact architectures considering, respectively the BT-UK and CONUS-60 network topologies for the channel launch powers of -2, 0 and 2 dBm. More details concerning these results are presented in appendix M, Tables M1-M18.

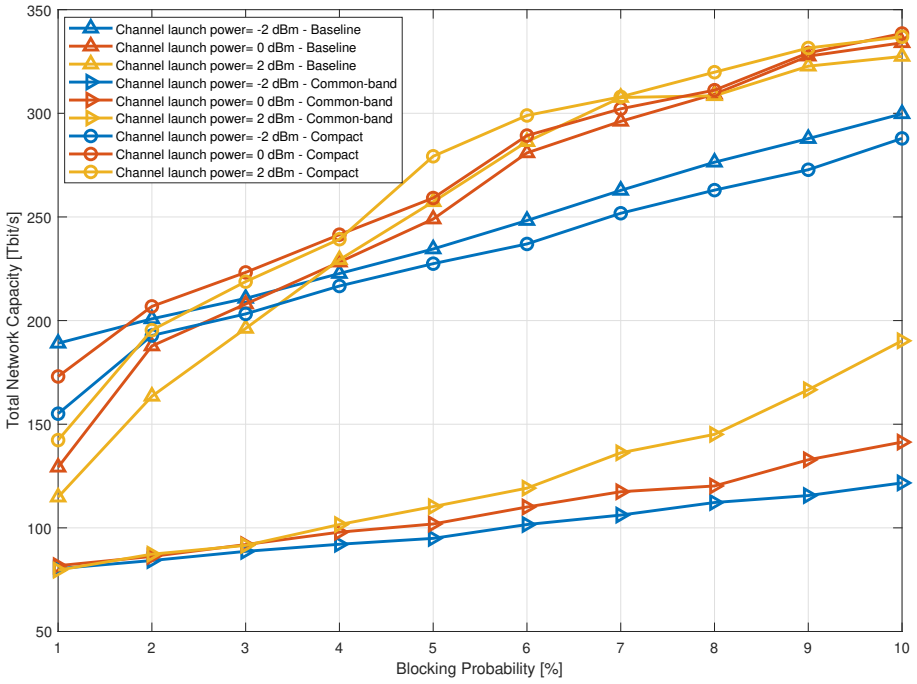

FIGURE 4.8. Total network capacity as a function of the blocking probability obtained for the BT-UK topology considering the baseline, common-band and compact MB node architectures, and the channel launch powers of -2, 0, and 2 dBm.

From Figure 4.8, it can be observed that the total network capacity increases for all three node architectures with the blocking probability and tends to the maximum network capacity as the blocking probability is further increased. It can be also observed that the total network capacity obtained for the common-band architecture is lower than the one obtained for the two other MB node architectures due to the lower number of available optical paths, as can be seen in Figure 4.4. For all results presented in Figure 4.8, for a blocking probability above around 3%, the total network capacity obtained with the common-band architecture is at least 100 Tbit/s lower than the one obtained with the other two architectures. In general, the total network capacity is similar for the baseline

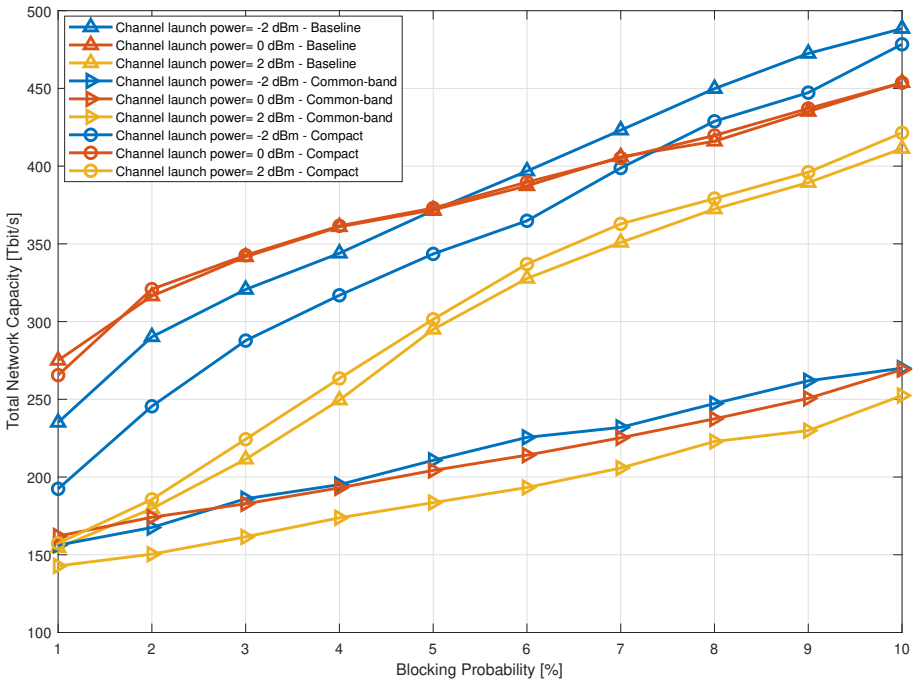

FIGURE 4.9. Total network capacity as a function of the blocking probability obtained for the CONUS-60 topology considering the baseline, common-band and compact MB node architectures, and the channel launch powers of -2, 0, and 2 dBm.

and compact architectures due to the similar number of available optical paths. Analyzing each architecture in particular, it can be observed that for the common-band architecture, the total network capacity reached for all channel launch powers considered is similar for a blocking probability lower than 3%. Finally, the channel launch power that ensures the highest total network capacity for a blocking probability of 1%, considering the baseline, common-band, and compact architectures is respectively, -2 dBm (189.06 Tbit/s), 0 dBm (81.75 Tbit/s) and 0 dBm (173.04 Tbit/s). In this situation, it can be seen that the baseline architecture has a lower channel launch power compared to the common-band and compact architectures.

For the CONUS-60 network, Figure 4.9 shows that, for 2 dBm, the total network capacity is lower than the total network capacities obtained with the channel launch powers of 0 and -2 dBm for all node architectures, differently from the behavior found in Figure 4.8, for the BT-UK network. Also, from Figure 4.9, it can also be seen that for a blocking probability higher than 6%, the total network capacity of the baseline and compact architectures for a channel launch power of 0 dBm becomes lower than the capacities obtained for a channel launch power of -2 dBm. This behavior can be justified

by noting that as the blocking probability increases, more paths of the total number of available optical paths can be assigned with FSs. But, most of these paths share the same links, due to the longer average link length of the CONUS-60 network, giving rise to more congested links and, ultimately, more paths are blocked and the transport capacity decreases. As observed also in Figure 4.8, the common-band architecture leads to the lower transport capacity. For example, for a blocking probability of 10%, the total network capacity is at least 140 Tbit/s lower than the one obtained with the other two architectures. The channel launch power of 0 dBm ensures the highest total network capacity for a blocking probability of 1%, for the baseline (275.03 Tbit/s), common-band (161.99 Tbit/s), and compact architectures (265.55 Tbit/s).

By comparing Figures 4.8 and 4.9, the most notorious difference is the higher total network capacity obtained for the CONUS-60 network in relation to the BT-UK total network capacity, mainly due to the higher number of available optical paths (Figures 4.4 and 4.5). However, for the compact architecture, a channel launch power of 2 dBm and a target blocking probability of 2%, the total network capacity obtained for the CONUS-60 is lower than in the BT-UK network, i.e., the capacity difference is 9.76 Tbit/s. For a blocking probability of 10%, the highest capacity found for the CONUS-60 network is 488.47 Tbit/s and occurs for the baseline architecture with a channel launch power of -2 dBm. In contrast, the highest capacity achieved for the BT-UK network is 338.51 Tbits/s, found for the compact architecture and a 0 dBm launch power. In this situation, the channel launch power corresponding to the highest total network capacity in the CONUS-60 topology (-2 dBm) is lower than the BT-UK (0 dBm) due to the higher average link length of the CONUS-60 network.

Tables 4.4 and 4.5 present the percentage of utilization of each band, respectively, for the BT-UK and CONUS-60 topologies. The percentage of utilization in each band is defined as the ratio between the number of demands assigned in each band (number of C- or L- or S-bands demands shown in Tables M1-M18) and the total number of served demands (Tables M1-M18).

From Tables 4.4 and 4.5, it can be observed that the C-band is more filled up, followed by the L- and then the S-bands for the three architectures. Moreover, for higher blocking probabilities, more demands are served, and the use of other bands is required to satisfy the increase of traffic requests, while decreasing the percentage of utilization of the C-band. The baseline and compact architectures lead to a similar utilization of each band.

TABLE 4.4. Percentage of utilization in each band, considering the baseline, common-band and compact architectures, a channel launch power of 0 dBm and the BT-UK topology.

Blocking probability [%]	BT-UK								
	Baseline			**Common-band**			**Compact**		
	C-band	**L-band**	**S-band**	**C-band**	**L-band**	**S-band**	**C-band**	**L-band**	**S-band**
1	83.3%	15.5%	0.1%	98.4%	0.5%	0.0%	74.9%	23.4%	0.7%
2	71.5%	25.4%	1.0%	96.8%	1.0%	0.0%	69.9%	26.4%	1.7%
3	67.1%	27.3%	2.5%	94.8%	2.0%	0.0%	65.6%	27.6%	3.8%
4	63.1%	27.8%	5.1%	92.3%	3.6%	0.0%	62.6%	27.6%	5.8%
5	60.0%	27.9%	7.0%	90.8%	4.1%	0.0%	59.6%	27.6%	7.8%
6	55.4%	27.9%	10.6%	88.3%	5.6%	0.0%	55.6%	27.7%	10.7%
7	53.3%	27.2%	12.5%	85.9%	7.0%	0.0%	53.5%	27.0%	12.4%
8	51.4%	26.6%	13.9%	83.9%	8.0%	0.0%	52.3%	26.6%	13.1%
9	49.5%	26.3%	15.2%	80.7%	10.2%	0.0%	50.0%	26.4%	14.6%
10	48.2%	26.1%	15.7%	78.2%	11.7%	0.0%	48.5%	25.9%	15.5%

TABLE 4.5. Percentage of utilization in each band, considering the baseline, common-band and compact architectures, a channel launch power of 0 dBm and the CONUS-60 topology.

Blocking probability [%]	CONUS-60								
	Baseline			**Common-band**			**Compact**		
	C-band	**L-band**	**S-band**	**C-band**	**L-band**	**S-band**	**C-band**	**L-band**	**S-band**
1	83.0%	15.9%	0.1%	98.1%	0.8%	0.0%	83.8%	15.1%	0.1%
2	78.5%	19.1%	0.3%	96.4%	1.5%	0.0%	78.2%	19.4%	0.4%
3	76.0%	20.2%	0.7%	94.7%	2.2%	0.0%	75.7%	20.4%	0.8%
4	74.0%	20.6%	1.3%	93.0%	3.0%	0.0%	74.0%	20.8%	1.2%
5	72.4%	20.9%	1.7%	90.7%	4.3%	0.0%	72.3%	21.1%	1.6%
6	71.1%	20.8%	2.0%	89.2%	4.7%	0.0%	70.9%	21.0%	2.1%
7	69.4%	21.0%	2.6%	87.2%	5.7%	0.0%	69.5%	20.9%	2.5%
8	68.0%	21.1%	2.9%	85.4%	6.5%	0.0%	68.0%	21.0%	3.0%
9	66.2%	21.1%	3.7%	83.7%	7.3%	0.0%	66.6%	20.8%	3.6%
10	64.8%	21.1%	4.1%	81.1%	8.9%	0.0%	65.2%	20.7%	4.1%

In the common-band architecture, the S-band is not used and the utilization of the L-band is lower than in the other architectures. This behavior happens due to additional noise from the AO-WCs in the L- and S-bands, which decreases the number of available optical paths. By comparing Tables 4.4 and 4.5, it can be observed that the S-band in the baseline and compact architectures is less used in the CONUS-60 network than in BT-UK due to the lower number of available paths (for example, 123 versus 63 for -2 dBm, 165 versus 97 for 0 dBm, and 190 versus 158 for 2 dBm, for the baseline architecture). The common-band architecture has a similar utilization of the C-, L-, and S-bands, for both network topologies.

The transport capacity in Tbit/s by modulation format is shown in Figures 4.10 and 4.11, respectively, for the BT-UK and CONUS-60 networks, whereas Table 4.6 shows the number of allocated demands for each modulation format, MB architecture and network topology. The target blocking probability of 1% and the channel launch power that ensures the maximum total network capacity for each MB architecture are considered. The best channel launch power for the baseline architecture is -2 dBm, and for the common-band

and compact architectures is 0 dBm, considering the BT-UK network. In the case of the CONUS-60 network, the best channel launch power is 0 dBm for all MB architectures. The transport capacity by modulation format is computed with the total number of allocated demands for all bands and the capacity of the demand (Table 4.6).

TABLE 4.6. Number of allocated demands for each modulation format and MB architecture, for a blocking probability of 1%.

Architecture	Number of allocated demands per modulation format					
	BT-UK			**CONUS-60**		
	QPSK	8-QAM	16-QAM	QPSK	8-QAM	16-QAM
Baseline	424	167.5	133.5	841.5	147.5	152
Common-band	116	77	87	500	90	89
Compact	303	204	151.5	814.5	150	148.5

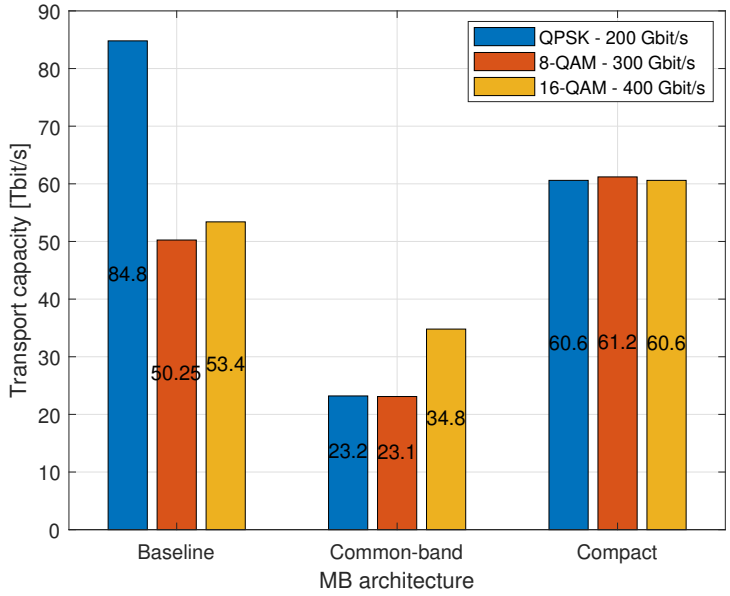

FIGURE 4.10. Transport capacity distribution among the three modulation formats considered for the BT-UK topology, considering a blocking probability of 1%, the baseline, common-band, and compact architectures.

From Figure 4.10, it can be observed that for the baseline architecture, the transport capacity for the three modulation formats is not as balanced as the one obtained with the common-band and compact architectures, being the QPSK format the dominant modulation format. For the common-band and compact architectures, there is a higher balance between the transport capacity of the three modulation formats because the channel launch power (0 dBm) is higher than in the baseline architecture (-2 dBm) (as can be seen in appendix M, Figures M1 and M2).

Figure 4.11 shows that for all MB node architectures, the QPSK transport capacity is higher compared to the remaining modulation formats due to the average longer link

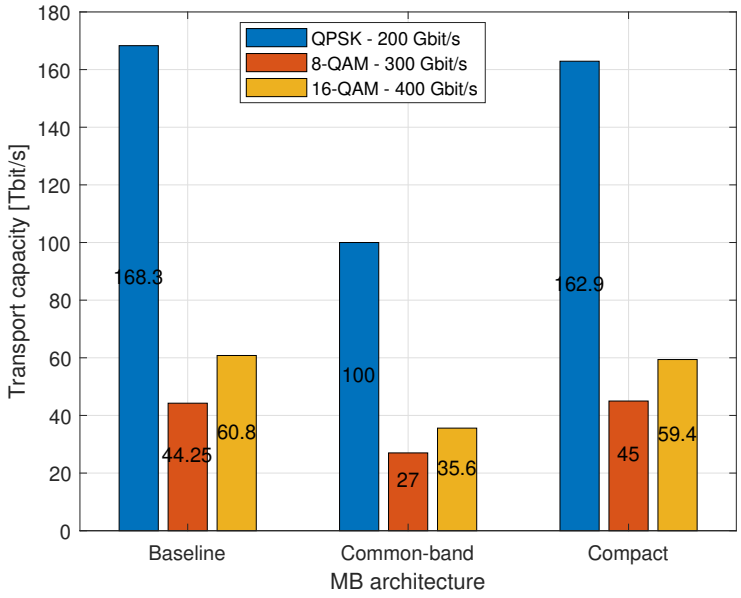

FIGURE 4.11. Transport capacity distribution among the three modulation formats considered for the CONUS-60 topology, considering a blocking probability of 1%, the baseline, common-band, and compact architectures.

length of the CONUS-60 network. In addition, the 16-QAM transport capacity is higher than the 8-QAM transport capacity due to a similar number of allocated demands (Table 4.6). Comparing Figures 4.10 and 4.11, it is possible to see that the QPSK transport capacity is preponderant in the CONUS-60 network than in BT-UK, due to the size of CONUS-60 network. For the BT-UK network, the size of the network, shorter link lengths and a more meshed network leads to a more balanced assignment of modulation formats.

Now, a comparison between the total network capacity obtained in Figures 4.8 and 4.9 with the results presented in chapter 2, for an A/D ratio of 25%, 640.8 Tbit/s (BT-UK) and 1427.6 Tbit/s (CONUS-60), is established. Note that in chapter 2, the total network capacity is obtained by the product of the total number of TRs with the capacity of each TR (100 Gbit/s). The total network capacity obtained with the impact of the PLIs and shown in Figures 4.8 and 4.9 is much lower compared to the one obtained in chapter 2 without the effect of the PLIs. In particular, for the BT-UK network, for the target blocking probability of 1% and the channel launch powers of -2 dBm (baseline architecture) and 0 dBm (common-band and compact architectures), the total network capacity when the PLIs are neglected is, respectively, 3.4, 7.8 and 3.7 times higher for the baseline, common-band and compact architectures, compared with the total network capacity calculated with the PLIs effect. In the case of the CONUS-60 network, for a target blocking probability of 1% and a channel launch power of 0 dBm, the capacity is,

respectively, 5.2, 8.8 and 5.4 times higher for the baseline, common-band and compact architectures. It can be concluded that the common-band node is more impaired by the PLIs than the other MB nodes, since the common-band architecture has additional noise from the AO-WCs, which impacts the total network capacity. Hence, the total network capacity calculated in chapter 2 is quite overestimated for the common-band architecture.

Finally, comparing the results obtained in Figures 4.8 and 4.9 with the results of Figure 7 (a) of [41], for the C+L+S 100 and 400 Gbit/s scenarios and for the blocking probabilities of 1% and 10%, it can be observed that the total network capacities obtained in this work, for the baseline architecture (that corresponds to the MB architecture considered in [41]), and the CONUS-60 topology (similar network topology, in terms of average link length, compared with the US-NET [41]), have the same behavior, regarding the increase of the total network capacity with the increase of the blocking probability, and the total network capacity values are in the same order of magnitude as those obtained in [41]. For the 0 dBm channel launch power and the blocking probability of 1%, the total network capacity obtained in this work for the baseline architecture is 275.03 Tbit/s, compared with the total network capacity obtained in [41], approximately, 400 Tbit/s for 400 Gbit/s requests and a 1% blocking probability. Note that in [41], different assumptions are considered to obtain the total network capacity: the US-NET topology is considered, the channel launch power is optimized to maximize the OSNR and achieve an acceptable OSNR flatness over the channels bandwidth, 100 and 400 Gbit/s requests are considered, gain and noise figures of the OAs dependent on the channel frequency and the NLI is considered over all the channels bandwidth.

4.5.2. Total cost-per-bit

In this subsection, we compute and discuss the total cost-per-bit for the MB architectures analyzed in the previous subsection, considering the BT-UK and the CONUS-60 networks. The total cost-per-bit is computed using (4.3). The total cost-per-bit is normalized to the cost-per-bit obtained with the baseline architecture, for a zero fiber lease cost, a launch power of -2 dBm, and the target blocking probability of 1%, which is typically a reference value for the blocking probability [8, 9, 32, 41]. Table 4.7 shows the total network capacity calculated for the BT-UK and CONUS-60 networks, and the cost-per-bit considering the baseline architecture for both network topologies. The cost-per-bit of the BT-UK network is given by $\frac{306019}{189.06\times10^{12}} = 1.62 \times 10^{-9}$ s/bit, and of the CONUS-60 is $\frac{680948}{235.142\times10^{12}} = 2.90 \times 10^{-9}$ s/bit.

TABLE 4.7. Parameters considered to compute the normalized cost-per-bit for the BT-UK and CONUS-60 topologies.

Total cost-per-bit parameters	Network	
	BT-UK	**CONUS-60**
Architecture	Baseline	
Blocking probability	1%	
Fiber lease cost	0	
Total network capacity [Tbit/s]	189.06	235.142
Total network cost	306019	680948
Cost-per-bit [s/bit]	1.62×10^{-9}	2.90×10^{-9}

Figure 4.12 shows the total cost-per-bit as a function of the fiber lease cost for the three MB architectures, channel launch powers of -2, 0, and 2 dBm, and the target blocking probability of 1%, considering the BT-UK topology. The total cost-per-bit is normalized to the cost-per-bit of the BT-UK network with the baseline architecture, a channel launch power of -2 dBm, and a blocking probability of 1%.

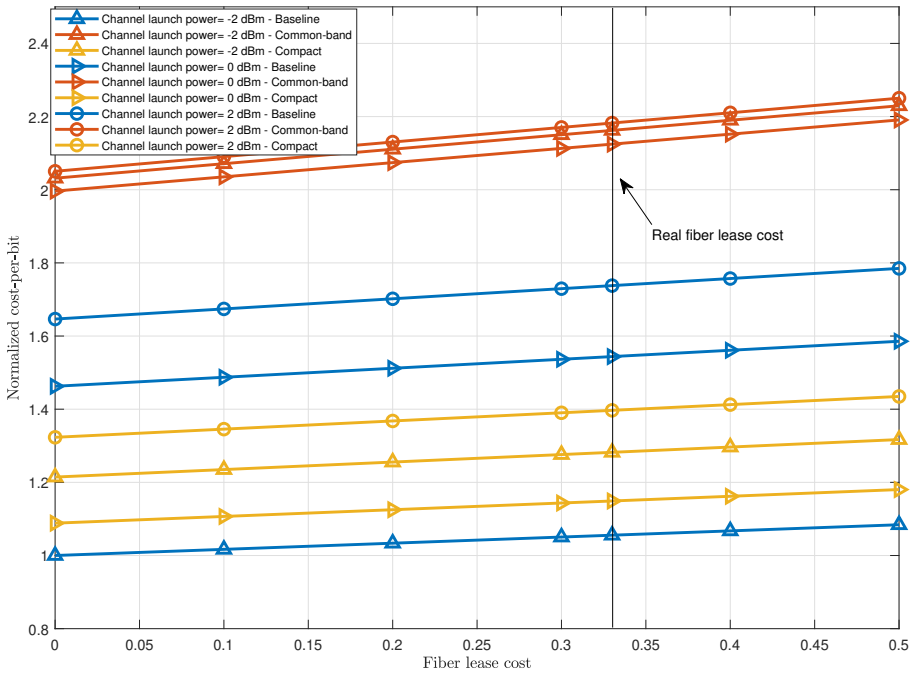

FIGURE 4.12. Cost-per-bit normalized to the baseline architecture as a function of the fiber lease cost considering the BT-UK network, a channel launch power of -2 dBm, and the blocking probability of 1%, for the baseline, common-band and compact architectures.

Figure 4.12 shows that the total cost-per-bit of all the MB architectures has a smooth increase with the fiber lease cost, since the BT-UK network is a network with a short average link length and the impact of the fiber lease cost is reduced. For all channel powers, the common-band architecture has the highest total cost-per-bit (above 2) due

to the lower total network capacity achieved, compared with the normalized cost-per-bit of the baseline and compact architectures. The channel launch power that leads to the lowest cost-per-bit for the common-band architecture is 0 dBm, but the remaining channel launch powers lead to similar cost-per-bit. For the baseline and compact architectures, the most cost effective channel launch powers are, respectively, -2 and 0 dBm. When the real fiber lease cost (0.33) is considered, the baseline architecture leads to the lowest cost-per-bit of 1.06, for the -2 dBm channel launch power.

Figure 4.13 shows the total cost-per-bit of the CONUS-60 network, for the three MB architectures, channel launch powers of -2, 0, and 2 dBm and the target blocking probability of 1%. The total cost-per-bit is normalized to the cost-per-bit of the CONUS-60 network with the baseline architecture, a channel launch power of -2 dBm, and a blocking probability of 1%.

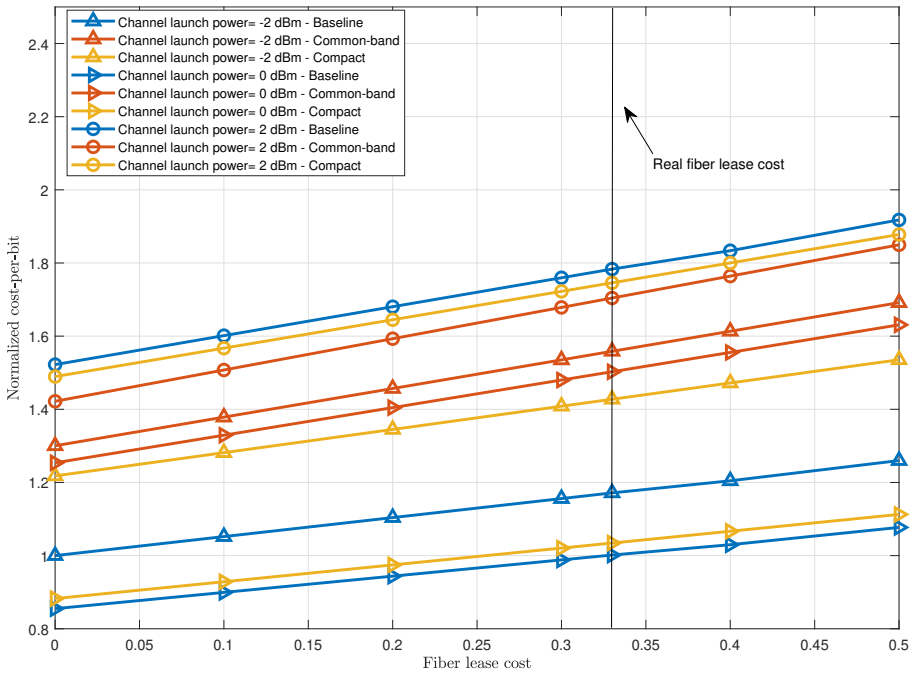

FIGURE 4.13. Cost-per-bit normalized to the baseline architecture as a function of the fiber lease cost considering the CONUS-60 network, a channel launch power of -2 dBm, and the blocking probability of 1%, for the baseline, common-band and compact architectures.

From Figure 4.13, it can be seen that the channel launch power of 0 dBm, leads to the lower cost-per-bit for the three MB architectures. For this power, the baseline and compact architectures have a much lower cost-per-bit than the common-band architecture. They are about 2/3 less expensive than the common-band architecture. For the real fiber

lease cost of 0.33, the baseline architecture for a channel launch power of 0 dBm leads to the lowest network cost-per-bit (1.0) in comparison with the other two architectures.

In order to compare the total cost-per-bit of Figures 4.12 and 4.13, the cost-per-bit obtained from the CONUS-60 network is normalized to the BT-UK network cost-per-bit, giving 1.79. With this, the total cost-per-bit of the CONUS-60 network is 1.79 times higher than the BT-UK network cost-per-bit. By comparing Figures 4.12 and 4.13, the total cost-per-bit for all architectures has a sharper increase with the fiber lease cost for the CONUS-60 network than for the BT-UK network, since the CONUS-60 network has a higher number of nodes and longer average link length. The most cost effective channel launch power of the baseline architecture for the BT-UK network (-2 dBm) is lower than the one obtained for the CONUS-60 (0 dBm) due to the higher average link length of the CONUS-60 network, demanding a higher channel launch power to achieve a lower total cost-per-bit. In the case of common-band and compact architectures, the same cost effective channel launch power (0 dBm) is obtained, for both network topologies.

Comparing the total cost-per-bit obtained in Figures 4.12 and 4.13 for the best situation (lower cost-per-bit obtained for a specific channel launch power) with the results from chapter 2 shown in Figures 2.24 and 2.25, the total cost-per-bit obtained for the common-band architecture with impact of the PLIs, is higher than the total cost-per-bit obtained for the remaining MB architectures. However, without the influence of the PLIs, the common-band architecture presented the lowest cost-per-bit in chapter 2. Hence, the advantages of this architecture become more limited when the effect of PLIs are considered. Regarding the baseline and compact architectures, in chapter 2, the total cost-per-bit obtained for both architectures is very similar. However, the total cost-per-bit of the baseline architecture is slightly lower than the compact architecture with the impact of the PLIs. Note that different normalizations are considered in chapter 2: the cost-per-bit is normalized to the R&S CD baseline scenario with 2 directions operating only in C-band and for an A/D ratio of 25%. This makes the values of the cost-per-bit presented in Figures 2.24 and 2.25 and Figures 4.12 and 4.13 hard to compare.

Finally, comparing the results obtained in Figures 4.12 and 4.13 with Figure 3 of [9], for α=1.5, β=2, it can be observed that the total cost-per-bit obtained in this work, follows the same behavior with the fiber lease cost as the one presented in [9]. Comparing the total cost-per-bit obtained in Figure 3 of [9], for α=1.5, β=2, with the total cost-per-bit from Figure 4.12, for the best channel launch powers of -2 dBm (baseline architecture) and

0 dBm (common-band architecture) (same MB architectures considered in [9]), and the BT-UK topology (similar network topology, in term of number of nodes and average node degree, compared with NSFNET [9]), the total cost-per-bit obtained in this work, for the common-band architecture is almost twice the baseline architecture cost-per-bit, while, in [9], the common-band architecture has a lower cost-per-bit (0.8 times below the baseline cost-per-bit). This worst performance of the common-band architecture observed in our work is due to the impact of the additional ASE noise coming from the amplifiers inside the AO-WC, which degrades significantly the OSNR, lowers the total network capacity and increases the cost-per-bit. As this behavior is not seen in [9], we suspect that in that work this additional noise has not been taken into account. Note also that in [9], the cost-per-bit is normalized to the cost-per-bit of the SDM architecture without consideration of the fiber lease cost, and without this normalization value, it is not possible to compare directly the values of the cost-per-bit that we have obtained with the cost-per-bit values presented in [9].

4.6. Conclusions

In this chapter, we developed a planning tool to solve the RMSA problem in C+L+S MB networks taking into account the node architecture and the PLIs impact. The flow-chart of the developed C+L+S MB RMSA simulator with three main steps is presented.

The number of available paths satisfying the defined residual margin for each MB architecture, network topology, and channel launch power is computed, considering a full-mesh logical topology. It has been concluded that with the increase of the channel launch power, the number of available optical paths increases until a maximum value is reached and then starts to decrease, for the BT-UK and CONUS-60 networks, due to the balance between the NLI and ASE noise powers in each band of the fiber. It is also concluded that the baseline and compact node architectures lead to a similar number of available optical paths, and that this number is much higher than the number of available optical paths provided by the common-band architecture.

The total network capacity for the baseline, common-band and compact architectures, considering the BT-UK and CONUS-60 networks is, then, computed. In the BT-UK network, the channel launch power that ensures the highest total network capacity, for a target blocking probability of 1% is -2 dBm (corresponding to a total network capacity of 189.06 Tbit/s) for the baseline architecture and 0 dBm for the common-band (81.75 Tbit/s) and compact architectures (173.04 Tbit/s). In the CONUS-60 network, for the

baseline (275.03 Tbit/s), common-band (161.99 Tbit/s) and compact architectures (265.55 Tbit/s), a channel launch power of 0 dBm guarantees the highest total network capacity for a blocking probability of 1%. For both networks, the common-band architecture has the lowest total network capacity compared with the remaining MB architectures due to the much lower number of available paths, in particular, in the L- and S-bands, due to the enhanced ASE noise caused by the AO-WCs.

The total cost-per-bit of the BT-UK and CONUS-60 networks has been computed for the baseline, common-band and compact architectures, for the channel launch powers of -2, 0 and 2 dBm, and the target blocking probability of 1%. The best channel launch powers for both network topologies are obtained for the three MB architectures, ensuring the lowest cost-per-bit. In particular, for these best channel launch powers obtained for the baseline (-2 dBm), common-band (0 dBm) and compact (0 dBm) architectures, and a real fiber lease cost of 0.33, the total cost-per-bit obtained are, respectively, 1.06, 2.12 and 1.15, for the BT-UK network, and 1.0, 1.50 and 1.03, for the CONUS-60 network, for the 0 dBm channel power.

From the results presented in this chapter, it can be concluded that the baseline architecture is a better option than the compact architecture due to its mature technology, since it does not require the use of MB WSSs that operate simultaneously in the C-, L-, and S-bands. Nevertheless, the compact architecture could be important in the future, as it has the switching capability between bands and requires a much lower number of components. The common-band architecture is hugely impacted by the effect of PLIs, degrading the total network capacity and cost-per-bit.

CHAPTER 5

Conclusions and future work

5.1. Final conclusions

In this dissertation, we have studied MB node architectures, such as the baseline, AO-WC, common-band and compact architectures, suitable for working on the C+L+S bands. Firstly, these four MB architectures were analyzed and compared in terms of their internal structure and cost-per-bit and compared with the SDM architecture. Finally, with the development of the C+L+S MB RMSA planning tool that incorporates the impact of PLIs, the total network capacity and cost-per-bit provided by these MB architectures in an optical network scenario has been obtained and discussed.

In chapter 2, a review of the ROADM node architectures proposed for MB transmission and a comparison with the SDM node architecture in terms of total node cost and cost-per-bit has been performed. It has been concluded that the TRs number and cost are the main contributors to the total node cost. However, in the AO-WC architecture, and apart from the TRs, the AO-WCs also affect significantly the total node cost. The common-band architecture presents the lower total node cost compared to the remaining MB node architectures, followed by the compact, baseline and AO-WC architectures. Then, the cost-per-bit without the influence of the fiber lease cost has been computed. In particular, it is concluded that the SDM architecture presents the lowest cost-per-bit compared to the remaining MB node architectures due to the lower cost of C-band TRs. The common-band architecture presents the lowest cost-per-bit compared to the remaining MB node architectures. Finally, the cost-per-bit of the MB architectures in the BT-UK and CONUS-60 networks has been studied. Again, the common-band architecture presents a lower cost-per-bit for a fiber lease cost higher than 0.05 and 0.15, respectively, for the CONUS-60 and BT-UK networks compared to the remaining MB node architectures. The AO-WC architecture has been excluded from the subsequent studies in the other chapters, due to its unbearable cost.

Chapter 3 assessed and analyzed the impact of several PLIs, such as the ASE, NLI noise powers, and ISRS, in a C+L+S MB ROADM-based network, considering the baseline, common-band and compact architectures, and the BT-UK network. Two WSS

technologies have been considered, the PICs and LCoS, being the LCoS technology the best option for the WSSs implementation, due to its lower ILs and higher availability. We have observed that the total NLI noise power is higher in the L-band, when compared with the C- and S-bands due to the ISRS effect and is independent of the node architecture. In this work, the total ASE noise power in the network is enhanced due to the use of high-gain OAs. From the total OSNR and residual margin computation, the baseline architecture has a better performance and allows higher modulation formats than the two other MB architectures, but at the expense of reduced switching capability.

In chapter 4, the total network capacity and cost-per-bit are obtained with the C+L+S MB network simulator. It has been concluded that for the BT-UK network, and a blocking probability of 1%, the baseline architecture requires a lower channel launch power of -2 dBm than the two other architectures, ensuring the highest total network capacity of 189.06 Tbit/s. In the common-band (81.75 Tbit/s) and compact architectures (173.04 Tbit/s), the same channel launch power of 0 dBm has been achieved. In the CONUS-60 network, the 0 dBm channel launch power is the one that leads to the higher network capacity, for the baseline (275.03 Tbit/s), common-band (161.99 Tbit/s) and compact architectures (265.55 Tbit/s) and a blocking probability of 1%. The same channel launch powers guarantee the lowest total cost-per-bit for the different MB architectures. For the BT-UK network, a real fiber lease cost of 0.33, and the baseline, common-band and compact architectures, the total cost-per-bit obtained is, respectively, 1.06, 2.12 and 1.15. In the case of the CONUS-60 network, for the baseline, common-band and compact architecture, the total cost-per-bit is, respectively, 1.0, 1.50 and 1.03. Hence, the common-band architecture is the most expensive MB node architecture studied as it is hugely impacted by the PLIs, while the baseline and compact architectures have similar cost-per-bit. Due to its mature technology and slightly lower cost-per-bit, the baseline architecture seems the best option for deployment in a MB optical network scenario, although it loses some switching capability.

5.2. Future work

In this section, some suggestions for future work are presented:

- Improve the Matlab simulator to solve the simplifications considered in this work: compute the NLI noise power along all channels bandwidth and including the ISRS tilt in the network optimization [40].

- Optimize the channel launch power and tilt to maximize the OSNR and network capacity [8, 9, 41].
- Improve the Matlab simulator to work with SDM node architectures so that a comparison between C+L+S MB and SDM networks can be performed [9, 32].
- Evaluation of the link saturation and average bit rate per optical path in the BT-UK and CONUS-60 topologies, and other optical networks, with the RMSA simulator developed [64].
- Improve the traffic model of the RMSA simulator to consider more realistic scenarios, such as the non-uniform population-based traffic scenario studied in [4].

References

[1] T. Zami, B. Lavigne, and M. Bertolini, "How 64 GBaud optical carriers maximize the capacity in core elastic WDM networks with fewer transponders per Gb/s," *Journal of Optical Communications and Networking*, vol. 11, no. 1, pp. A20–A32, January 2019.

[2] D. M. Marom, Y. Miyamoto, D. T. Neilson, and I. Tomkos, "Optical switching in future fiber-optic networks utilizing spectral and spatial degrees of freedom," *Proceedings of the IEEE*, vol. 110, no. 11, pp. 1835–1852, October 2022.

[3] R.-J. Essiambre, G. Kramer, P. J. Winzer, G. J. Foschini, and B. Goebel, "Capacity limits of optical fiber networks," *Journal of Lightwave Technology*, vol. 28, no. 4, pp. 662–701, February 2010.

[4] B. Correia, R. Sadeghi, E. Virgillito, A. Napoli, N. Costa, J. Pedro, and V. Curri, "Power control strategies and network performance assessment for C+L+S multiband optical transport," *Journal of Optical Communications and Networking*, vol. 13, no. 7, pp. 147–157, January 2021.

[5] A. Ferrari, A. Napoli, J. K. Fischer, N. Costa, A. D'Amico, J. Pedro, W. Forysiak, E. Pincemin, A. Lord, A. Stavdas *et al.*, "Assessment on the achievable throughput of multi-band ITU-T G.652.D fiber transmission systems," *Journal of Lightwave Technology*, vol. 38, no. 16, pp. 4279–4291, August 2020.

[6] M. Cantono, R. Schmogrow, M. Newland, V. Vusirikala, and T. Hofmeister, "Opportunities and challenges of C+L transmission systems," *Journal of Lightwave Technology*, vol. 38, no. 5, pp. 1050–1060, March 2020.

[7] H. Kawahara, M. Nakagawa, T. Seki, and T. Miyamura, "Experimental demonstration of wavelength-selective band/direction-switchable multi-band OXC using an inter-band all-optical wavelength converter," in *European Conference on Optical Communications (ECOC)*, Brussels, Belgium, December 2020.

[8] M. Nakagawa, H. Kawahara, T. Seki, and T. Miyamura, "Adaptive link-by-link band allocation: a novel adaptation scheme in multi-band optical networks," in *International Conference on Optical Network Design and Modeling (ONDM)*, Gothenburg,

Sweden, June 2021.

[9] M. Nakagawa, T. Seki, and T. Miyamura, "Techno-economic potential of wavelength-selective band-switchable OXC in S+C+L band optical ntworks," in *Optical Fiber Communications Conference and Exhibition (OFC)*, San Diego, CA, USA, March 2022, paper W2A.24.

[10] S. Yamamoto, H. Taniguchi, Y. Kisaka, S. Camatel, Y. Ma, D. Ogawa, K. Hadama, M. Fukutoku, T. Goh, and K. Suzuki, "First demonstration of a C+L band CDC-ROADM with a simple node configuration using multiband switching devices," *Optics Express*, vol. 29, no. 22, pp. 36 353–36 365, October 2021.

[11] N. Deng, L. Zong, H. Jiang, Y. Duan, and K. Zhang, "Challenges and enabling technologies for multi-band WDM optical networks," *Journal of Lightwave Technology*, vol. 40, no. 11, pp. 3385–3394, June 2022.

[12] M. Mehrabi, H. Beyranvand, and M. J. Emadi, "Multi-band elastic optical networks: inter-channel stimulated raman scattering-aware routing, modulation level and spectrum assignment," *Journal of Lightwave Technology*, vol. 39, no. 11, pp. 3360–3370, March 2021.

[13] P. J. Winzer, D. T. Neilson, and A. R. Chraplyvy, "Fiber-optic transmission and networking: the previous 20 and the next 20 years," *Optics Express*, vol. 26, no. 18, pp. 24 190–24 239, September 2018.

[14] A. Napoli and J. Pedro, "Getting the most from currently deployed optical fiber infrastructure," June 2017. [Online]. Available: https://www.fibre-systems.com/viewpoint/getting-most-currently-deployed-optical-fiber-infrastructure

[15] International Telecommunication Union, "Handbook – optical fibers, cables and systems," 2009. [Online]. Available: www.itu.int

[16] FS Community, "Is G.652 single mode fiber your right choice?" December 2021. [Online]. Available: https://community.fs.com/blog/what-kind-of-single-mode-fiber-should-you-choose.html

[17] JiangDong Group, "G.652D-Low water peak non-dispersion shift single-mode fiber," 2020. [Online]. Available: https://www.jdocable.com/product-detail/G-652D-Low-water-peak-non_pid-18f057e0c21d4403955f4b337e145490.html

[18] S. Woodward, M. D. Feuer, and P. Palacharla, "ROADM-node architectures for reconfigurable photonic networks," *Optical Fiber Telecommunications VIB: Chapter 15*, pp. 683–707, December 2013.

[19] M. Filer and S. Tibuleac, "N-degree ROADM architecture comparison: broadcast-and-select versus route-and-select in 120 Gb/s DP-QPSK transmission systems," in *Optical Fiber Communications Conference and Exhibition (OFC)*, San Francisco, CA, USA, March 2014, paper Th1I.2.

[20] B. C. Collings, "Advanced ROADM technologies and architectures," in *Optical Fiber Communications Conference and Exhibition (OFC)*, Los Angeles, CA, USA, March 2015, paper Tu3D.3.

[21] S. Gringeri, B. Basch, V. Shukla, R. Egorov, and T. J. Xia, "Flexible architectures for optical transport nodes and networks," *IEEE Communications Magazine*, vol. 48, no. 7, pp. 40–50, August 2010.

[22] R. Shankar, M. Florjańczyk, T. J. Hall, A. Vukovic, and H. Hua, "Multi-degree ROADM based on wavelength selective switches: architectures and scalability," *Optics Communications*, vol. 279, no. 1, pp. 94–100, November 2007.

[23] T. Zami, "High degree optical cross-connect based on multicast switch," in *Optical Fiber Communication Conference (OFC)*, San Francisco, CA, USA, March 2014, paper W2A.36.

[24] N. K. Fontaine, R. Ryf, and D. T. Neilson, "N × M wavelength selective cross-connect with flexible passbands," in *Optical Fiber Communication (OFC) Conference/National Fiber Optics Engineers Conference (NFOEC)*, Los Angeles, CA, USA, March 2012, paper PDP5B.2.

[25] J. M. Simmons, *Optical network design and planning*, 2nd ed. Springer International Publishing, 2014.

[26] A. Eira, N. Costa, and J. Pedro, "On the capacity and scalability of metro transport architectures for ubiquitous service delivery," in *20th International Conference on Transparent Optical Networks (ICTON)*, Bucharest, Romania, July 2018, paper Mo.B3.5.

[27] A. Eira and J. Pedro, "The role of metro transport node architectures in optimized edge data-center dimensioning," in *International Conference on Optical Network Design and Modeling (ONDM)*, Barcelona, Spain, May 2020.

[28] R. M. G. Kraemer, F. Nakamura, Y. Wang, H. Tsuda, and N. Calabretta, "High extinction ratio and low crosstalk C and L-band photonic integrated wavelength selective switching," in *22nd International Conference on Transparent Optical Networks (ICTON)*, July 2020, paper We.D2.1.

[29] K. Seno, K. Yamaguchi, K. Suzuki, and T. Hashimoto, "Wide-passband C + L-band wavelength selective switch by alternating wave-band arrangement on LCOS," in *European Conference on Optical Communication (ECOC)*, September 2018.

[30] J. M. Rivas-Moscoso, B. Shariati, D. M. Marom, D. Klonidis, and I. Tomkos, "Comparison of CD(C) ROADM architectures for space division multiplexed networks," in *Optical Fiber Communications Conference and Exhibition (OFC)*, Los Angeles, CA, USA, March 2017, paper Th2A.45.

[31] J. Alberto Hernandez, M. Quagliotti, L. Serra, L. Luque, R. Lopez da Silva, A. Rafel, O. Gonzalez de Dios, V. Lopez, A. Eira, R. Casellas, A. Lord, J. Pedro, and D. Larrabeiti, "Comprehensive model for technoeconomic studies of next-generation central offices for metro networks," *Journal of Optical Communications and Networking*, vol. 12, no. 12, pp. 414–427, December 2020.

[32] R. K. Jana, A. Mitra, A. Pradhan, K. Grattan, A. Srivastava, B. Mukherjee, and A. Lord, "When is operation over C+L bands more economical than multifiber for capacity upgrade of an optical backbone network?" in *European Conference on Optical Communications (ECOC)*, Brussels, Belgium, December 2020, paper Tu1H-4.

[33] F. Gomes, "Impact of physical layer impairments on multi-band metro networks," Master's thesis, ISCTE-IUL, Lisbon, Portugal, Master dissertation in Telecommunications and Computer Engineering, October 2021.

[34] F. Gomes, L. Cancela, and J. Rebola, "Impact of physical layer impairments on C+L-band metro networks," in *Proceedings of the 10th International Conference on Photonics, Optics and Laser Technology - Volume 1: PHOTOPTICS,*, INSTICC. SciTePress, 2022, pp. 134–143.

[35] M. Q. da Silva, "Impact of physical layer impairments on SDM networks based on ROADM nodes," Master's thesis, ISCTE-IUL, Lisbon, Portugal, Master dissertation in Telecommunications and Computer Engineering, October 2021.

[36] M. Q. Silva, L. G. Cancela, and J. L. Rebola, "Cost, power consumption and performance analysis in SDM ROADM architectures for uncoupled spatial channels," in *2022 13th International Symposium on Communication Systems, Networks and Digital Signal Processing (CSNDSP)*, July 2022, pp. 857–862.

[37] D. Semrau, E. Sillekens, R. I. Killey, and P. Bayvel, "The benefits of using the S-band in optical fiber communications and how to get there," in *IEEE Photonics Conference (IPC)*, Vancouver, BC, Canada, September 2020.

[38] I.-T. R. G. Telecommunication Standardization Sector of ITU, "Spectral grids for WDM applications: DWDM frequency grid," October 2020.

[39] A. Anchal and D. M. Marom, "Practical SDM-ROADM designs for uncoupled spatial channels and their switching capacity," in *2019 Optical Fiber Communications Conference and Exhibition (OFC)*, San Diego, CA, USA, March 2019, paper M1A.4.

[40] A. Souza, B. Correia, N. Costa, J. Pedro, and J. Pires, "Accurate and scalable quality of transmission estimation for wideband optical systems," in *2021 IEEE 26th International Workshop on Computer Aided Modeling and Design of Communication Links and Networks (CAMAD)*, October 2021, pp. 1–6.

[41] R. Sadeghi, B. Correia, A. Souza, N. Costa, J. Pedro, A. Napoli, and V. Curri, "Transparent vs translucent multi-band optical networking: capacity and energy analyses," *Journal of Lightwave Technology*, vol. 40, no. 11, pp. 3486–3498, April 2022.

[42] D. Semrau, E. Sillekens, R. I. Killey, and P. Bayvel, "A modulation format correction formula for the Gaussian noise model in the presence of inter-channel stimulated raman scattering," *Journal of Lightwave Technology*, vol. 37, no. 19, pp. 5122–5131, October 2019.

[43] R. Soref, "Design of low-energy on-chip electro-optical 1×M wavelength-selective switches," *Photon. Res.*, vol. 5, no. 4, pp. 340–345, August 2017.

[44] M. U. Masood *et al.*, "Networking analysis of photonics integrated multiband WSS based ROADM architecture," in *2022 International Conference on Software, Telecommunications and Computer Networks (SoftCOM)*, September 2022, pp. 1–6.

[45] Y. Ma, L. Stewart, J. Armstrong, I. G. Clarke, and G. Baxter, "Recent progress of wavelength selective switch," *Journal of Lightwave Technology*, vol. 39, no. 4, pp. 896–903, February 2021.

[46] *Wavelength selective switch (WSS) 1×9*, JDSU, November 2006. [Online]. Available: https://www.jdsu.com

[47] P. Momtahan, "Too many ROADMs? ICE6 can help," April 2023. [Online]. Available: https://www.infinera.com/blog/too-many-roadms-ice6-can-help/tag/optical/

[48] N. K. Fontaine, R. Ryf, D. T. Neilson, and H. Chen, "Low loss wavelength selective switch with 15-THz bandwidth," in *2018 European Conference on Optical Communication (ECOC)*, September 2018, pp. 1–3.

[49] N. K. Fontaine, M. Mazur, R. Ryf, H. Chen, L. Dallachiesa, and D. T. Neilson, "36-THz bandwidth wavelength selective switch," in *2021 European Conference on Optical Communication (ECOC)*, September 2021, pp. 1–4.

[50] T. Kato, S. Watanabe, T. Yamauchi, G. Nakagawa, H. Muranaka, Y. Tanaka, Y. Akiyama, and T. Hoshida, "Real-time transmission of 240×200-Gb/s signal in S+C+L triple-band WDM without S- or L-band transceivers," in *45th European Conference on Optical Communication (ECOC 2019)*, September 2019, pp. 1–4.

[51] T. Kato *et al.*, "Multi-band WDM transmission technology exceeding transceiver wavelength band," in *2020 Opto-Electronics and Communications Conference (OECC)*, October 2020, pp. 1–3.

[52] T. Yamauchi, T. Kato, G. Nakagawa, S. Watanabe, Y. Akiyama, and T. Hoshida, "Investigation on maximum transmission reach in wavelength converted systems," in *2019 24th OptoElectronics and Communications Conference (OECC) and 2019 International Conference on Photonics in Switching and Computing (PSC)*, July 2019, paper WB3-3.

[53] J. Pedro, "Designing transparent flexible-grid optical networks for maximum spectral efficiency [Invited]," *Journal of Optical Communications and Networking*, vol. 9, no. 4, pp. C35–C44, April 2017.

[54] Y. Li, J. Li, L. Zong, S. K. Bose, and G. Shen, "Upgrading nodes with colorless, directionless, and/or contentionless ROADMs in an optical transport network," in *2020 22nd International Conference on Transparent Optical Networks (ICTON)*, July 2020, paper Mo.C1.4.

[55] V. Curri, "Multiband optical transport: a cost-effective and seamless increase of network capacity," in *OSA Advanced Photonics Congress 2021*. Optica Publishing Group, July 2021, paper NeTu2C.3.

[56] FiberLabs Inc. [Online]. Available: https://www.fiberlabs.com/products/

[57] D. Semrau, R. I. Killey, and P. Bayvel, "A closed-form approximation of the Gaussian noise model in the presence of inter-channel stimulated raman scattering," *Journal of Lightwave Technology*, vol. 37, no. 9, pp. 1924–1936, May 2019.

[58] D. Semrau, E. Sillekens, R. I. Killey, and P. Bayvel, "Corrections to "A modulation format correction formula for the Gaussian noise model in the presence of inter-channel stimulated raman scattering"," *Journal of Lightwave Technology*, vol. 38, no. 6, pp. 1604–1604, March 2020.

[59] J. Pedro and S. Pato, "Capacity increase and hardware savings in DWDM networks exploiting next-generation optical line interfaces," in *2018 20th International Conference on Transparent Optical Networks (ICTON)*, July 2018, paper Th.A2.3.

[60] "OpenZR+ specifications, v. 3.0," September 2023. [Online]. Available: https://openzrplus.org/documents/

[61] T. Rahman, A. Napoli, D. Rafique, B. Spinnler, M. Kuschnerov, I. Lobato, B. Clouet, M. Bohn, C. Okonkwo, and H. de Waardt, "On the mitigation of optical filtering penalties originating from ROADM cascade," *IEEE Photonics Technology Letters*, vol. 26, no. 2, pp. 154–157, January 2014.

[62] X. Zhou and C. Xie, *Enabling technologies for high spectral-efficiency coherent optical communication networks*. John Wiley & Sons, 2016.

[63] *Series A Family of programmable optical processors, Finisar corporation, II-IV*, WaveShaper, 2020.

[64] V. Curri, M. Cantono, and R. Gaudino, "Elastic all-optical networks: a new paradigm enabled by the physical layer. how to optimize network performances?" *Journal of Lightwave Technology*, vol. 35, no. 6, pp. 1211–1221, January 2017.

[65] E. Amir, "K-shortest paths in a graph represented by a sparse matrix (Yen's algorithm)," 2012. [Online]. Available: https://www.mathworks.com/matlabcentral/fileexchange/35397-k-shortest-paths-in-a-graph-represented-by-a-sparse-matrix-yen-s-algorithm

Appendices

APPENDIX A

Number of components of C-band ROADMs

In this appendix, it is shown the list and the number of components needed for each C-band ROADM architecture. The components used to compute the total cost of the C-band node, are listed in Tables A1-A6.

TABLE A1. Number of components for CD C-band ROADM with A/D ratio of 25%.

Component	B&S				R&S			
	R=2	**R=4**	**R=8**	**R=16**	**R=2**	**R=4**	**R=8**	**R=16**
EDFA	4	8	16	32	4	8	16	32
$N_{A/D}$	3	5	5	9	3	5	5	9
1×2 S/C								
1×4 S/C	2							
1×8 S/C		4						
1×16 S/C			8					
1×32 S/C				16				
1×2 WSS	6				6			
1×4 WSS	2	10			4	10		
1×9 WSS		4	10			8	10	
1×20 WSS	6	10	8	18	6	10	16	18
1×40 WSS			10	34			10	50
TR	44	87	174	348	44	87	174	348

TABLE A2. Number of components for CD C-band ROADM with A/D ratio of 50%.

Component	B&S				R&S			
	R=2	**R=4**	**R=8**	**R=16**	**R=2**	**R=4**	**R=8**	**R=16**
EDFA	4	8	16	32	4	8	16	32
$N_{A/D}$	5	9	9	18	5	9	9	18
1×2 S/C								
1×4 S/C								
1×8 S/C	2							
1×16 S/C		4	8					
1×32 S/C								
1×64 S/C				16				
1×2 WSS	10				10			
1×4 WSS		18				18		
1×9 WSS	2		18		4		18	
1×20 WSS	10	22	8	32	10	26	18	36
1×40 WSS			18	52			18	104
TR	87	174	348	696	87	174	348	696

TABLE A3. Number of components for CDC MCS C-band ROADM with A/D ratio of 25%.

Component	B&S				R&S			
	R=2	**R=4**	**R=8**	**R=16**	**R=2**	**R=4**	**R=8**	**R=16**
EDFA	4	8	16	32	4	8	16	32
$N_{A/D}$	3	6	11	11	3	6	11	11
1×2 S/C								
1×4 S/C	2							
1×8 S/C								
1×16 S/C		4						
1×32 S/C			8	16				
1×64 S/C								
1×2 WSS								
1×4 WSS	2				4			
1×9 WSS		4				8		
1×20 WSS			8				16	
1×40 WSS				16				32
9×16 MCS	6	12	22	44	6	12	22	44
TR	44	87	174	348	44	87	174	348

TABLE A4. Number of components for CDC MCS C-band ROADM with A/D ratio of 50%.

Component	B&S				R&S			
	R=2	**R=4**	**R=8**	**R=16**	**R=2**	**R=4**	**R=8**	**R=16**
EDFA	4	8	16	32	4	8	16	32
$N_{A/D}$	6	11	22	22	6	11	22	22
1×2 S/C								
1×4 S/C								
1×8 S/C	2							
1×16 S/C		4						
1×32 S/C			8					
1×64 S/C				16				
1×2 WSS								
1×4 WSS								
1×9 WSS	2				4			
1×20 WSS		4				8		
1×40 WSS			8	16			16	32
9×16 MCS	12	22	44	88	12	22	22	88
TR	87	174	348	696	87	174	348	696

Some considerations were taken into account: in the case of CD A/D structure, for a ROADM with 8 and 16 directions, the use of 1×40 WSSs was considered, due to the high number of wavelengths to be inserted/extracted from the node, and for R=2 and 4, 1×20 WSSs were used in the A/D structure; On the CDC A/D structure of the node with degree 16, were used four MCSs or WSSs per card due to the low number of inputs, 9, being necessary 16, corresponding to the number of directions of the node, Figure A1.

TABLE A5. Number of components for CDC WSS C-band ROADM with A/D ratio of 25%.

Component	B&S				R&S			
	R=2	**R=4**	**R=8**	**R=16**	**R=2**	**R=4**	**R=8**	**R=16**
EDFA	4	8	16	32	4	8	16	32
$N_{A/D}$	3	5	10	10	3	5	10	10
1×2 S/C								
1×4 S/C	2							
1×8 S/C		4						
1×16 S/C								
1×32 S/C			8	16				
1×64 S/C								
1×2 WSS								
1×4 WSS	2				4			
1×9 WSS		4				8		
1×20 WSS			8				16	
1×40 WSS				16				32
9×18 WSS	6	10	20	40	6	10	20	40
TR	44	87	174	348	44	87	174	348

TABLE A6. Number of components for CDC WSS C-band ROADM with A/D ratio of 50%.

Component	B&S				R&S			
	R=2	**R=4**	**R=8**	**R=16**	**R=2**	**R=4**	**R=8**	**R=16**
EDFA	4	8	16	32	4	8	16	32
$N_{A/D}$	5	10	20	22	5	10	20	20
1×2 S/C								
1×4 S/C								
1×8 S/C	2							
1×16 S/C		4						
1×32 S/C			8					
1×64 S/C				16				
1×2 WSS								
1×4 WSS								
1×9 WSS	2				4			
1×20 WSS		4				8		
1×40 WSS			8	16			16	32
9×18 MCS	10	20	40	88	10	20	40	80
TR	87	174	348	696	87	174	348	696

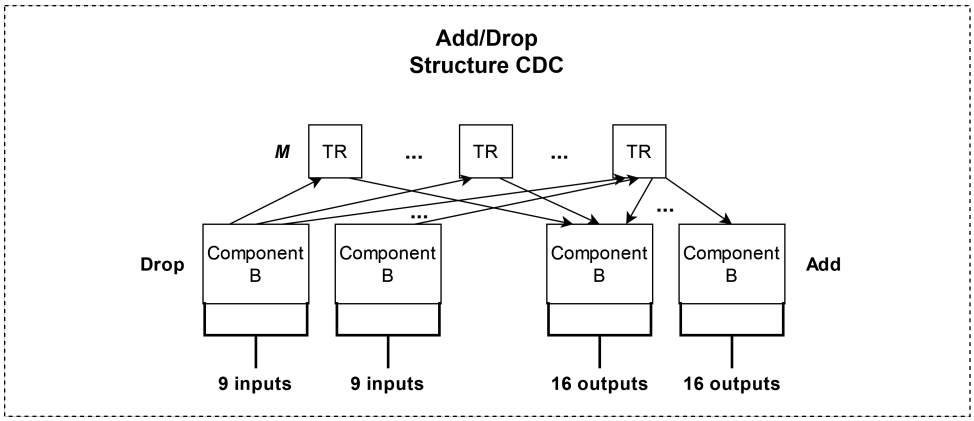

FIGURE A1. 16-degree CDC A/D structure.

APPENDIX B

Cost percentage increase of adding new bands to the AO-WC node

In this appendix, the cost increase values for the AO-WC architecture are shown when the L-band and L+S-bands are inserted into a C-band node (Table B1). Furthermore, the cost increase values are also shown when the S-band is inserted into a C+L node of the AO-WC architecture (Table B2).

TABLE B1. Approximate cost increase percentages of the additions of the L-band and the L+S bands in an R&S CD C-band node, for the AO-WC architecture, and an A/D ratio of 25% and 50%.

Degree	Percentage of node cost increase			
	L-band		L+S-bands	
	A/D ratio of 25%	**A/D ratio of 50%**	**A/D ratio of 25%**	**A/D ratio of 50%**
2	194.9%	187.5%	480.5%	459.9%
4	232.2%	205.1%	591.6%	514.6%
8	301.3%	242.1%	803.6%	621.6%
16	438.2%	313.0%	1207.0%	828.1%

TABLE B2. Approximate cost increase percentages of the addition of the S-band in an R&S CD C+L band node, for the AO-WC architecture, and an A/D ratio of 25% and 50%.

Degree	Percentage of node cost increase	
	A/D ratio of 25%	**A/D ratio of 50%**
2	96.8%	94.8%
4	108.2%	101.4%
8	125.2%	110.9%
16	142.8%	124.7%

APPENDIX C

Cost of the MB ROADM architectures for a more favorable scenario

In this appendix, the costs of the MB ROADM architectures are calculated for a more favorable cost scenario. Hence, tables C1-C4 show the total cost of the four MB ROADMs, considering CD, MCS-based CDC and WSS-based CDC A/D structures, for an A/D ratio of 25% and 50%, α=1.2 and β=0.5.

TABLE C1. Relative cost of the baseline MB ROADM architecture with an A/D ratio of 25% and 50%, R=2, 4, 8 and 16, considering the MB C+L and the C+L+S scenarios.

Add/Drop	Bands	Express	A/D ratio of 25%				A/D ratio of 50%			
			R=2	**R=4**	**R=8**	**R=16**	**R=2**	**R=4**	**R=8**	**R=16**
CD	C+L	**B&S**	4557	9092	18202	36705	9016	18074	36147	73096
		R&S	4573	9147	18333	37228	9037	18139	36277	73903
	C+L+S	**B&S**	7855	15724	31538	63419	15595	31269	62607	126484
		R&S	7883	15815	31813	64228	15628	31369	62880	127863
CDC	C+L MCS	**B&S**	4740	9424	18858	37838	9387	18703	37497	75282
		R&S	4756	9479	19061	38361	9414	18767	37757	76089
	C+L WSS	**B&S**	4732	9408	18860	37838	9365	18703	37489	75266
		R&S	4748	9463	19061	38361	9386	18767	37749	76073
	C+L+S MCS	**B&S**	8154	16264	32571	65264	16204	32334	64862	130010
		R&S	8181	16354	32916	66070	16248	32468	65407	131388
	C+L+S WSS	**B&S**	8186	16280	32629	65374	16214	32354	64814	130202
		R&S	8213	16370	32972	66182	16252	32452	65215	131580

TABLE C2. Relative cost of the MB ROADM architecture with AO-WCs, with an A/D ratio of 25% and 50%, R=2, 4, 8 and 16, considering the MB C+L and the C+L+S scenarios.

Add/Drop	Bands	Express	A/D ratio of 25%				A/D ratio of 50%			
			R=2	**R=4**	**R=8**	**R=16**	**R=2**	**R=4**	**R=8**	**R=16**
CD	C+L	**B&S**	4634	9534	20292	45637	9088	18507	38296	81976
		R&S	4655	9599	20421	46444	9109	18571	38485	83023
	C+L+S	**B&S**	8076	17031	37721	90161	15823	32638	68790	152652
		R&S	8109	17131	38125	90788	15868	32809	69192	153271
CDC	C+L MCS	**B&S**	4817	9866	20936	47010	9459	19171	39658	84162
		R&S	4838	9931	21197	48057	9486	19271	40061	85209
	C+L WSS	**B&S**	4809	9850	20936	46770	9443	19171	39650	84146
		R&S	4830	9915	21197	47577	9470	19271	40053	85193
	C+L+S MCS	**B&S**	8375	17572	38683	92004	16420	33666	71175	156758
		R&S	8407	17670	39084	93622	16464	33836	71983	158940
	C+L+S WSS	**B&S**	8407	17588	38739	92116	16436	33722	71271	156374
		R&S	8439	17686	39140	93734	16480	33892	72079	157980

TABLE C3. Relative cost of the MB ROADM architecture using a common-band, with an A/D ratio of 25% and 50%, R=2, 4, 8 and 16, considering the MB C+L and the C+L+S scenarios.

Add/Drop	Bands	Express	A/D ratio of 25%				A/D ratio of 50%			
			R=2	**R=4**	**R=8**	**R=16**	**R=2**	**R=4**	**R=8**	**R=16**
CD	C+L	**B&S**	4146	8311	16686	33855	8145	16459	32807	66093
		R&S	4166	8370	16924	34807	8174	16577	33043	67045
	C+L+S	**B&S**	7042	14208	28418	57556	13865	28070	56138	113716
		R&S	7087	14387	28772	58983	13954	28427	56852	116583
CDC	C+L MCS	**B&S**	4307	8596	17311	35105	8485	17029	34297	68593
		R&S	4326	8655	17549	36057	8514	17147	34773	69545
	C+L WSS	**B&S**	4307	8556	17231	34945	8445	16908	33817	68113
		R&S	4326	8615	17469	35897	8474	17027	34053	69065
	C+L+S MCS	**B&S**	7272	14598	29198	59116	14310	28618	57638	115289
		R&S	7317	14777	29552	60543	14399	28797	58352	116703
	C+L+S WSS	**B&S**	7232	14428	28958	58636	14230	28458	57278	114569
		R&S	7277	14517	29312	60063	14319	28637	57992	115983

TABLE C4. Relative cost of the MB ROADM compact architecture, with an A/D ratio of 25% and 50%, R=2, 4, 8 and 16, considering the MB C+L and the C+L+S scenarios.

Add/Drop	Bands	Express	A/D ratio of 25%				A/D ratio of 50%			
			R=2	**R=4**	**R=8**	**R=16**	**R=2**	**R=4**	**R=8**	**R=16**
CD	C+L	**B&S**	4556	9085	18127	36573	9011	18059	36040	73075
		R&S	4573	9133	18223	36955	9028	18107	36135	73839
	C+L+S	**B&S**	7842	15681	31320	63000	15577	31217	62451	125888
		R&S	7859	15729	31415	63382	15594	31265	62642	126652
CDC	C+L MCS	**B&S**	4739	9417	18856	37711	9383	18689	37444	75270
		R&S	4756	9465	19047	38093	9407	18736	37634	76034
	C+L WSS	**B&S**	4731	9387	18855	37709	9360	18673	37433	75249
		R&S	4748	9449	19046	38091	9377	18735	37623	76013
	C+L+S MCS	**B&S**	8141	16222	32425	64850	16182	32295	64712	129423
		R&S	8158	16270	32616	65230	16206	32391	65094	130187
	C+L+S WSS	**B&S**	8173	16237	32479	64957	16198	32302	64614	129610
		R&S	8190	16285	32670	65339	16222	32350	64804	130374

APPENDIX D

Cost percentage increase of the less favourable over the more favourable scenarios for AO-WC and common-band architectures

In this appendix, the cost percentage increase of the less favourable over the more favourable scenarios for AO-WC (Table D1) and common-band (Table D2) architectures are shown.

TABLE D1. Approximate cost percentages increase of the less favourable over the more favourable scenarios in an R&S CD node, for the AO-WC architecture, and an A/D ratio of 25% and 50%.

Degree	Percentage of node cost			
	A/D ratio of 25%		A/D ratio of 50%	
	C+L	**C+L+S**	**C+L**	**C+L+S**
2	4.7%	18.2%	2.4%	14.5%
4	13.5%	32.4%	6.9%	21.9%
8	29.7%	56.4%	15.8%	35.8%
16	55.8%	93.6%	31.2%	59.7%

TABLE D2. Approximate cost percentages increase of the less favourable over the more favourable scenarios in an R&S CD node, for the common-band architecture, and an A/D ratio of 25% and 50%.

Degree	Percentage of node cost			
	A/D ratio of 25%		A/D ratio of 50%	
	C+L	**C+L+S**	**C+L**	**C+L+S**
2	5.2%	6.1%	2.7%	3.1%
4	5.2%	6.0%	2.6%	3.1%
8	5.1%	6.0%	2.6%	3.1%
16	4.9%	5.9%	2.6%	2.9%

APPENDIX E

Networks topology

In this appendix, the network topologies of BT-UK and CONUS 60, used in subsection 2.4.3, are shown. The numbers represented in the links in Figures E1 and E2, represent the lengths of the links in km.

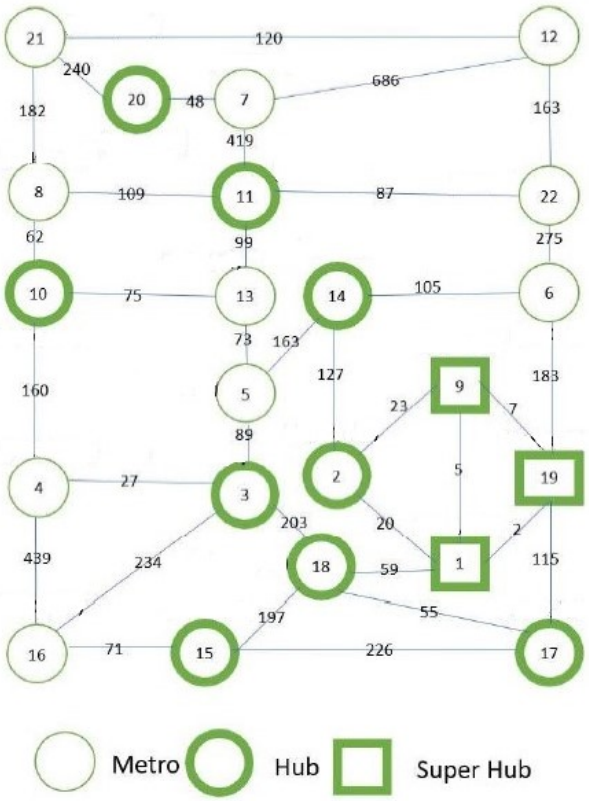

FIGURE E1. Physical topology of the BT-UK network.
Figure taken from [32].

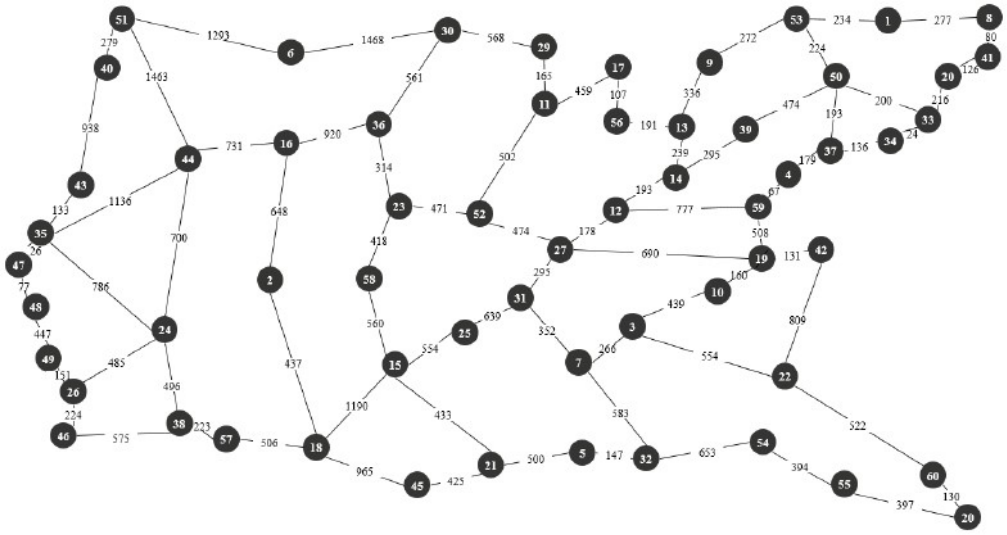

FIGURE E2. Physical topology of the CONUS 60 network.
Figure taken from [25].

APPENDIX F

Baseline architecture - components list and ILs of each optical path

In this appendix, the list and the number of components required for each optical path (express, add and drop paths) of the baseline architecture are shown. Tables F1-F3 show the components list for each optical path and band.

TABLE F1. Components list of the baseline architecture for the express path (1, 4 and 7), for each direction and band.

Directions	Components		
	C-band	**L-band**	**S-band**
2	2 WSSs 1 × 4	2 WSSs 1 × 9	
3	2 WSSs 1 × 9		
4	2 WSSs 1 × 9	2 WSSs 1 × 20	
8	2 WSSs 1 × 20		
16	2 WSSs 1 × 40		

From Table F1, it is observed that the size of the WSSs used increases with the number of directions due to the increase of the number of TRs which in turn leads to the increase in the number of A/D cards. The size of the express structure components is computed with (2.2). Note that the number of A/D cards of the C-band is smaller compared to the other bands due to the smaller number of C-band channels.

TABLE F2. Components list of the baseline architecture for the drop path (2, 5 and 8), for each direction and band.

Directions	Components		
	C-band	**L-band**	**S-band**
2	WSSs 1 × 4, WSS 2 × 1 and WSS 1 × 20	WSSs 1 × 9, WSS 2 × 1 and WSS 1 × 20	
3	WSSs 1 × 9, WSS 4 × 1 and WSS 1 × 20		
4	WSSs 1 × 9, WSS 4 × 1 and WSS 1 × 20	WSSs 1 × 20, WSS 4 × 1 and WSS 1 × 20	
8	WSSs 1 × 20, WSS 9 × 1 and WSS 1 × 40		
16	WSSs 1 × 40, WSS 20 × 1 and WSS 1 × 40		

From Tables F2 and F3, it is observed that the size of the WSSs used in the add and drop structures have 20 or 40 outputs, which is related to the number of TRs needed for each direction and band.

Table F4, shows the ILs for the express path, for each band and direction of the node.

From Table F4, the ILs of the express path for each direction are very similar, with about 1.2 dB (C-band), 0.8 dB (L-band) and 0.6 dB (S-band) of difference.

Appendix F *Components list and ILs of baseline architecture*

TABLE F3. Components list of the baseline architecture for the add path (3, 6 and 9), for each direction and band.

Directions	Components		
	C-band	**L-band**	**S-band**
2	WSS 20 × 1, WSSs 1 × 2, WSS 4 × 1	WSSs 20 × 1, WSS 1 × 2 and WSS 9 × 1	
3	WSSs 20 × 1, WSS 1 × 4 and WSS 9 × 1		
4	WSSs 20 × 1, WSS 1 × 4 and WSS 9 × 1	WSSs 20 × 1, WSS 1 × 4 and WSS 20 × 1	
8	WSSs 40 × 1, WSS 1 × 9 and WSS 20 × 1		
16	WSSs 40 × 1, WSS 1 × 20 and WSS 40 × 1		

TABLE F4. Insertion losses of the express path, for the baseline architecture for each direction and band.

Directions	Insertion losses [dB]		
	C-band	**L-band**	**S-band**
2	12.2	13.2	13.8
3	12.4	13.2	13.8
4	12.4	13.6	14.0
8	12.8	13.6	14.0
16	13.4	14.0	14.4

APPENDIX G

AO-WC architecture - components list and ILs of each optical path

In this appendix, it is shown the list and the number of components crossed by each optical path (express, add and drop paths) for the AO-WC architecture. Tables G1-G3 show the components list for each optical path and band.

TABLE G1. Components list of the AO-WC architecture for the express path (1, 2, 3, 6, 7, 8, 11, 12 and 13), for each direction and band.

Directions	Components		
	C-band	**L-band**	**S-band**
2	2 WSSs 1 × 9		
3	2 WSSs 1 × 20		
4	2 WSSs 1 × 20		
8	2 WSSs 1 × 40		
16	2 WSSs 1 × 80		

From Table G1, it is observed that the size of the WSSs used increases with the number of directions due to the increase of the number of TRs which in turn leads to the increase in the number of A/D cards. The size of the express structure components is computed with (2.8). When the node has 16 directions, a WSSs 1 × 80 is used, because of the high number of A/D cards (9, 13, 15, respectively, for C-, L- and S-bands) and the number of directions (16), using (2.8).

TABLE G2. Components list of the AO-WC architecture for the drop path (4, 9 and 14) for each direction and band.

Directions	Components
	C-band, L-band and S-band
2	WSSs 1 × 9, WSS 2 × 1 and WSS 1 × 20
3	WSSs 1 × 20, WSS 4 × 1 and WSS 1 × 20
4	WSSs 1 × 20, WSS 4 × 1 and WSS 1 × 20
8	WSSs 1 × 40, WSS 9 × 1 and WSS 1 × 40
16	WSSs 1 × 80, WSS 20 × 1 and WSS 1 × 40

From Tables G2 and G3, the components used in add and drop structures are the same used in the baseline architecture. Tables G4-G8, show the ILs for each express path shown in Figure 3.2.

From Tables G4-G8, it is possible to conclude that the express optical path with lower insertion losses is the path 1 (C-band→C-band), because of the smaller number of

TABLE G3. Components list of the AO-WC architecture for the add path (5, 10 and 15) for each direction and band.

Directions	Components
	C-band, L-band and S-band
2	WSSs 20 × 1, WSS 1 × 2 and WSS 9 × 1
3	WSSs 20 × 1, WSS 1 × 4 and WSS 20 × 1
4	WSSs 20 × 1, WSS 1 × 4 and WSS 20 × 1
8	WSSs 40 × 1, WSS 1 × 9 and WSS 40 × 1
16	WSSs 40 × 1, WSS 1 × 20 and WSS 80 × 1

TABLE G4. Insertion losses of the express paths of the AO-WC architecture with 2 directions, for C-, L- and S-bands.

Express path	Insertion losses [dB]
1 C-band→C-band	12.4
2 C-band→L-band	12.8
3 C-band→S-band	13.1
6 L-band→L-band	13.2
7 L-band→C-band	12.8
8 L-band→S-band	13.5
11 S-band→S-band	13.8
12 S-band→C-band	13.1
13 S-band→L-band	13.5

TABLE G5. Insertion losses of the express paths of the AO-WC architecture with 3 directions, for C-, L- and S-bands.

Express path	Insertion losses [dB]
1 C-band→C-band	12.8
2 C-band→L-band	13.2
3 C-band→S-band	13.4
6 L-band→L-band	13.6
7 L-band→C-band	13.2
8 L-band→S-band	13.8
11 S-band→S-band	14.0
12 S-band→C-band	13.4
13 S-band→L-band	13.8

TABLE G6. Insertion losses of the express paths of the AO-WC architecture with 4 directions, for C-, L- and S-bands.

Express path	Insertion losses [dB]
1 C-band→C-band	12.8
2 C-band→L-band	13.2
3 C-band→S-band	13.4
6 L-band→L-band	13.6
7 L-band→C-band	13.2
8 L-band→S-band	13.8
11 S-band→S-band	14.0
12 S-band→C-band	13.4
13 S-band→L-band	13.8

channels used by the C-band WSS when compared with the L- and S-bands. On the other hand, the express optical path 11 (S-band→S-band) has the highest insertion losses, for

TABLE G7. Insertion losses of the express paths of the AO-WC architecture with 8 directions, for C-, L- and S-bands.

Express path	Insertion losses [dB]
1 C-band→C-band	13.4
2 C-band→L-band	13.7
3 C-band→S-band	13.9
6 L-band→L-band	14.0
7 L-band→C-band	13.7
8 L-band→S-band	14.2
11 S-band→S-band	14.4
12 S-band→C-band	13.9
13 S-band→L-band	14.2

TABLE G8. Insertion losses of the express paths of the AO-WC architecture with 16 directions, for C-, L- and S-bands.

Express path	Insertion losses [dB]
1 C-band→C-band	14.4
2 C-band→L-band	14.6
3 C-band→S-band	14.8
6 L-band→L-band	14.8
7 L-band→C-band	14.6
8 L-band→S-band	15.0
11 S-band→S-band	15.2
12 S-band→C-band	14.8
13 S-band→L-band	15.0

all node directions, compared with the remaining express paths, due to the high number of channels of the S-band. In general, the ILs for each express path and direction are similar, for example, for the worst optical path (11), the ILs vary between 13.8 (2 directions) and 15.2 dB (16 directions), a difference of 1.4 dB.

APPENDIX H

Common-band architecture - components list and ILs of each optical path

In this appendix, the list and the number of components required for each optical path (express, add and drop) of the common-band architecture, are shown. Tables H1-H3 show the components list for each optical path. Note that all components used in the common-band architecture are C-band, due to the AO-WC. However, the AO-WC is not taken into account in the following tables, because its ILs are compensated by an OA inside each AO-WC device.

TABLE H1. Components list of the common-band architecture for the express path (1) and for each direction.

Directions	Components
2	2 WSSs 1 × 20
3	2 WSSs 1 × 20
4	2 WSSs 1 × 40
8	2 WSSs 1 × 40
16	2 WSSs 1 × 80

From Table H1, when the node has 16 directions, is used WSS 1 × 80, due to the high number of A/D cards (19) and due to the high number of directions of the node (16). In addition, the same WSSs are used when the node has 2 and 3 directions (WSSs 1 × 20) and when it has 4 and 8 directions (WSSs 1 × 40). The size of the WSSs used in the express path is computed with (2.8).

TABLE H2. Components list of the common-band architecture for the drop path (2), and for each direction.

Directions	Components
2	WSSs 1 × 20, WSS 9 × 1 and WSS 1 × 20
3	WSSs 1 × 20, WSS 9 × 1 and WSS 1 × 20
4	WSSs 1 × 40, WSS 20 × 1 and WSS 1 × 20
8	WSSs 1 × 40, WSS 40 × 1 and WSS 1 × 40
16	WSSs 1 × 80, WSS 80 × 1 and WSS 1 × 80

From Tables H2 and H3, when the node has 16 directions, the WSSs used in add and drop structure are WSSs 1 × 80, due to the same reason said previously. As expected, with the increase in the number of directions, the size of the WSSs of the add and drop paths increases. Table H4, shows the ILs for the express path.

TABLE H3. Components list of the common-band architecture for the add path (3) and for each direction.

Directions	Components
2	WSS 20 × 1, WSSs 1 × 9 and WSS 20 × 1
3	WSSs 20 × 1, WSS 1 × 9 and WSS 20 × 1
4	WSSs 20 × 1, WSS 1 × 20 and WSS 40 × 1
8	WSSs 40 × 1, WSS 1 × 40 and WSS 40 × 1
16	WSSs 80 × 1, WSS 1 × 80 and WSS 80 × 1

TABLE H4. Insertion losses of the express path, for the common-band architecture for each direction.

Directions	Insertion losses [dB]
2	12.8
3	12.8
4	13.4
8	13.4
16	14.4

From Table H4, is possible to see that the ILs of the express path are similar for each direction, ranging from 12.8 e 14.4, about 1.6 dB of difference between the node with 2 and 16 directions.

APPENDIX I

Compact architecture - components list and ILs of each optical path

In this appendix, the list and the number of components needed for each optical path (express, add and drop) of the compact architecture, are presented. Tables I1-I3 show the components list for each optical path.

TABLE I1. Components list of the compact architecture for the express path (1), for each direction and band.

Directions	Components		
	C-band	**L-band**	**S-band**
2	2 MB WSSs 1 × 9		
3	2 MB WSSs 1 × 9		
4	2 MB WSSs 1 × 20		
8	2 MB WSSs 1 × 20		
16	2 MB WSSs 1 × 40		

TABLE I2. Components list of the compact architecture for the drop path (2, 4 and 6), for each direction and band.

Directions	Components
	C-band, L-band and S-band
2	MB WSSs 1 × 9, MB-DEMUX, WSS 2 × 1 and WSS 1 × 20
3	MB WSSs 1 × 9, MB-DEMUX, WSS 4 × 1 and WSS 1 × 20
4	MB WSSs 1 × 20, MB-DEMUX, WSS 4 × 1 and WSS 1 × 20
8	MB WSSs 1 × 20, MB-DEMUX, WSS 9 × 1 and WSS 1 × 40
16	MB WSSs 1 × 40, MB-DEMUX, WSS 20 × 1 and WSS 1 × 40

TABLE I3. Components list of the compact architecture for the add path (3, 5 and 7), for each direction and band.

Directions	Components
	C-band, L-band and S-band
2	WSSs 20 × 1, WSS 1 × 2, MB-MUX and MB WSS 9 × 1
3	WSSs 20 × 1, WSS 1 × 4, MB-MUX and MB WSS 9 × 1
4	WSSs 20 × 1, WSS 1 × 4, MB-MUX and MB WSS 20 × 1
8	WSSs 40 × 1, WSS 1 × 9, MB-MUX and MB WSS 20 × 1
16	WSSs 40 × 1, WSS 1 × 20, MB-MUX and MB WSS 40 × 1

From Table I1, the size of the WSSs increase as expected with the increase in the number of directions. The size of the WSSs used in the express path is computed with (2.2). Furthermore, from Tables I2 and I3, in addition to the WSSs of the express, add

and drop structures, the MB-DEMUX/MUX, are also used. Table I4, show the ILs for the express path for each band and direction of the node.

TABLE I4. Insertion losses of the express path, for the compact architecture for each band and direction.

Directions	Insertion losses [dB]		
	C-band	**L-band**	**S-band**
2	16.2		
3	16.2		
4	16.2		
8	16.2		
16	16.4		

From Table I4, is possible to see that the ILs of the express path are similar for each direction, with about 0.2 dB of difference between the node with 2 and 16 directions.

APPENDIX J

ASE noise power for each band and link of the BT-UK topology considering the baseline, common-band and compact architectures

In this appendix, the number of in-line amplifiers for each link, pre-amplifier gain for each link, and ASE noise for each link, for the C-, L- and S-bands and for BT-UK topology, are presented. Tables J1-J3 show the ASE noise power for each band, link of the BT-UK topology (Figure E1) and for the baseline, common-band and compact architectures.

From Table J1, it is verified that the ASE noise power increases with the increase of the distance between links as expected, happening the same behavior to the remaining bands. The ASE noise power of the compact architecture for the C-band is higher compared with the ASE noise power obtained for the remaining MB architectures due to the higher C-band post-amplifier gain of the compact architecture (24.3 dB) compared with the C-band post-amplifier gain of the remaining architectures. In addition, the ASE noise power of the baseline architecture is lower compared with the ASE noise power of the remaining MB architectures due to a smaller post-amplifier gain (19.8 dB) compared with the post-amplifier gains of the common-band (21.6 dB) and compact (24.3 dB) architectures.

From Table J2, it is verified that the ASE noise power of the common-band architecture for the L-band is higher compared with the ASE noise power obtained for the baseline architecture due to the higher post-amplifier gain and due to the consideration of the ASE noise present in the OAs inside of the AO-WCs. In this situation for the common-band architecture, each link has 2 OAs to compensate the ILs of the 2 AO-WCs: the L-band path has one C-band EDFA and one L-band EDFA. Although, in this situation, the ASE noise power of the common-band architecture is slightly higher than the ASE noise power of the compact architecture, due to slightly the higher post-amplifier ASE noise power plus the additional ASE noise power due to AO-WCs (3.37+4.48=7.85 μW) of the common-band architecture for each link, compared to the post-amplifier ASE noise power of the compact architecture (7.39 μW) for each link. Finally, the baseline architecture

TABLE J1. Number of in-line amplifiers for each link, pre-amplifier gain for each link, and ASE noise for each link. These values are for the C-band, for the baseline, common-band and compact architectures and for the BT-UK topology.

Links	No. of in-line amplifiers ($N_{in,i}$)	Gain [dB]	ASE noise [μW]		
			Baseline	**Common-band**	**Compact**
1-2	0	9.70	2.25	3.32	6.04
1-9	0	6.93	2.15	3.22	5.94
1-18	0	16.92	3.12	4.19	6.91
1-19	0	6.37	2.14	3.21	5.92
2-9	0	10.26	2.27	3.34	6.07
2-14	1	14.75	3.32	4.39	7.12
3-4	0	11.00	2.32	3.39	6.11
3-5	0	22.47	5.89	6.97	9.69
3-16	1	24.65	14.75	15.82	18.54
3-18	1	21.78	8.60	9.67	12.39
4-10	1	17.80	4.65	5.72	8.44
4-16	3	21.80	15.21	16.28	19.00
5-13	0	19.51	3.99	5.06	7.78
5-14	1	18.08	4.83	5.90	8.62
6-14	0	25.43	9.66	10.73	13.45
6-19	1	19.93	6.32	7.39	10.11
6-22	2	18.96	7.15	8.22	10.95
7-11	2	27.84	41.83	42.90	45.62
7-12	4	26.58	51.66	52.73	55.45
7-20	0	14.88	2.71	3.78	6.51
8-10	0	17.47	3.26	4.33	7.05
8-11	0	26.17	11.07	12.14	14.87
8-21	1	19.84	6.23	7.30	10.02
9-19	0	7.30	2.16	3.23	5.95
10-13	0	19.88	4.16	5.23	7.96
11-13	0	24.32	7.94	9.01	11.73
11-22	0	22.10	5.58	6.65	9.37
12-21	0	28.20	16.47	17.54	20.26
12-22	1	18.08	4.83	5.90	8.62
15-16	0	19.14	3.83	4.90	7.62
15-17	1	23.91	12.75	13.83	16.55
15-18	1	21.22	7.81	8.88	11.60
17-18	0	16.18	2.95	4.02	6.74
17-19	0	27.28	13.70	14.77	17.50
20-21	1	25.20	16.48	17.55	20.28

has lower ASE noise power due to lower post-amplifier gain (20.8 dB) compared with the post-amplifier gain of the common-band (21.6 dB) and compact architectures (25.0 dB).

From Table J3, it is verified that the ASE noise power of the compact architecture for the S-band is higher compared with the ASE noise power obtained for the baseline architecture due to the higher post-amplifier gain (25.4 dB). In this situation for the common-band architecture, each link has 2 OAs to compensate the ILs of the 2 AO-WCs: the S-band path has one C-band EDFA and one S-band TDFA. Furthermore, the ASE noise power of the compact architecture is higher than the ASE noise power of the common-band architecture, due to the higher post-amplifier ASE noise power (12.74 μW)

TABLE J2. Number of in-line amplifiers for each link, pre-amplifier gain for each link, and ASE noise for each link. These values are for the L-band, for the baseline, common-band and compact architectures and for the BT-UK topology.

Links	No. of in-line amplifiers ($N_{in,i}$)	Gain [dB]	ASE noise [μW]		
			Baseline	**Common-band**	**Compact**
1-2	0	9.70	2.99	8.05	7.59
1-9	0	6.93	2.89	7.94	7.49
1-18	0	16.92	3.93	8.98	8.52
1-19	0	6.37	2.88	7.93	7.47
2-9	0	10.26	3.02	8.08	7.62
2-14	1	14.75	4.15	9.20	8.75
3-4	0	11.00	3.07	8.12	7.67
3-5	0	22.47	6.91	11.97	11.51
3-16	1	24.65	16.42	21.48	21.02
3-18	1	21.78	9.81	14.87	14.41
4-10	1	17.80	5.58	10.63	10.17
4-16	3	21.80	16.92	21.97	21.51
5-13	0	19.51	4.87	9.92	9.46
5-14	1	18.08	5.76	10.82	10.36
6-14	0	25.43	10.95	16.01	15.55
6-19	1	19.93	7.36	12.42	11.96
6-22	2	18.96	8.26	13.32	12.86
7-11	2	27.84	4.55	50.56	50.10
7-12	4	26.58	56.07	61.12	60.67
7-20	0	14.88	3.49	8.55	8.09
8-10	0	17.47	4.08	9.14	8.68
8-11	0	26.17	12.47	17.53	17.07
8-21	1	19.84	7.27	12.32	11.86
9-19	0	7.30	2.90	7.95	7.50
10-13	0	19.88	5.05	10.11	9.65
11-13	0	24.32	9.11	14.16	13.71
11-22	0	22.10	6.57	11.63	11.17
12-21	0	28.20	18.27	23.33	22.87
12-22	1	18.08	5.76	10.82	10.36
15-16	0	19.14	4.70	9.75	9.29
15-17	1	23.91	14.28	19.33	18.88
15-18	1	21.22	8.97	14.02	13.56
17-18	0	16.18	3.75	8.80	8.34
17-19	0	27.28	15.30	20.35	19.90
20-21	1	25.20	18.29	23.34	22.88

for each link, compared to the post-amplifier ASE noise power plus the additional ASE noise power due to AO-WCs (5.29+5.81=11.10 μW) of the common-band architecture for each link. Finally, as happens for the previous bands, the baseline architecture has lower ASE noise power due to lower post-amplifier gain (21.4 dB).

From Tables J1-J3, it is verified that the ASE noise power increases with the increase of the distance between links. Furthermore, as expected, the ASE noise power considering the S-band is higher than the ASE noise power obtained for the remaining bands due to the higher value of the noise figure, 6.40 dB, and the higher value of the nominal frequency of the central channel, 199.025 THz. In addition, the link with the highest ASE noise power

TABLE J3. Number of in-line amplifiers for each link, pre-amplifier gain for each link, and ASE noise for each link. These values are for the S-band, for the baseline, common-band and compact architectures and for the BT-UK topology.

Links	No. of in-line amplifiers ($N_{in,i}$)	Gain [dB]	ASE noise [μW]		
			Baseline	**Common-band**	**Compact**
1-2	0	10.00	5.38	11.43	13.07
1-9	0	7.00	5.20	11.25	12.89
1-18	0	17.80	7.23	13.28	14.92
1-19	0	6.40	5.17	11.22	12.86
2-9	0	10.60	5.43	11.48	13.12
2-14	1	15.70	7.71	13.76	15.40
3-4	0	11.40	5.52	11.57	13.21
3-5	0	23.80	13.85	19.90	21.54
3-16	1	26.40	37.14	43.19	44.83
3-18	1	23.30	20.73	26.78	28.42
4-10	1	19.00	10.83	16.88	18.52
4-16	3	23.45	37.52	43.56	45.20
5-13	0	20.60	9.24	15.29	16.93
5-14	1	19.30	11.25	17.30	18.94
6-14	0	27.00	23.48	29.53	31.17
6-19	1	21.30	14.91	20.96	22.60
6-22	2	20.33	16.87	22.92	24.56
7-11	2	29.93	113.78	119.83	121.47
7-12	4	28.64	139.55	145.60	147.24
7-20	0	15.60	6.35	12.40	14.04
8-10	0	18.40	7.56	13.61	15.25
8-11	0	27.80	27.21	33.26	34.90
8-21	1	21.20	14.69	20.74	22.38
9-19	0	7.40	5.21	11.26	12.90
10-13	0	21.00	9.65	15.70	17.34
11-13	0	25.80	19.02	25.07	26.71
11-22	0	23.40	13.07	19.12	20.76
12-21	0	30.00	41.85	47.90	49.54
12-22	1	19.30	11.25	17.30	18.94
15-16	0	20.20	8.87	14.92	16.56
15-17	1	25.60	31.73	37.78	39.42
15-18	1	22.70	18.70	24.74	26.38
17-18	0	17.00	6.86	12.91	14.55
17-19	0	29.00	34.28	40.33	41.97
20-21	1	27.00	41.90	47.95	49.59

is (7−12) due to the link length (686 km), moreover, this link has the highest number of in-line amplifiers, 4. Finally, the link with the lowest ASE noise power is (1−19) since it is the link with the shortest length, 2 km, for all bands, compared to the remaining links. For example, to compute the total ASE noise power for the L-band and for the candidate path $P_{3,4}$ is to sum the ASE noise power of the links for the common-band architecture and for the L-band with Table J2: (1−18) 8.98 μW, (18−3) 14.87 μW, (3−5) 11.97 μW, (5−13) 9.92 μW, (13−11) 14.16 μW, and (11−7) 50.56 μW, which summing up gives 110.46 μW, Table 3.10.

APPENDIX K

NLI coefficient with correction factor and NLI noise power for each band and link of the BT-UK topology

This appendix presents the NLI coefficient considering the modulation correction and NLI noise power for each link, for the C-, L- and S-bands and for BT-UK topology (Figure E1). Tables K1-K3 show the NLI coefficient with correction factor and NLI noise power with a coherent factor equal to 0, with modulation format correction for each band and link, and considering the modulation formats of 64-QAM, 16-QAM and QPSK.

From Tables K1-K3, it is observed that the length and number of spans affect the NLI coefficient with correction factor and the NLI noise power of each section, however, links with only one section have the same value of NLI noise power, due to the number of spans equal to 1 (see eq. (3.24)). For links with a number of spans greater than 1, the NLI coefficient with correction factor and the NLI noise power varies depending on the number and size of spans. It can be seen that the NLI noise power for the L-band is higher in relation to the other frequencies due to the ISRS effect, which consists of a wideband phenomenon that origins power transfers from high to low frequencies, the same behavior can be observed in [40]. In addition, the NLI noise power is higher for 64-QAM in comparison with the other modulation formats, due to the higher value of excess kurtosis (Table 3.11). Finally, it is found that link (7−12) present the highest NLI noise power for all three bands and modulation formats, due to the higher number of spans (5) and span length (137.20 km). In opposition, the links with only one span present the lowest NLI noise value comparatively with the remaining paths. For example, to compute the total NLI noise power for the L-band, QPSK modulation, and for the candidate path $P_{3,4}$ is to sum the NLI noise power of the links and for the L-band with Table K2: (1−18) 0.248 μW, (18−3) 0.487 μW, (3−5) 0.248 μW, (5−13) 0.248 μW, (13−11) 0.248 μW, and (11−7) 1.041 μW, which summing up gives 2.518 μW, Table 3.13.

Appendix K *NLI coefficient with correction factor and NLI noise power*

TABLE K1. NLI coefficient with correction factor and NLI noise power with correction considering the modulation formats of 64-QAM, 16-QAM and QPSK. These values are for the C-band, and for the BT-UK topology.

Links	Number of spans (N_{spans})	Span length [km] (L_{span})	NLI coefficient with correction factor [dB] ($\eta_{N_{spans}}$)			NLI noise power [μW] (p_{NLI})		
			64-QAM	**16-QAM**	**QPSK**	**64-QAM**	**16-QAM**	**QPSK**
1-2	1	20	24.81	24.54	22.73	0.303	0.284	0.188
1-9	1	5	24.81	24.54	22.73	0.303	0.284	0.188
1-18	1	59	24.81	24.54	22.73	0.303	0.284	0.188
1-19	1	2	24.81	24.54	22.73	0.303	0.284	0.188
2-9	1	23	24.81	24.54	22.73	0.303	0.284	0.188
2-14	2	63.50	27.18	26.78	23.80	0.522	0.477	0.240
3-4	1	27	24.81	24.54	22.73	0.303	0.284	0.188
3-5	1	89	24.81	24.54	22.73	0.303	0.284	0.188
3-16	2	117	28.10	27.88	26.44	0.646	0.613	0.440
3-18	2	101.50	27.95	27.70	26.06	0.624	0.588	0.404
4-10	2	80	27.62	27.31	25.19	0.578	0.538	0.330
4-16	4	109.75	31.64	31.49	30.61	1.460	1.411	1.152
5-13	1	73	24.81	24.54	22.73	0.303	0.284	0.188
5-14	2	81.50	27.65	27.35	25.27	0.582	0.543	0.337
6-14	1	105	24.81	24.54	22.73	0.303	0.284	0.188
6-19	2	91.50	27.82	27.54	25.73	0.605	0.568	0.374
6-22	3	91.67	30.01	29.80	28.53	1.002	0.956	0.713
7-11	3	139.67	30.41	30.26	29.39	1.099	1.062	0.870
7-12	5	137.20	32.90	32.79	32.15	1.951	1.901	1.642
7-20	1	48	24.81	24.54	22.73	0.303	0.284	0.188
8-10	1	62	24.81	24.54	22.73	0.303	0.284	0.188
8-11	1	109	24.81	24.54	22.73	0.303	0.284	0.188
8-21	2	91	27.81	27.54	25.71	0.604	0.567	0.372
9-19	1	7	24.81	24.54	22.73	0.303	0.284	0.188
10-13	1	75	24.81	24.54	22.73	0.303	0.284	0.188
11-13	1	99	24.81	24.54	22.73	0.303	0.284	0.188
11-22	1	87	24.81	24.54	22.73	0.303	0.284	0.188
12-21	1	120	24.81	24.54	22.73	0.303	0.284	0.188
12-22	2	81.50	27.65	27.35	25.27	0.582	0.543	0.337
15-16	1	71	24.81	24.54	22.73	0.303	0.284	0.188
15-17	2	113	28.07	27.83	26.35	0.641	0.607	0.432
15-18	2	98.50	27.91	27.65	25.97	0.618	0.583	0.395
17-18	1	55	24.81	24.54	22.73	0.303	0.284	0.188
17-19	1	115	24.81	24.54	22.73	0.303	0.284	0.188
20-21	2	120	28.13	27.90	26.49	0.650	0.617	0.446

Appendix K *NLI coefficient with correction factor and NLI noise power*

TABLE K2. NLI coefficient with correction factor and NLI noise power with correction considering the modulation formats of 64-QAM, 16-QAM and QPSK. These values are for the L-band, and for the BT-UK topology.

Links	Number of spans (N_{spans})	Span length [km] (L_{span})	NLI coefficient with correction factor [dB] ($\eta_{N_{spans}}$)			NLI noise power [μW] (p_{NLI})		
			64-QAM	**16-QAM**	**QPSK**	**64-QAM**	**16-QAM**	**QPSK**
1-2	1	20	25.76	25.51	23.94	0.376	0.356	0.248
1-9	1	5	25.76	25.51	23.94	0.376	0.356	0.248
1-18	1	59	25.76	25.51	23.94	0.376	0.356	0.248
1-19	1	2	25.76	25.51	23.94	0.376	0.356	0.248
2-9	1	23	25.76	25.51	23.94	0.376	0.356	0.248
2-14	2	63.50	27.92	27.52	24.46	0.619	0.565	0.279
3-4	1	27	25.76	25.51	23.94	0.376	0.356	0.248
3-5	1	89	25.76	25.51	23.94	0.376	0.356	0.248
3-16	2	117	28.90	28.67	27.26	0.776	0.737	0.533
3-18	2	101.50	28.73	28.49	26.87	0.747	0.706	0.487
4-10	2	80	28.39	28.08	25.95	0.690	0.642	0.394
4-16	4	109.75	32.39	32.24	31.34	1.736	1.676	1.363
5-13	1	73	25.76	25.51	23.94	0.376	0.356	0.248
5-14	2	81.50	28.42	28.11	26.04	0.695	0.648	0.402
6-14	1	105	25.76	25.51	23.94	0.376	0.356	0.248
6-19	2	91.50	28.60	28.32	26.52	0.724	0.680	0.449
6-22	3	91.67	30.76	30.55	29.26	1.191	1.135	0.843
7-11	3	139.67	31.18	31.04	30.17	1.313	1.270	1.041
7-12	5	137.20	33.66	33.54	32.90	2.321	2.261	1.948
7-20	1	48	25.76	25.51	23.94	0.376	0.356	0.248
8-10	1	62	25.76	25.51	23.94	0.376	0.356	0.248
8-11	1	109	25.76	25.51	23.94	0.376	0.356	0.248
8-21	2	91	28.59	28.31	26.50	0.722	0.678	0.447
9-19	1	7	25.76	25.51	23.94	0.376	0.356	0.248
10-13	1	75	25.76	25.51	23.94	0.376	0.356	0.248
11-13	1	99	25.76	25.51	23.94	0.376	0.356	0.248
11-22	1	87	25.76	25.51	23.94	0.376	0.356	0.248
12-21	1	120	25.76	25.51	23.94	0.376	0.356	0.248
12-22	2	81.50	28.42	28.11	26.04	0.695	0.648	0.402
15-16	1	71	25.76	25.51	23.94	0.376	0.356	0.248
15-17	2	113	28.86	28.63	27.18	0.769	0.729	0.522
15-18	2	98.50	28.70	28.44	26.78	0.741	0.698	0.476
17-18	1	55	25.76	25.51	23.94	0.376	0.356	0.248
17-19	1	115	25.76	25.51	23.94	0.376	0.356	0.248
20-21	2	120	28.92	28.70	27.32	0.780	0.742	0.540

TABLE K3. NLI coefficient with correction factor and NLI noise power with correction considering the modulation formats of 64-QAM, 16-QAM and QPSK. These values are for the S-band, and for the BT-UK topology.

Links	Number of spans (N_{spans})	Span length [km] (L_{span})	NLI coefficient with correction factor [dB] ($\eta_{N_{spans}}$)			NLI noise power [μW] (p_{NLI})		
			64-QAM	**16-QAM**	**QPSK**	**64-QAM**	**16-QAM**	**QPSK**
1-2	1	20	23.46	23.16	21.08	0.222	0.207	0.128
1-9	1	5	23.46	23.16	21.08	0.222	0.207	0.128
1-18	1	59	23.46	23.16	21.08	0.222	0.207	0.128
1-19	1	2	23.46	23.16	21.08	0.222	0.207	0.128
2-9	1	23	23.46	23.16	21.08	0.222	0.207	0.128
2-14	2	63.50	26.28	25.94	23.53	0.425	0.393	0.226
3-4	1	27	23.46	23.16	21.08	0.222	0.207	0.128
3-5	1	89	23.46	23.16	21.08	0.222	0.207	0.128
3-16	2	117	27.02	26.80	25.47	0.503	0.479	0.352
3-18	2	101.50	26.89	26.66	25.18	0.489	0.463	0.329
4-10	2	80	26.63	26.35	24.51	0.460	0.432	0.283
4-16	4	109.75	30.59	30.46	29.69	1.147	1.112	0.931
5-13	1	73	23.46	23.16	21.08	0.222	0.207	0.128
5-14	2	81.50	26.65	26.38	24.58	0.463	0.435	0.287
6-14	1	105	23.46	23.16	21.08	0.222	0.207	0.128
6-19	2	91.50	26.79	26.54	24.92	0.477	0.451	0.310
6-22	3	91.67	28.99	28.81	27.70	0.792	0.760	0.589
7-11	3	139.67	29.31	29.18	28.38	0.854	0.827	0.688
7-12	5	137.20	31.82	31.72	31.16	1.521	1.486	1.305
7-20	1	48	23.46	23.16	21.08	0.222	0.207	0.128
8-10	1	62	23.46	23.16	21.08	0.222	0.207	0.128
8-11	1	109	23.46	23.16	21.08	0.222	0.207	0.128
8-21	2	91	26.78	26.53	24.90	0.477	0.450	0.309
9-19	1	7	23.46	23.16	21.08	0.222	0.207	0.128
10-13	1	75	23.46	23.16	21.08	0.222	0.207	0.128
11-13	1	99	23.46	23.16	21.08	0.222	0.207	0.128
11-22	1	87	23.46	23.16	21.08	0.222	0.207	0.128
12-21	1	120	23.46	23.16	21.08	0.222	0.207	0.128
12-22	2	81.50	26.65	26.38	24.58	0.463	0.435	0.287
15-16	1	71	23.46	23.16	21.08	0.222	0.207	0.128
15-17	2	113	26.99	26.77	25.40	0.500	0.475	0.347
15-18	2	98.50	26.86	26.63	25.11	0.486	0.460	0.324
17-18	1	55	23.46	23.16	21.08	0.222	0.207	0.128
17-19	1	115	23.46	23.16	21.08	0.222	0.207	0.128
20-21	2	120	27.04	26.83	25.51	0.506	0.482	0.356

APPENDIX L

Total NLI noise power for each band and candidate path of the BT-UK topology

This appendix presents the total NLI noise power for each candidate path, for the C-, L- and S-bands and for BT-UK network (Figure E1). Table L1 shows the total number of spans in each candidate path of the three demands considered previously (1−2, 1−3 and 1−7) and the total NLI noise power calculated at the end of each candidate path for the C-, L- and S-bands, assessed with (3.17), considering Φ=0 (Gaussian modulation).

TABLE L1. Total NLI noise power for the candidate paths considering the Gaussian modulation and for the C-, L- and S-bands.

Paths	Distance [km]	Total number of spans	Total NLI noise power [μW] (p_{NLI})		
			C-band	**L-band**	**S-band**
$\boldsymbol{P}_{1,1}$	20	1	0.490	0.585	0.374
$\boldsymbol{P}_{1,2}$	28	2	0.981	1.171	0.749
$\boldsymbol{P}_{1,3}$	32	3	1.471	1.756	1.123
$\boldsymbol{P}_{1,4}$	417	6	2.942	3.512	2.246
$\boldsymbol{P}_{1,5}$	427	7	3.433	4.097	2.620
$\boldsymbol{P}_{2,1}$	262	3	1.471	1.756	1.123
$\boldsymbol{P}_{2,2}$	375	5	2.452	2.926	1.872
$\boldsymbol{P}_{2,3}$	385	6	2.942	3.512	2.246
$\boldsymbol{P}_{2,4}$	399	6	2.942	3.512	2.246
$\boldsymbol{P}_{2,5}$	407	7	3.433	4.097	2.620
$\boldsymbol{P}_{3,1}$	901	10	4.904	5.853	3.743
$\boldsymbol{P}_{3,2}$	909	11	5.394	6.438	4.117
$\boldsymbol{P}_{3,3}$	913	12	5.885	7.023	4.492
$\boldsymbol{P}_{3,4}$	942	9	4.414	5.268	3.369
$\boldsymbol{P}_{3,5}$	956	12	5.885	7.023	4.492

From Table L1, it is observed that the total NLI noise power in the L-band is higher than in the C- and S-bands due to the ISRS effect. In addition, we find out that the total NLI noise power in the L-band increases 1.2 times when compared to the C-band, in the case of the L- and S-bands, the total NLI noise power increases 1.6 times, and the total NLI noise power in C-band increases 1.3 times when compared to the S-band, for all the paths presented in Table L1. Furthermore, the candidate paths with the same number of spans have the same total NLI noise power due to dependency on the number of spans. Moreover, the candidate path $P_{1,1}$ shows the lowest total NLI noise power since it has only one span. The paths $P_{1,5}$, $P_{2,5}$ and $P_{3,5}$, for all bands, have the highest total NLI

noise power accumulated compared with the other candidate paths, due to the higher number of spans crossed.

APPENDIX M

Auxiliary results considering BT-UK and CONUS-60 network topologies and the baseline, common-band and compact architectures

This appendix presents auxiliary results of the simulations performed by the Matlab simulator, for the baseline, common-band, and compact architectures, using the parameters shown in Tables 4.2 and 4.3. Tables M1-M18 show the blocking probability (4.1), total network capacity (4.2), total demands number, number of blocked demands, and the number of C-, L- and S-bands demands. In addition, in Figures M1 and M2, the transport capacity in Tbit/s for each modulation format (QPSK, 8-QAM and 16-QAM), for the baseline, common-band and compact architectures, a blocking probability of 1%, the channel launch powers of -2 and 0 dBm and considering the BT-UK network.

TABLE M1. Auxiliary results obtained using the Matlab simulator, considering the BT-UK topology, the baseline architecture, and a channel launch power of -2 dBm.

Blocking probability limit [%]	Blocking probability [%]	Total network capacity [Tbit/s]	Total Demands number	Number of blocked demands	Number of C-band demands	Number of L-band demands	Number of S-band demands
1	1.06	189.06	734.56	7.82	518.60	202.62	5.52
2	2.06	200.84	794.12	16.34	535.52	227.06	15.20
3	3.05	210.71	845.00	25.76	548.94	244.06	26.24
4	4.05	222.70	904.26	36.62	569.12	259.08	39.44
5	5.04	234.54	966.06	48.68	582.60	276.34	58.44
6	6.04	248.27	1035.54	62.52	598.12	295.46	79.44
7	7.03	262.81	1109.10	77.98	618.60	311.90	100.62
8	8.03	276.40	1180.12	94.78	633.38	326.14	125.82
9	9.03	287.80	1248.02	112.74	649.12	337.70	148.46
10	10.03	299.76	1313.80	131.80	662.06	349.64	170.30

TABLE M2. Auxiliary results obtained using the Matlab simulator, considering the BT-UK topology, the common-band architecture, and a channel launch power of -2 dBm.

Blocking probability limit [%]	Blocking probability [%]	Total network capacity [Tbit/s]	Total Demands number	Number of blocked demands	Number of C-band demands	Number of L-band demands	Number of S-band demands
1	1.14	80.33	299.80	3.44	294.86	1.50	0.00
2	2.16	84.24	318.34	6.86	308.72	2.76	0.00
3	3.12	88.66	339.70	10.58	323.06	6.06	0.00
4	4.12	92.09	358.24	14.76	335.06	8.42	0.00
5	5.13	94.93	372.72	19.12	344.52	9.08	0.00
6	6.10	101.60	406.34	24.78	367.40	14.16	0.00
7	7.09	106.16	428.38	30.36	380.40	17.62	0.00
8	8.09	112.23	459.52	37.18	399.28	23.06	0.00
9	9.08	115.58	480.26	43.62	410.18	26.46	0.00
10	10.08	121.69	514.06	51.82	428.14	34.10	0.00

TABLE M3. Auxiliary results obtained using the Matlab simulator, considering the BT-UK topology, the compact architecture, and a channel launch power of -2 dBm.

Blocking probability limit [%]	Blocking probability [%]	Total network capacity [Tbit/s]	Total Demands number	Number of blocked demands	Number of C-band demands	Number of L-band demands	Number of S-band demands
1	1.08	155.08	613.84	6.60	471.36	134.74	1.14
2	2.06	192.80	775.60	16.00	539.64	211.88	8.08
3	3.06	203.22	825.94	25.24	557.40	227.48	15.82
4	4.05	216.68	895.30	36.26	577.56	251.06	30.42
5	5.05	227.46	950.78	48.04	587.80	270.08	44.86
6	6.04	236.97	1003.62	60.66	603.72	282.60	56.64
7	7.04	251.78	1079.84	75.98	626.50	300.24	77.12
8	8.03	262.94	1142.90	91.82	636.14	317.74	97.20
9	9.03	272.77	1201.18	108.50	649.98	326.46	116.24
10	10.03	287.89	1279.26	128.36	663.04	341.54	146.32

TABLE M4. Auxiliary results obtained using the Matlab simulator, considering the CONUS-60 topology, the baseline architecture, and a channel launch power of -2 dBm.

Blocking probability limit [%]	Blocking probability [%]	Total network capacity [Tbit/s]	Total Demands number	Number of blocked demands	Number of C-band demands	Number of L-band demands	Number of S-band demands
1	1.04	235.14	980.16	10.20	872.04	97.82	0.10
2	2.03	290.16	1223.16	24.88	1009.80	185.92	2.56
3	3.04	320.65	1369.48	41.58	1081.56	237.36	8.98
4	4.03	343.95	1486.04	59.84	1127.42	281.32	17.46
5	5.02	371.45	1620.28	81.40	1179.10	325.66	34.12
6	6.02	396.80	1746.52	105.12	1232.54	364.90	43.96
7	7.02	423.12	1884.06	132.32	1283.10	413.32	55.32
8	8.02	449.84	2025.36	162.44	1335.30	450.88	76.74
9	9.02	472.48	2147.86	193.66	1380.12	480.88	93.20
10	10.02	488.47	2251.26	225.58	1410.30	506.24	109.14

TABLE M5. Auxiliary results obtained using the Matlab simulator, considering the CONUS-60 topology, the common-band architecture, and a channel launch power of -2 dBm.

Blocking probability limit [%]	Blocking probability [%]	Total network capacity [Tbit/s]	Total Demands number	Number of blocked demands	Number of C-band demands	Number of L-band demands	Number of S-band demands
1	1.07	156.18	651.86	6.98	640.06	4.82	0.00
2	2.06	167.52	706.98	14.56	682.64	9.78	0.00
3	3.06	186.03	793.86	24.28	751.34	18.24	0.00
4	4.05	195.11	839.68	34.02	782.42	23.24	0.00
5	5.04	210.75	915.94	46.16	836.12	33.66	0.00
6	6.05	225.51	988.82	59.78	884.24	44.80	0.00
7	7.04	231.95	1032.58	72.68	903.52	56.38	0.00
8	8.04	247.29	1109.68	89.20	949.92	70.56	0.00
9	9.03	261.91	1190.42	107.54	996.50	86.38	0.00
10	10.03	270.01	1239.92	124.38	1016.90	98.64	0.00

TABLE M6. Auxiliary results obtained using the Matlab simulator, considering the CONUS-60 topology, the compact architecture, and a channel launch power of -2 dBm.

Blocking probability limit [%]	Blocking probability [%]	Total network capacity [Tbit/s]	Total Demands number	Number of blocked demands	Number of C-band demands	Number of L-band demands	Number of S-band demands
1	1.05	192.42	819.74	8.64	763.84	47.26	0.00
2	2.04	245.52	1053.40	21.50	921.22	110.56	0.12
3	3.03	287.77	1247.34	37.80	1031.18	177.14	1.22
4	4.03	316.93	1387.56	55.86	1106.92	219.34	5.44
5	5.03	343.53	1517.46	76.28	1162.32	265.60	13.26
6	6.03	364.83	1630.44	98.24	1206.56	303.40	22.24
7	7.02	398.80	1798.86	126.28	1273.14	365.86	33.58
8	8.02	428.84	1951.62	156.54	1333.08	414.58	47.42
9	9.02	447.26	2059.10	185.68	1368.10	446.20	59.12
10	10.02	478.38	2227.34	223.16	1430.64	491.34	82.20

TABLE M7. Auxiliary results obtained using the Matlab simulator, considering the BT-UK topology, the baseline architecture, and a channel launch power of 0 dBm.

Blocking probability limit [%]	Blocking probability [%]	Total network capacity [Tbit/s]	Total Demands number	Number of blocked demands	Number of C-band demands	Number of L-band demands	Number of S-band demands
1	1.09	129.26	463.3	5.04	385.98	71.76	0.52
2	2.07	187.74	683.00	14.12	488.60	173.38	6.90
3	3.05	207.98	769.94	23.48	516.36	210.48	19.62
4	4.05	228.21	856.28	34.70	540.32	237.74	43.52
5	5.04	248.98	946.38	47.74	568.08	264.22	66.34
6	6.04	280.90	1086.84	65.60	602.20	303.48	115.56
7	7.03	296.13	1163.86	81.86	620.04	316.72	145.24
8	8.03	309.24	1229.44	98.76	632.14	327.38	171.16
9	9.03	327.58	1317.42	118.92	651.70	346.34	200.46
10	10.03	334.02	1360.80	136.50	655.26	355.38	213.66

TABLE M8. Auxiliary results obtained using the Matlab simulator, considering the BT-UK topology, the common-band architecture, and a channel launch power of 0 dBm.

Blocking probability limit [%]	Blocking probability [%]	Total network capacity [Tbit/s]	Total Demands number	Number of blocked demands	Number of C-band demands	Number of L-band demands	Number of S-band demands
1	1.12	81.75	286.32	3.20	281.80	1.32	0.00
2	2.14	86.21	306.00	6.54	296.36	3.10	0.00
3	3.13	91.93	331.28	10.36	314.16	6.76	0.00
4	4.11	97.92	357.12	14.68	329.66	12.78	0.00
5	5.10	101.87	375.72	19.18	341.04	15.50	0.00
6	6.10	110.06	411.36	25.08	363.12	23.16	0.00
7	7.09	117.43	446.06	31.64	383.06	31.36	0.00
8	8.09	120.21	464.54	37.56	389.80	37.18	0.00
9	9.07	132.84	523.18	47.44	422.12	53.62	0.00
10	10.07	141.37	561.68	56.56	439.20	65.92	0.00

TABLE M9. Auxiliary results obtained using the Matlab simulator, considering the BT-UK topology, the compact architecture, and a channel launch power of 0 dBm.

Blocking probability limit [%]	Blocking probability [%]	Total network capacity [Tbit/s]	Total Demands number	Number of blocked demands	Number of C-band demands	Number of L-band demands	Number of S-band demands
1	1.06	173.04	629.84	6.68	471.88	147.18	4.10
2	2.06	206.84	762.36	15.70	532.54	201.14	12.98
3	3.05	223.24	836.92	25.54	549.26	230.60	31.52
4	4.05	241.46	917.04	37.10	573.94	252.66	53.34
5	5.04	259.13	998.50	50.34	595.18	275.14	77.84
6	6.04	289.26	1131.54	68.32	629.52	313.06	120.64
7	7.03	302.17	1200.88	84.42	643.06	323.96	149.44
8	8.03	311.16	1252.34	100.58	655.14	333.06	163.56
9	9.03	329.14	1341.30	121.10	670.84	353.98	195.38
10	10.03	338.51	1397.56	140.18	678.14	362.50	216.74

TABLE M10. Auxiliary results obtained using the Matlab simulator, considering the CONUS-60 topology, the baseline architecture, and a channel launch power of 0 dBm.

Blocking probability limit [%]	Blocking probability [%]	Total network capacity [Tbit/s]	Total Demands number	Number of blocked demands	Number of C-band demands	Number of L-band demands	Number of S-band demands
1	1.04	275.03	1163.48	12.12	965.40	185.32	0.64
2	2.03	316.44	1349.02	27.42	1059.62	257.82	4.16
3	3.03	341.66	1468.72	44.52	1116.50	297.02	10.68
4	4.03	360.98	1571.54	63.30	1163.48	324.38	20.38
5	5.03	371.86	1634.44	82.14	1183.26	341.24	27.80
6	6.02	387.31	1717.24	103.42	1221.68	358.00	34.14
7	7.02	405.96	1819.32	127.74	1262.10	382.72	46.76
8	8.02	415.98	1883.94	151.12	1281.58	396.70	54.54
9	9.02	435.11	1990.54	179.58	1317.16	420.02	73.78
10	10.02	453.70	2096.40	210.08	1357.96	442.12	86.24

TABLE M11. Auxiliary results obtained using the Matlab simulator, considering the CONUS-60 topology, the common-band architecture, and a channel launch power of 0 dBm.

Blocking probability limit [%]	Blocking probability [%]	Total network capacity [Tbit/s]	Total Demands number	Number of blocked demands	Number of C-band demands	Number of L-band demands	Number of S-band demands
1	1.07	161.99	683.02	7.32	670.22	5.48	0.00
2	2.06	174.14	742.18	15.28	715.54	11.36	0.00
3	3.05	182.80	786.34	24.00	745.04	17.30	0.00
4	4.05	193.05	838.66	33.98	779.78	24.90	0.00
5	5.05	204.28	897.22	45.28	813.48	38.46	0.00
6	6.04	214.08	948.72	57.32	846.68	44.72	0.00
7	7.04	225.25	1010.20	71.08	881.20	57.92	0.00
8	8.04	237.43	1077.78	86.64	920.58	70.56	0.00
9	9.03	250.62	1149.56	103.78	962.16	83.62	0.00
10	10.03	269.12	1249.24	125.28	1012.52	111.44	0.00

TABLE M12. Auxiliary results obtained using the Matlab simulator, considering the CONUS-60 topology, the compact architecture, and a channel launch power of 0 dBm.

Blocking probability limit [%]	Blocking probability [%]	Total network capacity [Tbit/s]	Total Demands number	Number of blocked demands	Number of C-band demands	Number of L-band demands	Number of S-band demands
1	1.04	265.55	1118.52	11.62	937.36	168.84	0.70
2	2.04	320.86	1365.46	27.80	1068.16	264.68	4.82
3	3.03	342.65	1474.68	44.68	1116.14	301.36	12.50
4	4.03	361.58	1570.04	63.30	1162.12	326.54	18.08
5	5.03	373.03	1636.12	82.32	1182.24	345.22	26.34
6	6.02	389.67	1724.16	103.86	1222.52	361.48	36.30
7	7.02	405.24	1817.28	127.58	1263.70	380.24	45.76
8	8.02	419.72	1897.74	152.22	1290.74	397.84	56.94
9	9.02	437.07	1995.76	180.02	1328.22	416.10	71.42
10	10.02	453.65	2091.74	209.58	1363.80	432.48	85.88

TABLE M13. Auxiliary results obtained using the Matlab simulator, considering the BT-UK topology, the baseline architecture, and a channel launch power of 2 dBm.

Blocking probability limit [%]	Blocking probability [%]	Total network capacity [Tbit/s]	Total Demands number	Number of blocked demands	Number of C-band demands	Number of L-band demands	Number of S-band demands
1	1.10	114.83	402.76	4.42	345.34	52.72	0.28
2	2.06	163.47	587.64	12.12	433.98	137.02	4.52
3	3.06	196.21	716.08	21.88	484.76	190.04	19.40
4	4.04	229.34	850.36	34.34	531.14	230.74	54.14
5	5.04	257.33	970.30	48.94	561.52	265.44	94.40
6	6.03	286.32	1093.40	65.94	590.28	293.64	143.54
7	7.03	307.63	1186.56	83.46	614.86	314.64	173.60
8	8.03	308.46	1205.04	96.82	613.76	314.04	180.42
9	9.03	322.74	1275.18	115.18	631.82	326.86	201.32
10	10.03	327.44	1311.84	131.62	635.68	332.64	211.90

TABLE M14. Auxiliary results obtained using the Matlab simulator, considering the BT-UK topology, the common-band architecture, and a channel launch power of 2 dBm.

Blocking probability limit [%]	Blocking probability [%]	Total network capacity [Tbit/s]	Total Demands number	Number of blocked demands	Number of C-band demands	Number of L-band demands	Number of S-band demands
1	1.14	79.59	276.48	3.14	269.68	3.66	0.00
2	2.16	87.30	306.68	6.62	291.60	8.46	0.00
3	3.14	91.53	326.52	10.24	302.54	13.74	0.00
4	4.11	101.60	366.44	15.08	328.26	23.10	0.00
5	5.11	110.26	404.02	20.62	346.36	37.04	0.00
6	6.08	119.15	444.02	27.00	366.50	50.52	0.00
7	7.07	136.21	513.94	36.34	405.88	71.70	0.02
8	8.06	145.11	558.56	45.04	421.44	92.02	0.06
9	9.06	166.64	652.02	59.04	464.24	128.38	0.36
10	10.07	190.26	760.40	76.56	499.82	181.44	2.58

TABLE M15. Auxiliary results obtained using the Matlab simulator, considering the BT-UK topology, the compact architecture, and a channel launch power of 2 dBm.

Blocking probability limit [%]	Blocking probability [%]	Total network capacity [Tbit/s]	Total Demands number	Number of blocked demands	Number of C-band demands	Number of L-band demands	Number of S-band demands
1	1.08	142.34	506.68	5.46	403.14	96.84	1.24
2	2.05	195.40	710.84	14.60	492.64	187.82	15.78
3	3.05	218.79	807.04	24.62	526.50	220.86	35.06
4	4.04	239.26	895.46	36.20	544.30	249.64	65.32
5	5.04	279.27	1061.40	53.50	593.90	291.20	122.80
6	6.04	298.96	1152.24	69.60	613.50	305.34	163.80
7	7.03	307.95	1199.28	84.30	621.64	314.50	178.84
8	8.03	319.84	1258.16	101.04	640.32	320.36	196.44
9	9.03	331.50	1317.78	119.02	653.12	335.10	210.54
10	10.03	336.92	1355.60	136.02	657.44	341.58	220.56

TABLE M16. Auxiliary results obtained using the Matlab simulator, considering the CONUS-60 topology, the baseline architecture, and a channel launch power of 2 dBm.

Blocking probability limit [%]	Blocking probability [%]	Total network capacity [Tbit/s]	Total Demands number	Number of blocked demands	Number of C-band demands	Number of L-band demands	Number of S-band demands
1	1.07	154.47	662.50	7.10	635.92	19.48	0.00
2	2.06	179.67	776.54	15.96	714.12	46.46	0.00
3	3.04	211.44	921.44	28.02	801.40	92.02	0.00
4	4.04	249.49	1099.28	44.38	902.30	152.40	0.20
5	5.03	294.98	1313.14	66.02	1014.48	229.78	2.86
6	6.03	327.76	1473.14	88.82	1090.26	282.30	11.76
7	7.03	350.90	1594.40	112.02	1147.32	313.90	21.16
8	8.02	372.39	1714.22	137.56	1197.58	343.30	35.78
9	9.02	389.41	1807.56	163.04	1232.04	364.66	47.82
10	10.02	411.27	1931.04	193.46	1276.98	395.94	64.66

TABLE M17. Auxiliary results obtained using the Matlab simulator, considering the CONUS-60 topology, the common-band architecture, and a channel launch power of 2 dBm.

Blocking probability limit [%]	Blocking probability [%]	Total network capacity [Tbit/s]	Total Demands number	Number of blocked demands	Number of C-band demands	Number of L-band demands	Number of S-band demands
1	1.09	142.83	610.24	6.62	598.04	5.58	0.00
2	2.07	150.40	650.42	13.48	628.20	8.74	0.00
3	3.06	161.52	704.26	21.54	667.46	15.26	0.00
4	4.06	173.79	766.58	31.10	709.60	25.88	0.00
5	5.06	183.54	815.14	41.22	739.92	34.00	0.00
6	6.05	193.28	870.80	52.66	771.58	46.56	0.00
7	7.04	205.80	933.40	65.74	811.48	56.18	0.00
8	8.04	222.88	1023.96	82.32	864.14	77.50	0.00
9	9.03	229.87	1070.34	96.70	887.86	85.78	0.00
10	10.03	252.44	1187.82	119.18	951.40	117.24	0.00

TABLE M18. Auxiliary results obtained using the Matlab simulator, considering the CONUS-60 topology, the compact architecture, and a channel launch power of 2 dBm.

Blocking probability limit [%]	Blocking probability [%]	Total network capacity [Tbit/s]	Total Demands number	Number of blocked demands	Number of C-band demands	Number of L-band demands	Number of S-band demands
1	1.07	157.34	675.98	7.22	646.12	22.64	0.00
2	2.05	185.63	803.14	16.48	736.12	50.54	0.00
3	3.05	224.31	982.48	29.92	845.38	107.18	0.00
4	4.03	263.43	1164.74	46.94	947.10	169.88	0.82
5	5.03	301.47	1346.32	67.66	1042.04	232.02	4.60
6	6.03	337.01	1521.12	91.66	1124.74	290.66	14.06
7	7.02	362.85	1655.20	116.24	1189.32	324.08	25.56
8	8.02	379.13	1746.92	140.14	1227.08	342.48	37.22
9	9.02	396.08	1843.06	166.28	1261.02	363.94	51.82
10	10.02	421.41	1980.42	198.48	1310.94	397.42	73.58

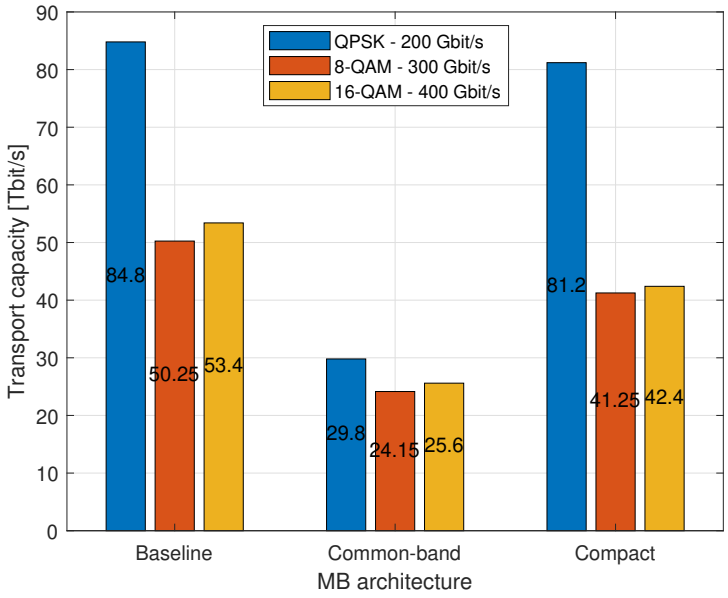

FIGURE M1. Transport capacity distribution among the three modulation formats considered for the BT-UK topology, considering a blocking probability of 1%, a channel launch power of -2 dBm, the baseline, common-band, and compact architectures.

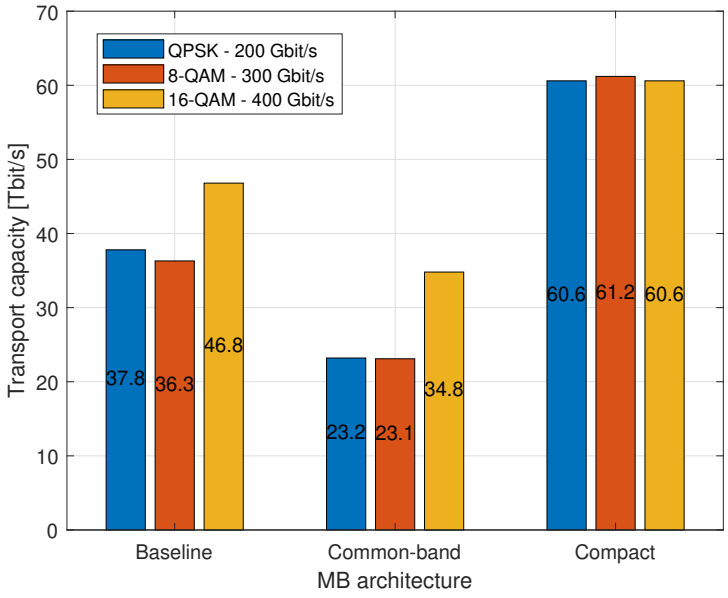

FIGURE M2. Transport capacity distribution among the three modulation formats considered for the BT-UK topology, considering a blocking probability of 1%, a channel launch power of 0 dBm, the baseline, common-band, and compact architectures.

APPENDIX N

Scientific contributions

Influence of the ROADM architecture on the cost-per-bit in C+L+S multi-band optical networks

João Frederico Ó Ramos [2], Luís Cancela [1,2], and João Rebola [1,2]

[1] *Optical Communications and Photonics Group, Instituto de Telecomunicações, Lisboa, Portugal*
[2] *Instituto Universitário de Lisboa (ISCTE-IUL), Lisboa, Portugal*
e-mail: Frederico_O@iscte-iul.pt, luis.cancela@iscte-iul.pt ,joao.rebola@iscte-iul.pt

ABSTRACT
A detailed cost-per-bit analysis of four C+L+S multi-band (MB) reconfigurable optical add-drop multiplexers architectures is presented and discussed. A network cost analysis, including these MB nodes is also presented. The MB common-band architecture, based mainly on C-band components, is the most cost effective architecture in almost all the network scenarios considered.
Keywords: cost-per-bit, multi-band, optical networks, reconfigurable optical add-drop multiplexers.

1. INTRODUCTION

Nowadays, optical networks are required to have more capacity and flexibility due to the growth of new services, such as autonomous driving, virtual reality, cloud and 5G services. The foreseeable traffic generated by these new services will consume all available C-band resources in a near future, and, so, multi-band (MB) and spatial division multiplexing (SDM) solutions have been being explored in recent years to increase network capacity [1].

The MB solution consists in the exploitation of the full low attenuation spectrum available in a single mode optical fiber, allowing transmission beyond the C-band, and is seen as a near to medium-term solution to solve the capacity problem [1]. Several studies have already addressed both transmission issues, and node architecture solutions for operating a MB network [2–4]. In particular, in [3], a cost analysis considering a C+L+S network scenario is studied considering both transmission and node architecture issues. The node architectures considered were the MB baseline, where switching between bands is not allowed, and the MB common-band architectures, that uses mainly C-band components. In [2], a MB all-optical wavelength converter (AO-WC) architecture was presented and , in [4], a MB architecture called compact architecture that uses only components that work in all bands has been proposed and a network performance analysis has been done. Despite there are already, at least, four types of MB ROADM architectures proposed in the literature to the authors best knowledge a comprehensive cost analysis comparison between these architectures remains to be done.

In this paper, a detailed cost-per-bit analysis of all four MB reconfigurable optical add-drop multiplexer (ROADM) architectures proposed in the literature - the MB baseline, the MB AO-WC, the MB common-band and the MB compact architectures - is presented and discussed considering the C+L+S band scenario. A comparison with a SDM node scenario is also performed.

This paper is organized as follows. In section 2, the four MB architectures are presented, as well as their cost model. In section 3, the cost-per-bit of the four MB architectures is calculated and the cost-per-bit considering the British Telecom (BT-UK) and CONUS networks is studied considering the four MB node architectures. A comparison with a SDM node is also performed. In section 4, the main conclusions are drawn.

2. C+L+S MULTI-BAND ROADM ARCHITECTURES COST MODELLING

This section presents the MB architectures studied in this work, as well as the cost of each one of the components used to build these MB architectures. Fig. 1 shows the four *R*-degree MB architectures studied: the MB baseline architecture is shown in Fig. 1a [3], the MB AO-WC architecture is shown in Fig. 1b [2], the MB common-band architecture is shown in Fig. 1c [2, 3], and the MB compact architecture is shown in Fig. 1d [4].

The MB baseline architecture shown in Fig. 1a, consists of a MB demultiplexer (DEMUX) and MB multiplexer (MUX), optical amplifiers (two Erbium-doped fiber amplifiers (EDFAs) for C- and L-bands and one Thulium-doped fiber amplifier (TDFA) for S-band) at the DEMUX output and at the MUX input, and a bank of parallel single-band wavelength selective switches (WSSs), which are connected to single-band WSSs at the output ROADM directions. The wavelengths can be switched to any direction within each band, however, switching between bands is not possible. As a main advantage, the equipment dedicated to other bands may not be acquired at the beginning of network operation, when the network traffic is not enough to justify the use of other bands [4].

To add the possibility of switching wavelengths between bands, the MB architectures presented in Figs. 1b, 1c and 1d were proposed in [2–4]. The AO-WC and common-band architectures use AO-WCs, which have the function of converting multiple wavelengths between bands. The AO-WC architecture uses dedicated band components in the express and add/drop (A/D) structures, whereas the common-band architecture uses only C-band components on express and A/D structures thanks to the AO-WCs, reducing the node complexity and cost. A disadvantage of using the AO-WC and common-band architectures is the use of AO-WCs, which is a technology,

979-8-3503-0302-5/23/$31.00 ©2023 IEEE

that is still in a research phase [3]. The compact architecture uses in the express structure, MB WSSs that work simultaneously in multiple bands and reduce the amount of equipment needed. However, the use of this architecture requires the acquisition of MB components at the beginning of the network operation, leading to a high initial investment as opposed to the previous architectures.

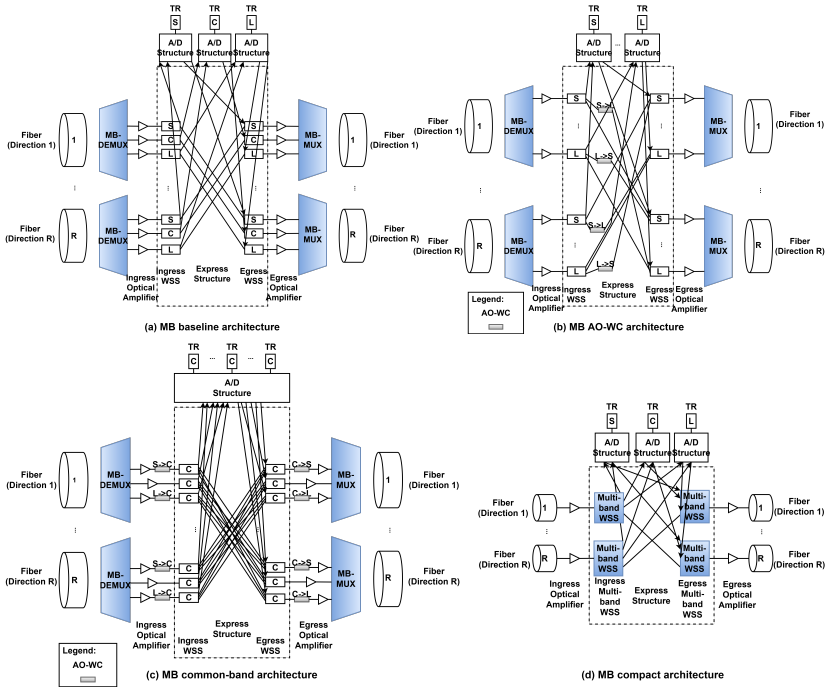

Fig. 1: R-degree MB route-and-select (R&S) architectures.

To compute the cost of each MB ROADMs, the number of channels considered in the C-, L- and S-bands is, respectively, 87, 130 and 148 channels for a 50 GHz channel spacing, and a R&S ROADM architecture with colorless and directionless (CD) A/D structure with an A/D ratio of 25% is considered. The component costs, presented in Table 1 are extracted from [3], and are calculated in relation to the cost of a C-band EDFA. The L-band components are assumed 20% more expensive than C-band components, and the cost of the S-band components depends on a multiplicative factor α, which ranges from 1.2 to 1.5 [3, 5]. The AO-WC cost depends on the C-band transponder (TR) cost, with the parameter β ranging from 0.5 to 2, and the fiber lease cost is 0.33 per fiber/km/year [3, 5]. In our calculations, we considered α=1.5 and β=2, which corresponds to a less favourable cost scenario.

Table 1: Relative cost of components for C-, L- and S-bands

Components	Cost			
	C-band	**L-band**	**S-band**	**Variable name**
EDFA	1	1.2	-	$Cost_{xDFA,b}$
TDFA	-	-	α	$Cost_{xDFA,b}$
1×2 WSS	1.25	1.5	1.25α	$Cost_{WSS,b}$
1×4 WSS	2.5	3	2.5α	$Cost_{WSS,b}$
1×9 WSS	5	6	5α	$Cost_{WSS,b}$
1×20 WSS	7.5	9	7.5α	$Cost_{WSS,b}$
1×40 WSS	15	18	15α	$Cost_{WSS,b}$
1×80 WSS	30	36	30α	$Cost_{WSS,b}$
Transponder (TR)	36	43.2	36α	$Cost_{TR,b}$

Components	Cost	
	C+L+S-bands	**Variable name**
Optical Amplifier (C+L+S bands)	2.2167+α	$Cost_{MB,EDFA}$
1×N_{bands} MB MUX/DEMUX	0.04	$Cost_{MB,MUX/DEMUX}$
AO-WC	36β	$Cost_{AO-WC}$
1×9 MB WSS	7α	$Cost_{MB,WSS}$
1×20 MB WSS	10α	$Cost_{MB,WSS}$
1×40 MB WSS	20α	$Cost_{MB,WSS}$
Cost per fiber/km/year	0.33	-

The cost of the CD A/D structure of the MB ROADM is given by

$$Cost_{A/D,CD,b} = 2N_{A/D}Cost_{WSS,R\times1,b} + 2N_{A/D}Cost_{WSS,1\times M,b} + MCost_{TR,b} \quad (1)$$

where $N_{A/D}$ is the number of A/D cards, M is the number of TRs and the variable b identifies the band dependence, with b=C, L or S, since (1) can be used to calculate the cost of the CD A/D structure for any of the bands. The express structure total cost of the baseline, AO-WC and common-band architectures (Fig. 1) is given by,

$$Cost_{Express} = \Sigma_b^{N_{bands}}(Cost_{Express,b}) + N_{AO-WC}Cost_{AO-WC} + 2RCost_{MB,MUX/DEMUX} \quad (2)$$

where N_{AO-WC} is the number of AO-WCs and $Cost_{express,b}$ is the express structure cost in each band given by

$$Cost_{Express,b} = R(2Cost_{WSS,a} + 2Cost_{xDFA,b}) \quad (3)$$

where a=b, for the baseline and AO-WC architectures express structure cost and a=C, for the common-band architecture express structure cost. The express structure total cost of the MB compact architecture is given by

$$Cost_{Compact,Express} = R(2Cost_{MB,WSS} + 2Cost_{MB,EDFA}) + 6RCost_{MB,MUX/DEMUX} \quad (4)$$

For comparison purposes, we also model the cost of a SDM ROADM architecture with wavelength granularity switching without lane changes [6]. The SDM ROADM A/D structure and the express structure costs are given, respectively, by $3\times Cost_{A/D,CD,b}$ and $3\times Cost_{Express,C}$, since we use 3 fibers working on the C-band.

3. RESULTS ANALYSIS

In this section, a cost-per-bit analysis of the four MB ROADM architectures is performed in section 3.1, alongside with a comparison with a SDM ROADM with 3 fibers per direction. In section 3.2, a MB network scenario is analysed, and two different networks (BT-UK and CONUS 60) are considered.

3.1. Cost comparison between MB node architectures

This subsection studies the cost-per-bit of the four MB architectures presented in section 2. The cost-per-bit is defined as the ratio between the total node cost and the total node A/D capacity, which depends on each TR bit rate (100 Gb/s per transponder is assumed) and on their number. The cost-per-bit is normalized to the cost of a reference scenario, a R&S C-band node with 2 directions, where the total node A/D capacity is 4.4 Tb/s.

Fig. 2a shows the normalized cost-per-bit of each R&S CD MB ROADM architecture and of the SDM ROADM considering 2, 4, 8 and 16 directions. In addition, Fig. 2b shows the required number of AO-WCs considering R=2, 4, 8 and 16, for the AO-WC and common-band architectures.

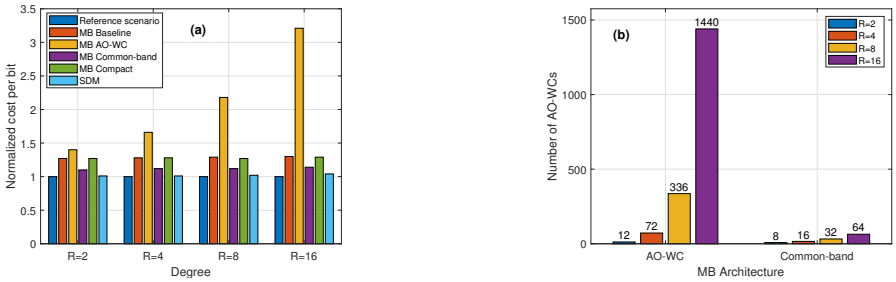

Fig. 2: Normalized cost-per-bit of the MB and SDM ROADM architectures (a) and number of AO-WCs for AO-WC and common-band architectures (b).

As can be observed in Fig. 2a, the cost-per-bit of the SDM architecture is quite similar (only approximately 2% higher) to the reference scenario cost, since both SDM architecture total cost and the node A/D capacity depend practically only on the TRs number. The cost-per-bit of the SDM architecture is lower compared to the four MB architectures due to the lower cost of the C-band TRs. The cost-per-bit of the SDM, baseline, common-band and compact architectures remains unchanged with the number of directions increase since their cost is mainly dependent on the TRs cost (the number of TRs roughly doubles with the number of directions, for R=2, 4, 8 and 16 are, respectively, 183, 365, 730 and 1460 TRs). The common-band architecture cost-per-bit is very similar to the reference scenario cost, being the compact and MB baseline architectures slightly expensive. For the common-band architecture, the number of AO-WC doubles with the number of directions, Fig. 2b, but their contribution to the total node cost is low. While, for the AO-WC architecture, the number of AO-WCs increases hugely with the number of directions, resulting in a significant contribution to the total node cost for a higher number of directions, as shown in Fig. 2a, being the AO-WC architecture the most costly architecture. The results obtained in Fig. 2a for the baseline, common-band and SDM architectures, are very similar to the results of Fig. 3 of [3], for α=1.5, β=2, without considering the fiber lease cost.

3.2. Cost comparison between two MB networks

This subsection studies the cost-per-bit of two MB networks, a smaller network - BT-UK, and a larger one - CONUS 60 [5, 7]. The BT-UK network topology has 22 nodes, an average link length of 147 km and an average node degree of 3.2. In the CONUS 60 network, the total number of nodes is 60, the average link length is 445 km and the average node degree of 2.6.

Figs. 3a and 3b show the cost-per-bit for the BT-UK and CONUS 60 networks, respectively, as a function of the fiber lease cost per km and year considering MB and SDM R&S CD ROADM architecture with an A/D ratio

of 25%. The duration of the fiber lease considered is 5 years. From Figs. 3a and 3b, it is observed that the cost-per-bit of MB architectures has a smooth increase with the fiber lease cost since only one fiber per direction is used, as opposed to the sharper increase in the SDM network scenario where 3 fibers per direction are considered. Fig. 3 also shows that, the compact and baseline architectures present a similar cost-per-bit due to the use of a similar A/D structure. The common-band architecture presents the lower cost-per-bit compared to the other MB architectures for both topologies due to the use of only C-band components. For the real fiber lease cost (0.33), the common-band architecture presents the lowest cost-per-bit compared to the other MB architectures for both topologies. The cost-per-bit in Fig. 3a increases less than in Fig. 3b for all the architectures, since the CONUS 60 network has a higher number of nodes and a longer total network length, than the BT-UK network. Furthermore, in the CONUS 60 network, the SDM architecture exceeds the cost-per-bit of all MB architectures before the real fiber lease cost (0.33) is reached. In the BT-UK network, below the fiber real cost, only the cost-per-bit of the common-band architecture is exceeded by the SDM solution cost. As concluded previously, the AO-WC architecture is not a good choice in terms of cost-per-bit compared to the other MB architectures.

The results presented in Fig. 3 are similar to the ones presented in Fig. 3 of [3], for α=1.5 and β=2 and in Figure 3 of [5], for the MB baseline, common-band and SDM architectures.

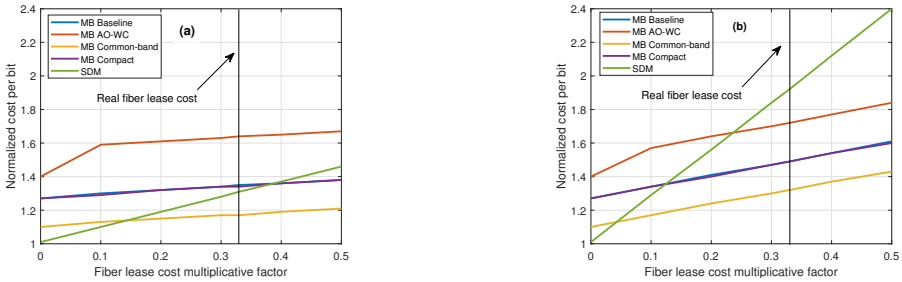

Fig. 3: Normalized cost-per-bit as a function of the fiber lease cost considering both MB and SDM ROADMs for the (a) BT-UK network, and (b) CONUS 60 network.

4. CONCLUSIONS

In this work, we have studied the required number of hardware components, cost-per-bit and suitability of four C+L+S MB node architectures and their impact in network scenarios. We have concluded that the AO-WC node architecture presents the highest cost-per-bit compared to the other MB architectures, due to the high number of AO-WCs and is regarded has an architecture to be discarded. The common-band architecture presents the lowest cost-per-bit due to the use of only C-band components, decreasing the total cost of the node. Both compact and baseline MB node architectures have similar costs. In the BT-UK and CONUS 60 networks scenarios, the most economically promising architecture is the common-band architecture, since it is less expensive than SDM for fiber lease costs above 0.15, however, it relies on a technologically immature component, the AO-WC. For an immediate network deployment, the MB baseline architecture seems advantageous over the compact architecture, although their very similar cost-per-bit, due to its use of commercially available hardware components.

ACKNOWLEDGEMENTS

This work was supported under the project of Instituto de Telecomunicações UIDB/EEA/50008/2020.

REFERENCES

[1] B. Correia *et al.*, "Power control strategies and network performance assessment for C+L+S multiband optical transport," *Journal of Optical Communications and Networking*, vol. 13, no. 7, pp. 147–157, January 2021.

[2] M. Nakagawa *et al.*, "Adaptive Link-by-Link Band Allocation: A Novel Adaptation Scheme in Multi-Band Optical Networks," in *ONDM*, (Gothenburg, Sweden), June 2021.

[3] M. Nakagawa, T. Seki, and T. Miyamura, "Techno-Economic Potential of Wavelength-Selective Band-Switchable OXC in S+C+L Band Optical Networks," in *OFC*, (San Diego, CA, USA), March 2022.

[4] N. Deng *et al.*, "Challenges and Enabling Technologies for Multi-Band WDM Optical Networks," *Journal of Lightwave Technology*, vol. 40, pp. 3385–3394, June 2022.

[5] R. K. Jana *et al.*, "When is operation over C + L bands more economical than multifiber for capacity upgrade of an optical backbone network?," in *ECOC*, (Brussels, Belgium), December 2020.

[6] A. Anchal and D. M. Marom, "Practical SDM-ROADM Designs for Uncoupled Spatial Channels and Their Switching Capacity," in *OFC*, (San Diego, CA, USA), March 2019.

[7] J. M. Simmons, *Optical network design and planning*. Springer International Publishing, second ed., 2014.